Institute of Materials Science and Testing of Polymers

Master thesis

# Investigating novel concepts to characterize the resistance against rapid crack propagation of polyamide 12 pipe grades

Christoph Waly, BSc.

Leoben, February 2021

About the master thesis

This master thesis was written by

Christoph Waly, BSc.

Conducted at

Polymer Compentence Center Leoben GmbH

Submitted to

Institute of Materials Science and Testing of Polymers
Department Polymer Engineering and Science
Montanuniversität Leoben

Academic Supervisor

Univ.-Prof. Dipl.- Ing. Dr. mont Gerald Pinter
Institute of Materials Science and Testing of Polymers
Department Polymer Engineering and Science
Montanuniversität Leoben

Supervisor

Dipl.- Ing. Mario Messiha
Polymer Compentence Center Leoben GmbH

# EIDESSTATTLICHE ERKLÄRUNG

Ich erkläre an Eides statt, dass ich diese Arbeit selbstständig verfasst, andere als die angegebenen Quellen und Hilfsmittel nicht benutzt und mich auch sonst keiner unerlaubter Hilfsmittel bedient habe.

# AFFIDAVIT

I declare in lieu of oath, that I wrote this thesis and performed the associated research myself, using only literature cited in this volume.

**LEOBEN, February 2021** **Christoph Waly, BSc.**

# ACKNOWLEDGEMENTS

First of all, I would like to express my deepest gratitude to all the people who supported me during the progress of this thesis.

I would like to express my special thanks to Univ.-Prof. Dr. mont. Gerald Pinter (Chair of Materials Science and Testing of Polymers, Montanuniversität Leoben) for the time he invested in technical discussions, suggestions for improvement and last but not least for the academic supervision of this thesis. Furthermore, I would like to thank him for giving me unrestricted access to the testing equipment at the chair.

Very special thanks to my supervisor Dipl.-Ing. Mario Messiha (Polymer Competence Center Leoben GmbH, PCCL) for the opportunity, trust, willingness to discuss and share his knowledge in the complex fields of polymer physics and fracture mechanics. Through his critical assessment and patience, he has contributed significantly to the completion of this thesis.

On behalf of the PCCL, I would like to offer my sincere thanks to Dipl.-Ing. Dr. mont. Andreas Frank for making this thesis possible and for the kind reception into the "pipe group". Further thanks go to my colleague Ivaylo Mitev for his support during the measurements. From the chair of Materials Science and Testing of Polymers, I would specially like to thank Dr.mont. Florian Arbeiter for his support at the servo-hydraulic testing machines and helpful professional inputs. At this point I would also like to thank Dipl.-Ing. Sandra Petersmann for her assistance at the drop tower.

The present work was part of the COMET- project “Fracture mechanical failure mechanisms in polyamide pipe grades” (Project-No.: VI-3.08c) at the Polymer Compentence Center Leoben GmbH (PCCL, Austria) within the competence center program COMET of the Federal Ministry for Transport, Innovation an Technology (Austria) and Federal Ministry for Economy, Family and Youth (Austria) with contributions by Evonik Operations GmbH (Germany) an the Montanuniversität Leoben, Department of Material Science and Testing (Austria). The PCCL is funded by the federal government and the states of Styria, Lower Austria and Upper Austria.

Finally, I would like to thank my parents with all my heart for making it possible for me to study. Without them it would not be possible to write these lines at all. Many thanks to my long-time girlfriend Dajana for her unconditional love, patience and constant support during the whole study time.

# ABSTRACT

In the present work, polyamide 12 (PA12) pipe grades, which differ in their molecular structure (neat PA12 or compounded) and use of additives (i.e. impact modification and/or pigmentation), were tested by three new accelerated test methods, aiming to characterise the resistance against Rapid Crack Propagation (RCP). These include a modified form of a Charpy impact test (so-called "Modified Charpy"), a novel test apparatus designed to imitate the stress conditions in a pipe under internal pressure, called the "Notched Hoop-stressed Impact (NHI)" test and finally the presentation of a fracture mechanics test method, termed "Quasi-dynamic $K_{ID,eq}$". While the modified Charpy test is based on an already existing test concept, the NHI test as well as the quasi-dynamic $K_{ID,eq}$ test represent completely new approaches for the characterization of RCP. In order to quantify a reliable material ranking with regard to RCP resistances, all PA12 grades were tested via standardized Small-Scale Steady-State (S4) test according ISO 13477. Results of newly developed approaches were then compared to S4 results in order to check for their reliability and quantitative significance with regard to RCP resistances.

Using the modified Charpy test, the materials showed a different ranking related to the critical pressure values $p_{c\text{-}S4}$ from the S4 test and therefore could not be classified correctly. If the critical temperature values $T_{c\text{-}S4}$ are considered, a ranking of the pipe grades results which agrees positively with the S4 test. However, the underlying idea of reaching a plateau of unchanging ideal brittleness was not achieved due to measurement restrictions. With the NHI test it was possible to evoke different stress states and the associated failure modes in the test specimens, ranging from brittle to ductile. The results of the NHI test also did not provide agreement with respect to $p_{c\text{-}S4}$ from S4 ranking. A ranking in terms of $T_{c\text{-}S4}$ in contrast seems possible. The quasi-dynamic $K_{ID,eq}$ test shows high potential for similar ranking of the materials with regard to their RCP resistance as provided by the S4 test, by using low temperatures, appropriate loading speeds and the advantages of dominating plane strain conditions of Cracked Round Bar (CRB) test specimens. Using this method, it seems possible to rank the investigated materials by $p_{c\text{-}S4}$.

It was demonstrated that all methods were able to rank the PA12 types as long as the classification refers to $p_{c\text{-}S4}$ or $T_{c\text{-}S4}$. Furthermore, a significant advantage of the accelerated

methods in terms of shortened testing times, reduced testing effort and lower costs compared to the S4 test can be attested.

# KURZFASSUNG

In der vorliegenden Arbeit wurden Polyamid 12 (PA12)-Rohrtypen, die sich in ihrer molekularen Struktur (reines PA12 oder compoundiert) und der Verwendung von Additiven (d.h. Schlagzähmodifikation und/oder Pigmentierung) unterscheiden, in drei neuen beschleunigten Prüfverfahren getestet, die darauf abzielen, den Widerstand gegen „Rapid Crack Propagation (RCP)“ zu charakterisieren. Dazu gehören eine modifizierte Form eines Charpy-Schlagversuches (sogenannter "Modified Charpy"), eine neuartiges Prüfverfahren zur Nachahmung der Spannungsbedingungen in einem Rohr unter Innendruck, genannt "Notched Hoop-stressed Impact (NHI)" Test und schließlich die Vorstellung einer bruchmechanischen Prüfmethode, die als "Quasi-dynamischer $K_{ID,eq}$" bezeichnet wird. Während der modifizierte Charpy-Test auf einem bereits bestehenden Prüfkonzept basiert, stellen sowohl der NHI Test als auch der quasi-dynamische $K_{ID,eq}$ Test völlig neue Ansätze für die RCP Charakterisierung von PA12 dar. Um eine verlässliche Materialeinstufung hinsichtlich der RCP Beständigkeit zu quantifizieren, wurden alle PA12-Typen mittels standardisiertem „Small-Scale Steady-State (S4)“ Test nach ISO 13477 geprüft. Die Ergebnisse der neu entwickelten Ansätze wurden dann mit den S4-Ergebnissen verglichen, um ihre Zuverlässigkeit und quantitative Aussagekraft in Bezug auf die RCP Beständigkeit zu überprüfen.

Mit dem modifizierten Charpy-Test zeigten die Materialien, bezogen auf die kritischen Druckwerte $p_{c\text{-}S4}$ aus dem S4 Test, eine andere Rangfolge und konnten daher nicht korrekt klassifiziert werden. Betrachtet man die kritischen Temperaturwerte $T_{c\text{-}S4}$, so ergibt sich eine Rangfolge der Rohrtypen, die mit dem S4-Test positiv übereinstimmt. Die zugrundeliegende Idee, ein Plateau gleichbleibender idealer Sprödigkeit zu erreichen, wurde aufgrund der messtechnischen Einschränkungen nicht erreicht. Mit dem NHI-Test war es möglich, unterschiedliche Spannungszustände und die damit verbundenen Versagensarten in den Probekörpern hervorzurufen, die von spröde bis duktil reichen. Die Ergebnisse des NHI Tests lieferten jedoch keine Übereinstimmung bezüglich der Rangfolge $p_{c\text{-}S4}$ von S4. Eine Reihung in Bezug auf $T_{c\text{-}S4}$ scheint hingegen möglich. Der quasi-dynamische $K_{ID,eq}$ Test zeigt durch die Verwendung niedriger Temperaturen, geeigneter Belastungsgeschwindigkeiten und den Vorteilen des dominierenden ebenen

Spannungszustand von „Cracked Round Bar (CRB)“-Prüfkörpern ein hohes Potenzial für eine ähnliche Reihung der Rohrtypen hinsichtlich ihrer RCP-Beständigkeit, wie sie der S4 Test liefert. Mit dieser Methode scheint es möglich zu sein, eine Rangfolge der unteruschten Materialien nach $p_{c\text{-}S4}$ festzulegen.

Es konnte gezeigt werden, dass alle Methoden in der Lage waren, die PA12-Typen zu reihen, solange sich die Klassifizierung auf $p_{c\text{-}S4}$ oder $T_{c\text{-}S4}$ bezieht. Darüber hinaus kann den beschleunigten Verfahren ein deutlicher Vorteil in Bezug auf verkürzte Prüfzeiten, reduzierten Prüfaufwand und geringere Kosten im Vergleich zum S4 Test attestiert werden.

# TABLE OF CONTENTS

# 1 INTRODUCTION AND OBJECTIVES

In infrastructural pressure pipe applications, the resistance of thermoplastic materials against failure by Rapid Crack Propagation (RCP) is an important property. This kind of catastrophic fracture is caused by a fast-growing crack which is exposed to a continuous crack driving force, and which could undergo the length of several hundred meters almost at the speed of sound. Although this form of failure is infrequent in its kind, polymer materials used in pressurized pipelines, such as PolyEthylene (PE) and PolyAmide (PA), can suffer RCP (Kopp et al. 2018). It is therefore important to characterize the resistance against RCP in order to ensure a safe and reliable structural design and use of polymeric pressure pipes. The evaluation of RCP resistances of thermoplastic pipes is based on the Full-Scale (FS) test according to ISO 13478, and the Small-Scale Steady-State test (S4 test), which is standardized in ISO 13477. However, both testing methods are very cost-intensive and require relatively large pipe specimens for testing (Argyrakis 2010). This has led to the development of accelerated laboratory-scale techniques, which typically use standard tensile, Charpy or Single-Edge-Notched-Bending (SENB) test specimens.

In that context, three newly developed methods are being investigated within this thesis. The main focus of the research is laid upon the development of suitable test conditions and parameters for these methods in order to rank materials according to their RCP resistance. A further objective addresses possible relationships between molecular and morphological structures as well as different additives of various PA12 grades and their RCP resistance.

A theoretical part at the beginning of this thesis was based upon a fundamental literature research in order to better understand the complex nature of a material`s behavior during rapid fracture and further to recognize important structure-property relationships with regard to RCP in PA12. In the experimental part, some general information about the selected grades are given and the new concepts are presented. In the fourth chapter, the results obtained from each method are presented and discussed in detail. Finally, the main outcomes of the thesis are briefly summarized and an outlook on possible future work is given.

# 2 BACKGROUND

This chapter provides a brief overview about basic information on PA12 as a pipe material. Furthermore, the linear-elastic fracture mechanical approaches relevant for this thesis are described, which provide an important basis for the understanding of RCP as well as the development of suitable methods for its characterisation.

## 2.1 Polyamide 12 Pipe Grades

In addition to traditional metallic materials, thermoplastic materials have been increasingly used as pipe materials for decades. By using plastic pipes, costs can be saved in terms of corrosion protection and maintenance work (Weßing et al. 2007). Further benefits that plastic pipes offer over steel pipes include easier installation (lower weight, fast welding techniques, no need of sand bedding) and the ability to wind pipes (long pipe lengths, reduced welding, faster installation, simplified transport and handling, increased safety) (Jareneck and Armstrong 2010). Since some years PA12 has been used as material for Standard Dimension Ratios (SDR) 11 gas piping systems in the range of pressures up to 18 bar (Hartmann 2014; Hitesh 2006; Lohmar 2006). While modern PE gas pipe grades such as PE100 and PE100 RC can be operated up to maximum pressures of 10 bar, PA12 has become an attractive alternative to steel in the high-pressure range (Lohmar 2006; Messiha et al. 2020). This can be attributed in part to its high mechanical properties and chemical resistance (Bonten 2016; Weßing et al. 2007). Current material developments are focusing on a further increase of the operating pressure. Though, a major challenge for the development and classification of PA12 pipe grades is the validation of the material against RCP (Weßing et al. 2007).

### 2.1.1 Chemical Structure and Related Properties

There is a large number of different PA12 types for manifold applications available on the market, which essentially differ in the used monomer and the resulting polymer structure (Alewelt et al. 1998; Domininghaus et al. 2012). In terms of pipe application, a semi-crystalline aliphatic PA12 material is commonly used, which is produced by polycondensation of Laurolactam (Alewelt et al. 1998; Baron et al. 1998). The monomer

and polymer units are shown in Fig. 2.1. The property profile of all PA is mainly determined by the amide group CO-NH (red marking), which connects the beginnings and ends of opened rings. The distance between these groups has a decisive effect on the intermolecular forces, which in turn have an influence on the melting temperature and the absorption of water. The higher the amide bond frequency the higher the melting temperature and the absorption of water (Domininghaus et al. 2012).

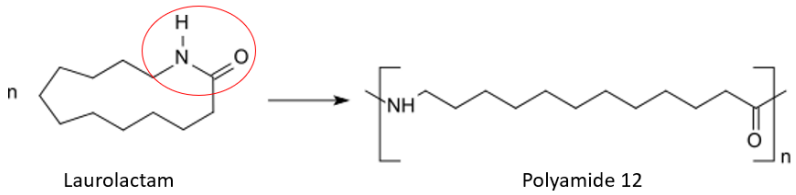


**Fig. 2.1:** Polycondensation of PA12 by Laurolactam (Domininghaus et al. 2012).

Whether an even or uneven number of $CH_2$ groups exists in the main chain between two amide bonds, additionally affects the properties of PA. An uneven number means that the forces between the chains (e.g. van der Waal forces) are generally lower than for those with an even number of methylene groups. The reason for this is shown schematically in Fig. 2.2. If the number of methylene groups is even, the amide groups are always opposite to each other, so that each functional group can form a hydrogen bridge without chain deformation. If the number of methylene groups is odd, only every second amide group is more probable to form a bridge (Alewelt et al. 1998; Domininghaus et al. 2012).

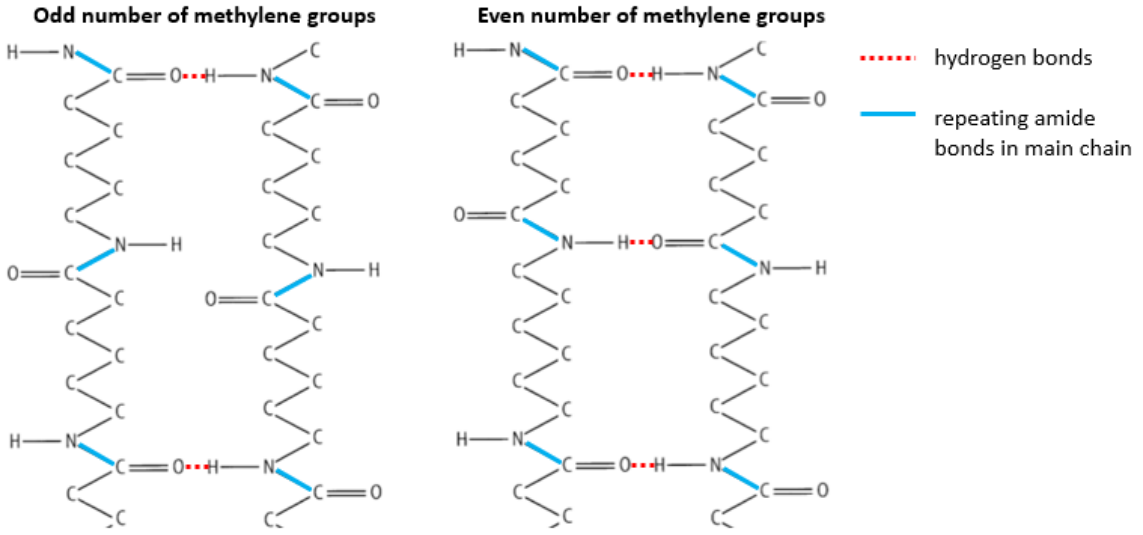


**Fig. 2.2:** Influence of the amount of $CH_3$ groups on the formation of hydrogen bonds in PA (Domininghaus et al. 2012).

### 2.1.2 PA12 Compounds

Commercially available PA12 compounds are mainly available in modified form by means of additives, such as Pigments (PGM) or Impact Modifier (IM). The production of compounds can be done in two ways. Additives can either be added to the reactor before or during polycondensation, or incorporated into the melt (e.g. during reactive extrusion) after polycondensation. The former assumes that the additives do not disturb the reaction (i.e. chain control) and that additives themselves are not damaged by the temperatures in the reactor (Alewelt et al. 1998).

***Pigments (PGM)***

Pigments can be either organic or inorganic substances. They are insoluble in polyamides and are dispersed in the polymer melt. Typically, they must be resistant to heat, light and different weather conditions, in order to satisfy decorative purposes or, as in the case of pipes, to mark different kinds of pipelines (Alewelt et al. 1998). For polyamides, almost all inorganic PGM with a temperature resistance up to or above 300 °C can be used. However, the choice of organic PGM is very limited, as the majority of available colorants are attacked by the chemically aggressive polymer melt (Jandke Joachim and Reinicker Roger A. 2016). Janostik and Senkerik (2017) tested the influence of different PGM in injection molded PolyCarbonate (PC) tensile specimens. Results showed an increase in stiffness but no significant increase in tensile strength. Kurzböck et al. (2012) tested the influence of carbon black on the tensile strength in PolyPropylene (PP). The results exhibits slightly higher tensile strength and lower strain at break values. Shnean (2012) made tests with a mixture of carbon black and titanium dioxide in High-Density PolyEthylen (HDPE). He showed that with increasing weight content of carbon black and titanium dioxide, the modulus of elasticity and impact strength increase, but the compressive strength decreases. Kanu et al. (2001) investigated the effect of organic and inorganic PGM on the tensile and impact properties of injection molded PP. They showed that both properties are improved by the addition of PGM. They also exhibited that the property improvement with organic PGM was higher than with inorganic PGM. Lodeiro et al. (2000) investigated the influence of PGM on the impact behavior of injection molded HDPE sheets using an instrumented falling weight impact machine. They observed that virgin HDPE exhibits higher impact energy than those containing a PGM.

***Impact modifier (IM)***

Impact modifiers are added to thermoplastic materials in order to resist cracking under certain loading rates. Polymers like PA have a glass transition temperature ($T_g$) above room temperature (RT). As a result, they behave more brittle below RT, which must be considered for the final application. In order to be able to use such materials below $T_g$ for end applications, often suitable IM such as rubbers or elastomers, which activate some energy absorption mechanisms like crazing, shear yielding, caviation or voiding, are added to the material. Most important properties of such additives are a sufficiently low $T_g$, optimum particle size, suitable particle size distribution, homogeneous dispersion, good adhesion to thermoplastic matrix and sufficient effectiveness at minimum quantities. Furthermore, the molecular characteristics of the matrix material as well as the manufacturing process also influence the effectiveness of the impact modification (Höffin 1995; Pritchard 1998; Wang et al. 2019; Yilmaz et al. 2015). According to Partridge (1992), the $T_g$ of the matrix should be almost unchanged after the addition of an IM. He also comments that a polymer has been successfully modified when its fracture resistance is increased by a factor of 10 under certain conditions, while its low-strain stiffness does not decrease by more than 25 %. According to Leevers (1996) and Perkins (1999), each rubber toughened system has a temperature limit below which the toughening becomes ineffective. When a system reaches such a temperature limit, at a given strain rate, the rubber becomes too slow to respond to an applied stress. This means that the rubber behaves like glass. Processes such as crack pinning then contribute to the toughness, which absorbs much less energy than crazing or shear yielding. Furthermore, due to their viscoelasticity, polymeric materials exhibit a geometry and strain-rate dependent brittle-tough transition. The influence of IM on the brittle-tough transition behavior has been investigated by several researchers in different materials: Hassan and Haworth (2006), Taib et al. (2012), Gensler et al. (2000), Nijhof et al. (1999). In summary, it can be inferred from the papers that there is a shift in the brittle-tough transition to lower temperatures when IM are added to the pure material. This shift increases with smaller rubber particle sizes (Hassan and Haworth 2006). A decrease in yield stress and elastic modulus was also observed with the addition of rubber particles. In contrast, an increase in elongation to break and notched impact strength was noted (Nijhof et al. 1999; Taib et

al. 2012). Gensler et al. (2000) investigated the influence of impact velocity on an neat isotactic PP (iPP) and an impact modified iPP/Ethylene-Propylene Rubber (EPR) blend. While a tough-brittle transition occurred in iPP, iPP/EPR blend showed no transition in the considered impact speed range. For iPP, the loss in ductility can be attributed to a change in the deformation mechanism. This change in the mechanism could be seen in the load-displacement curve as well as on the fracture surface. Shear processes dominate at lower impact speeds, whereas crazing predominates at higher impact speeds. In contrast, most of the deformation energy in iPP/EPR was absorbed in the iPP matrix, through shear processes.

## 2.2 Fracture Mechanics

In classical continuum mechanics theory, mainly defect-free continua are considered. Fracture mechanics, on the contrary, deals with components that contain inherent defects, that may occur during production of the materials (e.g. pores, voids material inhomogeneities, etc.) or due to mechanical, or thermal loads. If flawed components are additionally submitted to external forces, defects may grow together to form macroscopic cracks. In the worst case this leads to premature structural failure (Wagner 2009). In case of polymers, such a failure can, for example, be due to a break in molecular chains ("chain scission") or due to the chain disentanglements (Grellmann and Altstädt 2011).

In general, there are two different concepts in fracture mechanics which can be used to investigate failure criteria, the linear-elastic (LEFM) and the elastics- plastics (EPFM) fracture mechanics. In both cases it is possible to describe the stress and deformation fields in front of the crack tip by a single parameter, which can partly be transferred into each other. The stress intensity factor $K$ is used for the LEFM, whereas the $J$- integral can be used in frame of the EPFM (Pinter 2019; Schöngrundner 2010; Wagner 2009). The following section describes the concepts and theories of LEFM relevant to this thesis. Extensive works on this topic are available in the literature: Maiti (2015), Kolednik (2012), Gross and Seelig (2016), Anderson (2005b).

### 2.2.1 Linear elastic fracture mechanics

The LEFM provides concepts for the description of crack behavior in an isotropic and linear elastic material. Two main requirements are linked to the applicability of the concept (Anderson 2005b; Pinter 2019):

- linear- elastic material behavior and
- Small Scale Yielding (SSY) at the tip of the crack.

Basically, there are three types of loads (Mode I: opening, Mode II: sliding, Mode III: tearing) which can be applied to a flawed body (Albiter 2018; Anderson 2005b; Özbek 2008). The following descriptions and relationships refer to Mode I, as this type of loading is most relevant for this work.

### 2.2.2 Concept of the energy release rate (G- Concept)

One way to describe the conditions at the crack front is the concept of energy release rate introduced by Griffith. According to this approach, the energy required to form two new crack surfaces is equal to the energy released during a fracture process. Applying an energy conservation approach to a fracture of an elastic body (see Fig. 2.3), the energy supplied to the system ($\partial U_{in}$) can be divided into three components during an increase of the fracture surface $A$ by an infinitesimal amount $\partial A$. These are (Argyrakis 2010; Griffith 1921; Kolednik 2012; Özbek 2008):

- the change in dissipated energy for crack propagation ($\partial U_{diss}$),
- the change in stored energy ($\partial U_{el}$) and
- the change in kinetic ($\partial U_{kin}$) energy of the system.

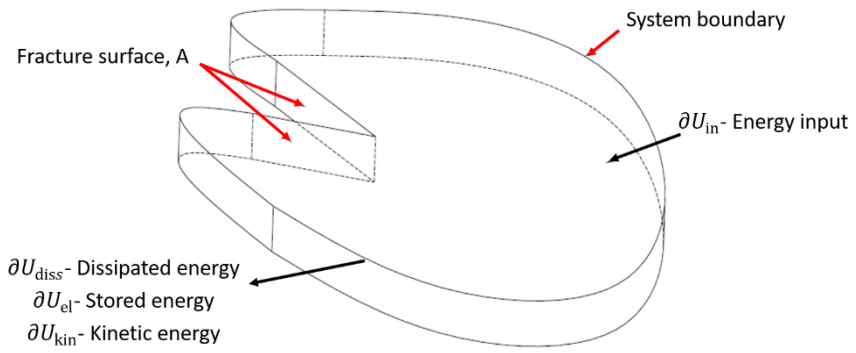


**Fig. 2.3:** Energy balance on a bounded system according to Argyrakis (2010).

The fracture resistance $G_C$ is also defined as $\partial U_{diss}/\partial A$. The difference between the change in input energy $\partial U_{in}$ and the energy stored in the system $\partial U_{el}$ (both related to the area $\partial A$) is better known as the energy release rate or crack driving force $G$. If the crack propagation speed is low, the kinetic part can be neglected and $G$ is equal to $G_C$ (crack initiation toughness for quasi- static conditions) at the onset of fracture. If the crack propagation rate is high, the kinetic component $\partial U_{kin}/\partial A$ can no longer be neglected. In this case, the condition for crack initiation becomes $G = G_D$, with $G_D$ being the dynamic fracture toughness of a material.

### 2.2.3 Concept of stress intensity (K- Concept)

The second approach used in LEFM is the concept of the stress intensity factor $K$, which was established by Irwin in 1957 and is a measure for the intensity of the stress field in the crack tip area (Anderson 2005b; Irwin 1957). The $K_I$ factor can be calculated using the following Eq. 2.1 (Irwin 1957):

$$K_I = \sigma \cdot \sqrt{\pi \cdot a} \cdot f(a/w) \tag{2.1}$$

Where $a$ represents the crack length and $w$ the specimen width. The dimensionless correction function $f(a/w)$, also called geometry factor, depends on the specimen type and its dimensions. The applied stress in front of the crack tip is given by $\sigma$. If $K_I$ in a stressed sample exceeds a critical value $K_C$, crack growth is assumed to occur (Wagner 2009).

### 2.2.4 Plane Stress & Plane Strain Conditions

If a cracked body is loaded e.g. under Mode I, two extreme cases, plane stress and plane strain conditions, can be distinguished. The first occurs within relatively thin bodies, where the principal stresses are always parallel to the given crack plane and are negligible in the normal direction. In thicker components, however, there is a region of material that is relatively far from the free surfaces. This region is not free to deform and displays a distinctive plane strain state where the displacements in the body are parallel to its crack plane (Özbek 2008).

In principle, it must be considered that different specimen thicknesses lead to different $K_C$ values (Fig. 2.4), due to changes in the stress state. In case of very thin bodies, a very high

$K_C$ in plane stress state is present. As the thickness of the component increases, this value passes through a range known as the mixed mode, where neither of the two extreme cases predominates but are simultaneously present. With further increase in component thickness the fracture toughness decreases to a minimum plane strain value $K_{IC}$.

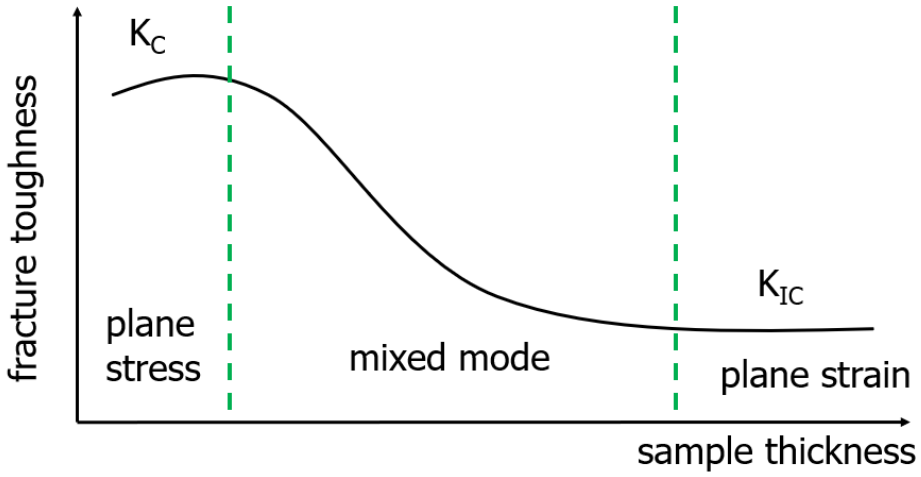


**Fig. 2.4:** Influence of specimen thickness on fracture toughness according to Anderson (2005b) and Pinter (2019).

## 2.3 Dynamic Fracture in Plastic Pipes

When a pressurized pipe fails, it is usually due to unforeseen external factors acting on stress concentration locations, such as defects within the material itself. The most commonly observed type of failure is Slow Crack Growth (SCG), which is characterised by crack initiation followed by slow crack extension (Frank et al. 2019; Pinter 1999). In practice, however, RCP, although very rare, may occur under adverse conditions, such as high pressure and/or low temperature. Above a critical internal pressure $p_c$, a crack can propagate, often sinusoidally, at high-speeds (e.g. 100-300 m/s) for several hundreds of metres along the pipe (Ivankovic and Venizelos 1998; Kopp et al. 2018). In addition, external loading situations, material structure, pipe dimensions and production, as well as the properties of the pressurizing fluid can affect the crack growth behavior (Flüeler and Farshad 1995). However, to simplify the complex issue of dynamic fracture mechanics, it helps to consider the loading situation and the material response to a given dynamic loading separately, whereby the material response can be divided into Rapid Crack Initiation (RCI) and RCP.

### 2.3.1 Time- dependent Material Response – RCI & RCP

Rapid or abrupt loading on a component can come from several sources (e.g. excavator hits a pressurized pipe while digging) causing the mechanical material response to become dependent on time. Very high stress rates often result in an overshooting of $K_I$ at the crack tip, which is regarded as the main reason for sudden brittle failure. In terms of LEFM, the quasi-static $K_I$ quickly becomes dependent on time and is represented by $K_I(t)$ (Bertram 2008; Gross and Seelig 2016).

Crack initiation begins when $K_I(t)$ reaches a critical value, the so-called dynamic crack initiation toughness $K_{Ic}(t)$, or from an energy-based perspective $G_I(t) = G_{Ic}(t)$ (Bertram 2008). Basically speaking, $K_{Ic}(t)$ is not a material constant, but it is dependent on temperature and the stress state in a structure and therefore also on the geometry and shape of a specimen. Thus, the $K_{Ic}(t)$ is strongly dependent on the size of the plastic zone and the materials yield strength. As it is well known for polymers that the yield strength as well as the plastic deformation process can be influenced by loading rate $v$, it becomes possible to rewrite $K_{Ic}(t)$ as $K_{Ic}(v)$, since $v$ is a function of time $t$ (Bertram 2008). Leevers (1995) as well as Buchar (1987) report a decrease of $K_{Ic}(v)$ with increasing loading rates until a minimum value is reached. Other researcher, like Ravi-Chandar and Knauss (1984), support a rising $K_{Ic}(v)$ at higher loading rates. Kalthoff (1990) and Anderson (2005a) mention the complex dependence of the fracture initiation toughness on $v$, especially when dealing with rate sensitive thermoplastics such as PA or HDPE. Instead of suppressing plastic deformations at the crack tip at increasing loading rates, an increase of plastic deformations due to adiabatic heating can be observed. Therefore, it can be concluded that a decrease in $K_{Ic}(v)$ with increasing v is only observed when embrittlement predominates. Conversely, an increase in $K_{Ic}(v)$ is observed when ductility increases. A schematic representation of $G_{Ic}(v)$ (energetic counterpart to $K_{Ic}(v)$) as a function of loading rate for rate sensitive materials with dominating embrittlement is given in Fig. 2.5.

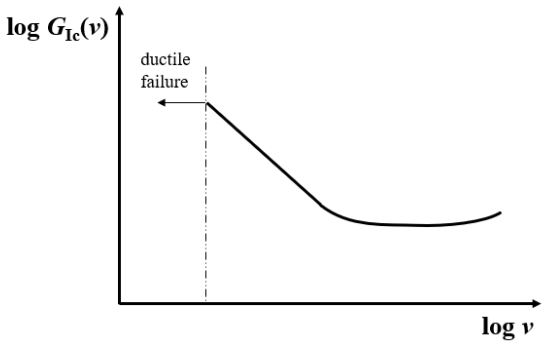


**Fig. 2.5:** Initiation energy release rate $G_{Ic}$(v) as a function of loading rate v, for rate sensitive materials with dominating embrittlement according to Buchar (1987) and Messiha (unpublished).

Similar to $G_{Ic}(v)$, the crack propagation toughness strongly depends on the plastic deformation behavior of the material at the crack tip, and thus also on the strain rate (Deblieck et al. 2017). In case of rate sensitive materials, the resistance to rapid crack propagation, is expressed as dynamic fracture toughness $G_{Id}(\dot{a})$ and is a function of the crack propagation speed $\dot{a}$ (Broek 1982). Assuming dominating embrittlement at increasing local strain rates during RCP (in the case of rate sensitive materials), $G_{Id}(\dot{a})$ passes through a minimum before increasing asymptoticly at the maximum possible crack propagation speed a specific material can achieve ($\dot{a}_{max}$, see Fig. 2.6) (Deblieck et al. 2017; Gross and Seelig 2016). In comparison, $G_{Id}$ for an ideally brittle material remains constant before approaching $\dot{a}_{max}$ (Broek 1982; Hahn et al. 1973). This increase at higher $\dot{a}$ can be explained by the fact that successively increasing amount of the introduced energy is converted into pure kinetic energy in order to reach $\dot{a}_{max}$. However, in this limiting case no more energy would be available for crack growth, which drives $G_{Id}(\dot{a})$ to infinite.

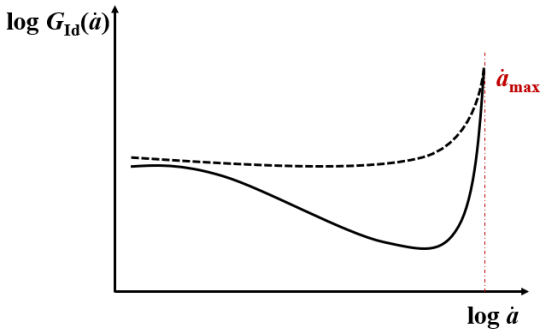


**Fig. 2.6:** Schematic relationship between propagation energy release rate $G_{Id}(\dot{a})$ as a function of propagation speed $\dot{a}$ of a running crack for a rate insensitive material (dashed line) and a rate sensitive material (continuous line) according to Kanninen (1983) and Messiha (unpublished).

### 2.3.2 Fracture Mechanisms- Adiabatic Decohesion

The adiabatic decohesion model developed by Leevers is a theory based on experimental observations and describes what possibly happens during RCP within semi-crystalline thermoplastics. In brief, the decohesion model describes the short-term failure by introducing a melt fracture mechanism based on adiabatic heating effects, which is able to predict the fracture initiation resistance to high speed impact $G_{Ic}(v)$ and the fracture resistance to stable RCP $G_{Id}(\dot{a})$ (Leevers 2004). When a crack propagates rapidly, a large amount of energy is released which is converted into heat (adiabatic conditions). In the case of SCG, where a crack grows slowly, there is enough time for the surrounding bulk material to dissipate the heat from the crack tip, resulting in almost isothermal conditions (Leevers et al. 2000; Leevers 2004). Polymers are very poor heat conductors and therefore comparatively low crack propagation speeds are sufficient to generate adiabatic conditions at the crack tip (Weichert and Schönert 1974). In addition, this poor heat conduction of semi-crystalline polymers causes local melting zones to form due to heat. Referring to Fig. 2.7a, polymer chains from the surrounding bulk material are drawn through a thin active layer into the crack zone. In this active layer the temperatures can locally increase by adiabatic heating up to the melting point of the material. As soon as a chain is pulled through the active layer, it drags new chains from the surrounding bulk material along with it. These processes generate heat, which cannot be removed quickly enough, resulting in an enlargement of a so-called melt zone left behind the active layer. At a certain point where the melt layer thickness reaches a critical value $s_c$ (Fig. 2.7b) the chains become too short, the system becomes mechanically unstable and the cohesive strength collapses. The energy required to separate the fibrils through the melt layer is significantly lower than the energy required to expand the melt zone. For this reason, the separation mechanism can be interpreted as a low-energy disentanglement process of polymer chains promoted by adiabatic heating (Leevers 1995; Leevers 2004; Leevers and Morgan 1995). Further details of this model can be found in the literature: Leevers (1995), Leevers and Morgan (1995), Leevers et al. (2000), Leevers (2004).

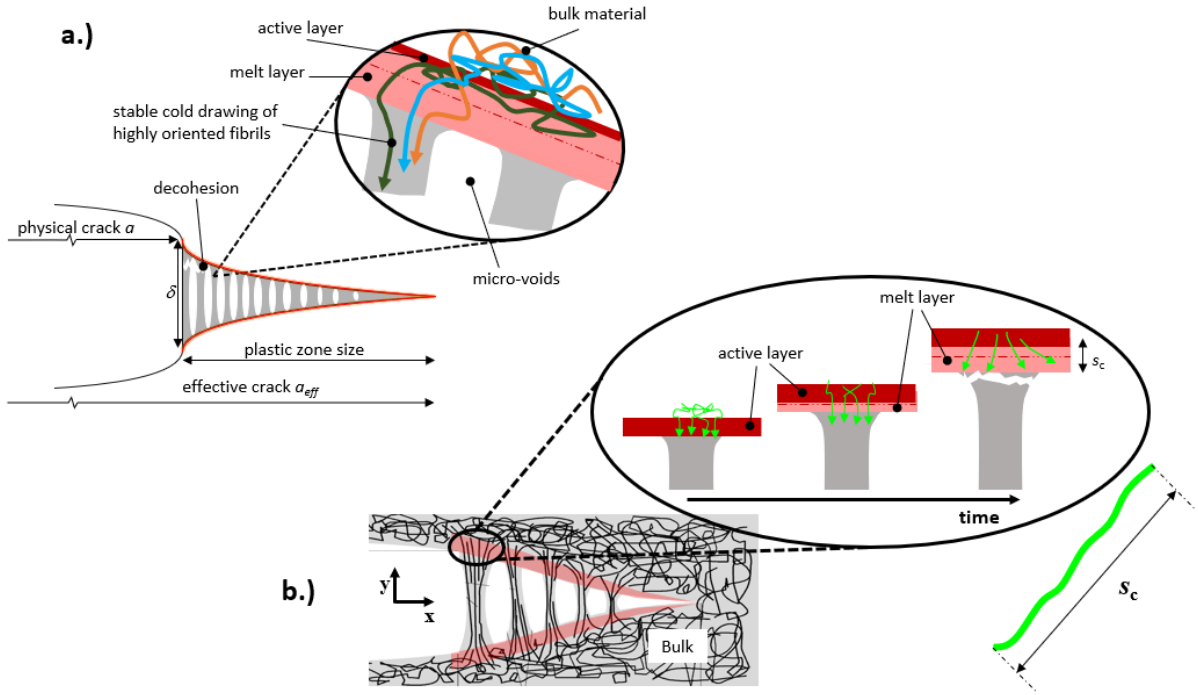


**Fig. 2.7:** Crack-tip craze in a polymer, modelled as a cohesive zone (a); stages of decohesion at a craze-fibril (b) (Hertlin 1999; Leevers 2004; Messiha unpublished).

### 2.3.3 Approaches to assess RCP behavior of plastic pipes

Plastic pipes, which are often used in infrastructural applications to transport gases or fluids, can fail under the conditions of RCP (Zhuang et al. 2014). It is therefore necessary to have knowledge of the resistance to RCP in order to ensure safe installation and operation, especially when new pipe grades are developed. Currently, different analytical and experimental methods are available. Experimental methods include e.g. the FS test, according to ISO 13478 as well as the S4 test, according to ISO 13477. Other experimental methods use fracture mechanics to characterise RCP, such as the High-Speed Double Torsion (HSDT) test or the Essential work of Fracture (EWF) model using deep double edge notched tension test specimens (DDENT) (Argyrakis 2010). Analytical methods, in contrast, include e.g. the Basic Physical RCP Model, which was developed to determine $G$ as a function of $\dot{a}$, as well as the Adiabatic Decohesion Model (Argyrakis 2010; Leevers 1995; Özbek 2008). In the following, however, a technical overview of the most important experimental methods is given. These include the FS and the S4. Finally, a brief overview of the concepts used in this work is given.

***FS- Test***

The FS-test simulates the actual conditions for a pipe in operation according to ISO 13478. This test is designed to determine the critical pressure $p_{c\text{-}FS}$ above which RCP occurs (Brömstrup 2012; Özbek 2008).

In order to simulate real operating conditions, a 25 m long pipe sample with a maximum diameter of 0,5 m is placed about 0,1 m below the surface and covered with gravel. To create constant temperatures (0 °C ± 1,5 °C) cooling water is used which circulates around the pipe (Argyrakis 2010). At both ends of the pipe a steel pipe is fixed to simulate an even longer pipe system. Nitrogen or air is then introduced into the pipe to pressurize the system. Close to one end of the pipe (initiation zone) a crack of about 0,4 m length is inserted through a steel blade and cooled down to approx. -70 °C; inside the pipe an axial notch is added to ensure that the crack propagates at a very high speed (Argyrakis 2010; Özbek 2008). If a propagating crack extends over 90 % of the pipe's total length, valid RCP is given, otherwise the crack is considered as an arrested crack (Özbek 2008).

This test is very time-consuming and expensive. From preparation to data acquisition it approximately takes up to a week. About six tests should be carried out per pipe material in order to obtain accurate results, which increases the factor of time, costs and material input enormously. This finally led to the development of the S4 test (Özbek 2008; Yayla 1991).

***S4 Test***

The S4 test, according to ISO 13477, initiates a fast moving crack in a pipe under internal pressure, which can propagate or arrest depending on the test conditions (Argyrakis 2010). An essential difference to the FS test is the use of significantly shorter pipes of a length about 7 times the pipe diameter. A typical test setup of the S4 test is given in Fig. 2.8. After cooling down to 0 °C the pipe is pressurized with air and sealed at both ends. Near one end the impact of a projectile is applied (10-20 m/s), which drives the fast propagating crack into the pipe. To prevent decompression, baffle plates are positioned at certain distances. They ensure an equal test pressure in the individual chambers before the crack reaches them. Only by maintaining the pressure in front of the crack tip it becomes possible to use

shorter test specimens. The illustrated containment cage, which serves to stabilise the crack propagation above critical conditions, is designed to prevent flaring of the pipe walls when compressed air escapes (Argyrakis 2010; Özbek 2008).

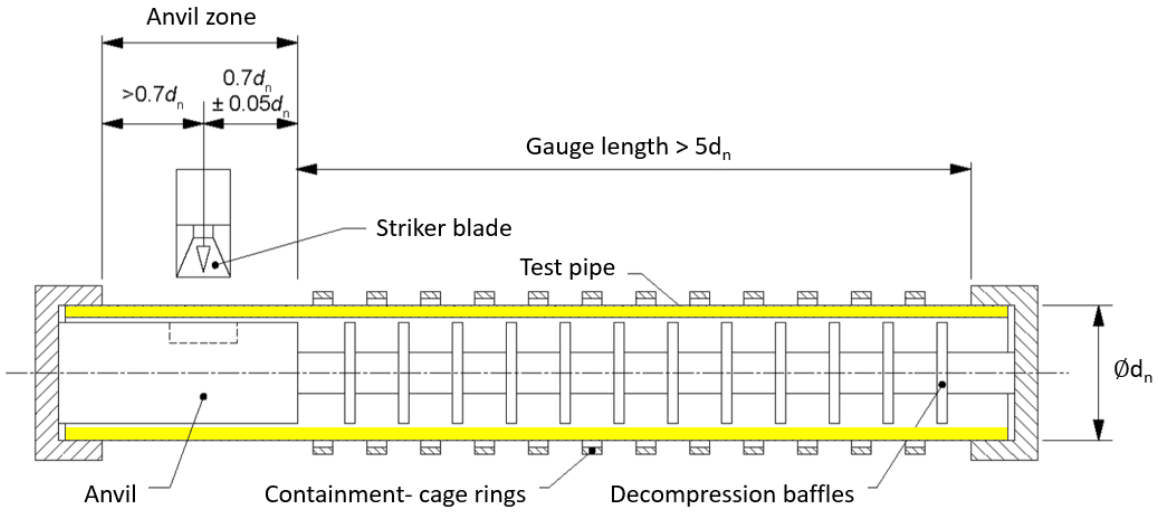


**Fig. 2.8:** Schematic representation of an S4 test setup (Argyrakis 2010).

However, the aim of this test is to determine a critical test pressure ($p_{c\text{-}S4}$) or temperature ($T_{c\text{-}S4}$) under steady state conditions. To determine the critical pressure, the pipe specimens are loaded at different pressures but at constant temperature. The lowest pressure at which a crack propagates is called critical pressure $p_{c\text{-}S4}$. The determination of the critical temperature $T_{c\text{-}S4}$ follows the same scheme, except that in this case the pressure is kept constant and the temperature is varied. The critical temperature is then the temperature below which RCP is able to occur (Argyrakis 2010; Özbek 2008; Yayla 1991). The arrest and propagation regime in terms of temperature and pressure can be taken schematically from Fig. 2.9. If a high enough pressure is selected and the temperature is varied, the critical temperature ($T_{c\text{-}S4,3}$) can be determined. If the same is done for the pressure at a constant low temperature, the critical pressure ($p_{c\text{-}S4,1}$) can be determined. It follows, that a pipe material which is used above its critical S4 temperature or below it's critical S4 pressure is resistant to RCP (Özbek 2008).

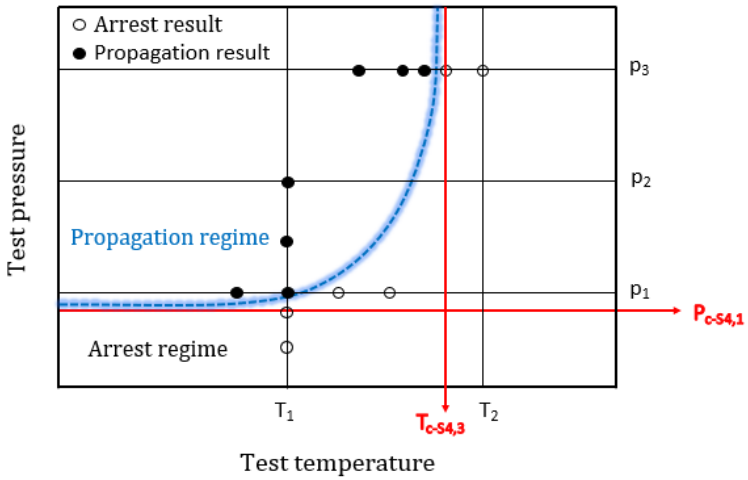


**Fig. 2.9:** Propagation and arrest regime in an S4 test according to Argyrakis (2010).

**Novel Concepts**

All abovementioned methods are very time-consuming and costly, as the FS and S4 tests require extruded pipes for testing, which drives costs up (Özbek 2008). Hence, this thesis is dedicated to the development of accelerated methods on laboratory scale to classify polymeric materials according to their dynamic fracture toughness in terms of mechanical and fracture mechanics approaches on behalf of commonly used specimens for quality assurances. These include, the modification of a standard Charpy impact test ("modified Charpy"), which is based on an already existing test concept. The presentation of a new fracture mechanics test method termed "quasi-dynamic $K_{ID,eq}$" method, and a novel test which was intended to simulate the stress states in a pipe under internal pressure - the "NHI test".

# 3 EXPERIMENTAL

The following experimental chapter is divided in two parts. The first implies an introduction of the selected materials which were investigated to rank them in terms of resistance to RCP. Hereafter, principles of the novel concepts are explained. In each case, the essential basic idea, test setup, used material, specimen preparation, test conditions and evaluation are briefly discussed.

## 3.1 Material selection

A total of five different PA12 materials (see Table 3.1) were investigated, which were all provided by Evonik Operations GmbH, Essen (GER). The materials differ primarily in the use or non-use of special additives, such as an IM or a yellow inorganic PGM. For some materials, both are combined. The first material in the table, PA12-base, is a neat PA12. The other five materials are high viscosity compounds (labelled with "C"), which were developed from PA12-base and other neat PA12 types. The numbers (2 to 5) next to the letter "C" indicate increasing molecular masses ($M_w$). However, it can be noted that the compounds are strongly related to each other so that they form a systematic series. Material C3-nc can be classified as a compound that is non-colored (nc) and without an IM. By adding an IM, C4-im-nc is obtained. Further addition of a yellow PGM (yw) results in C2-im-yw. Material C5-im-yw is basically the same as C2-im-yw, except that it has been intentionally modified to obtain a longer average chain length (Messiha unpublished).

The weight average molecular mass $M_w$ and the number average molecular mass $M_n$ were determined by gel permeation chromatography (GPC). Samples were dissolved with a concentration of 5 g/l in hexaflourisopropanol (HFIP) + 0,05 mol potassium trifluoroacetate at RT. The polydispersity (PD) results from the ratio of $M_w$ to $M_n$. The density ($\rho$) was determined according to DIN EN ISO 1183-1 (immersion method). A complete overview of the data obtained is summarized in Table 3.1. Damping peaks (i.e. glass transition, secondary relaxation region) of the respective pipe grades obtained from dynamic-mechanical analysis (DMA) can be taken from Fig. 3.1. For determination a DMA8000 test equipment from PerkinElmer, Massachusetts (US), was used. Measurements were carried out on tenisle specimens, according to ISO 6721-4 in a

temperature range from -130 °C to 130 °C. The results from the DMA exhibit similar shapes for all investigated materials.

**Table 3.1:** General material characterisation of used PA12 pipe grades. Abbreviations: IM (impact modifier), PGM (inorganic yellow pigment), weight average molecular mass ($M_w$), polydispersity (PD), density (ρ).

| Material | IM | PGM | $M_w$ [g/mol] | PD [-] | ρ [g/cm³] |
|---|---|---|---|---|---|
| **PA12-base** | - | - | 102000 | 1,970 | 1,016 |
| **C2-im-yw** | + | + | 123000 | 1,940 | 1,008 |
| **C3-nc** | - | - | 143000 | 2,290 | 1,015 |
| **C4-im-nc** | + | - | 147000 | 2,220 | 1,007 |
| **C5-im-yw** | + | + | 157000 | 2,380 | 1,009 |

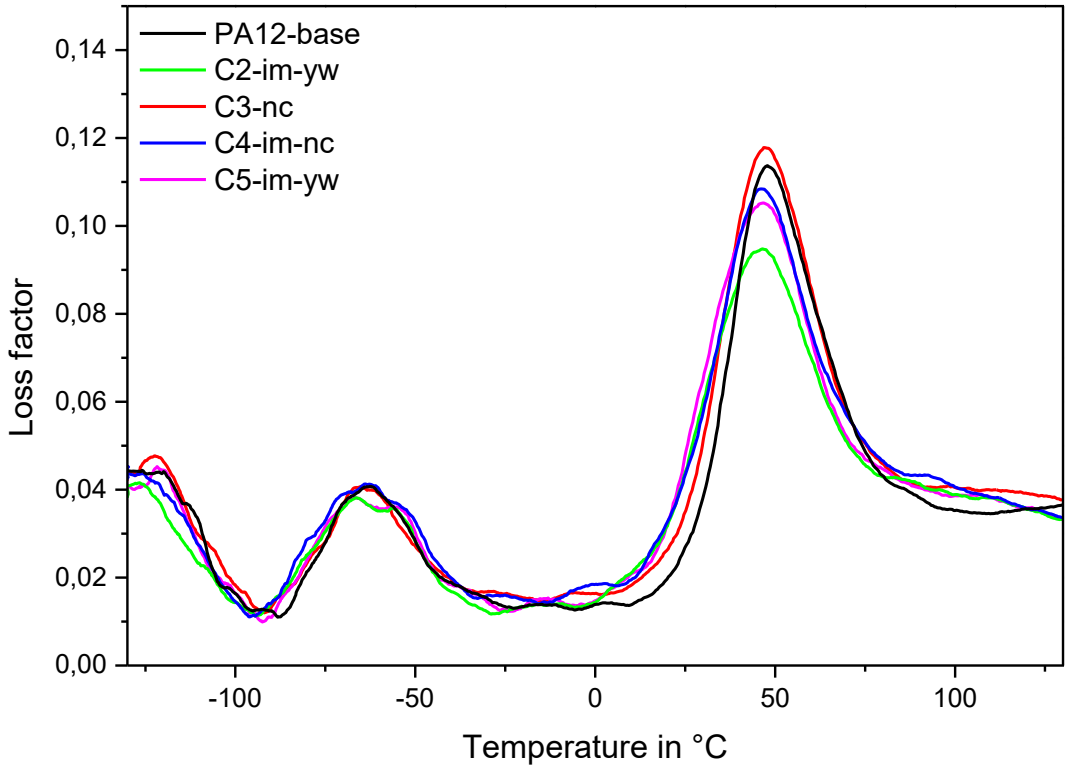


**Fig. 3.1:** Loss factor as a function of temperature in a range of -130 °C to 130 °C for the selected PA12 pipe grades.

## 3.2 Novel Concepts

Three methods are presented in this chapter, the modified Charpy, the NHI test and the quasi-dynamic $K_{ID,eq}$ test (Messiha unpublished). All methods focus on ranking materials in terms of their resistance against RCP as determined via the S4 test.

### 3.2.1 Modified Charpy

In a standard Charpy impact bending test (DIN EN ISO 179), a pendulum impact striker is used to assess the toughness behavior of plastics. Impact energies of 0,5 J to 50 J and impact velocities of 2,9 m/s to 3,8 m/s are normally used for these tests. (Grellmann and Altstädt 2011). The fundamental idea behind the modified Charpy approach is to rank materials by reaching a plateau of ideal brittleness, as it might be the case during RCP. Using a standard Charpy test, limitations of test setups are soon met at impact velocities higher than 4 m/s due to successively increasing dynamic effects (e.g. significant oscillations in load-displacement data, etc.). Yet, RCP is considered to occur at extremely high crack propagation speeds and is often initiated at impact velocities above 10 m/s (Leevers 1995, 1996). Taking into account that these ideally brittle behavior must be strongly linear elastic, the validity of a time-temperature shift can be expected. Instead of increasing the impact velocity which results in an adverse dynamic effect, the temperature is drastically decreased aiming to reach a state of ultimate unchanging brittleness (see Fig. 3.2), while avoiding dynamic effects at low loading rates. Considering three different materials (A, B and C) over a wide temperature range, an absorption of different impact energies can be expected, depending on the material composition. As illustrated, the fracture behavior at high temperatures is ductile and changes to brittle as the temperature decreases, with a sharp transition in between, which is represented as a tough-brittle transition. Ranking of different grades should be done in the brittle region (e.g. at -120 °C), where theoretically a point of ultimate unchanging brittleness is reached. This approach was intended to provide a quick and easy tool to rank materials in terms of their RCP resistance.

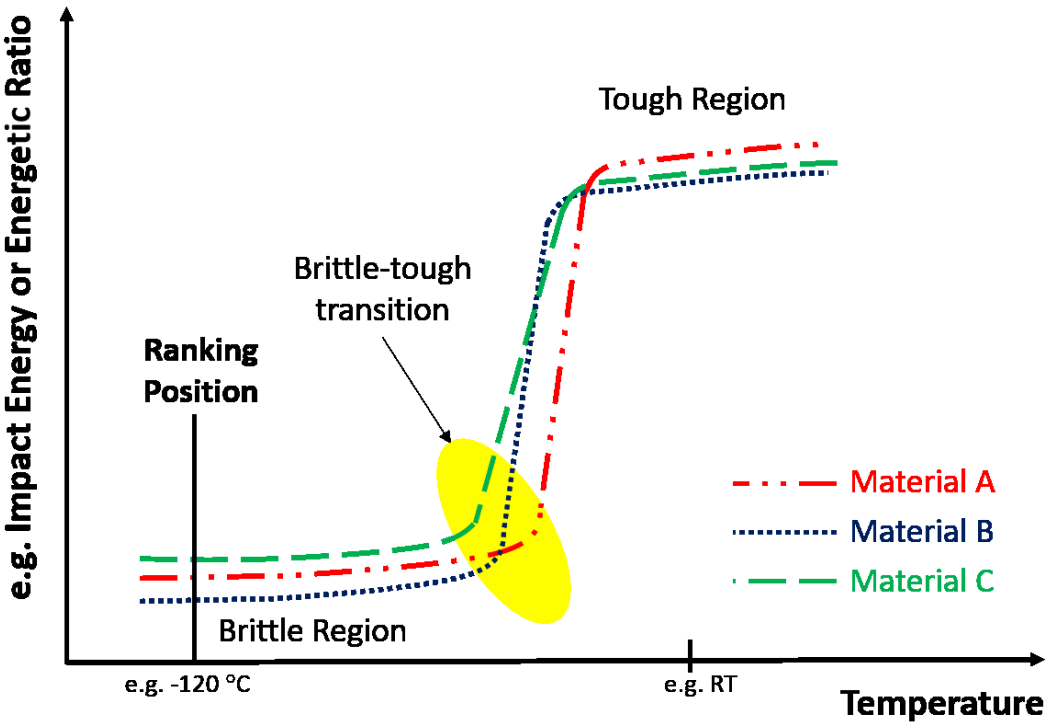


**Fig. 3.2:** Schematic representation showing the basic idea behind the modified Charpy approach.

In order to prove the method, a servo-hydraulic testing machine of the type 331.05S from MTS Systems Corporation, Eden Prairie (US), (see Fig. 3.3), which was equipped with a maximum load cell capacity of 15 kN was used. Temperature was controlled by a temperature chamber BT2A1 from BISCUIT, Saugerties (US). The chamber itself can be heated to a maximum of 300 °C or cooled with nitrogen to a minimum of -130 °C, depending on the desired conditions. A temperature sensor was located in the chamber, which monitored the set conditions during the measurements. For the modified Charpy test, a three-point bending arrangement was set up in the chamber on which the specimens were placed. The support distance was set at 62 mm in accordance with the standard DIN EN ISO 179-1. A fin, which was connected to the moving piston of the machine, provided the impact load. The fin had a radius of 3 mm and the supports a radius of 1 mm. To characterize the specimens after testing, a light microscope SZX-ILLB2-200 from the Company Olympus Corporation, Tokyo (J), was used to measure the fractured ligament area ($A_n$) of the specimens. Standard "V" notched Charpy specimens according to DIN EN ISO 179/1eA that were cut out from injection-moulded multi-purpose test specimens were used, which were provided by Evonik Operations GmbH. A schematic

representation of the test specimen dimensions is shown in Fig. 3.4. The impact speed was set to 100 mm/s and measurements were carried out at eleven different temperatures: -120/ -100/ -80/ -60/ -45/ -30/ -15/ 0/ 24/ 40/ 60 °C. Three samples per material and temperature were used for statistical validation. For this method, all PA12 grades were selected (shown in Table 3.1).

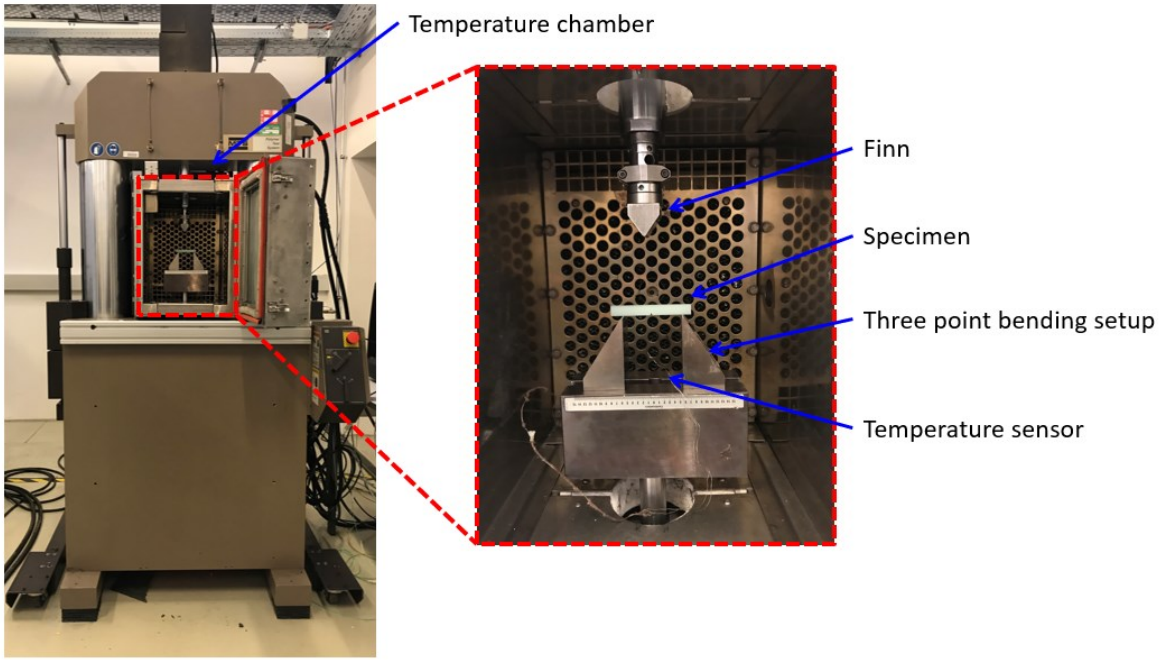


**Fig. 3.3:** Machine 331.05S from MTS Systems Corporation with temperature chamber BT2A1 from BISCUIT (left); test arrangement for the modified Charpy test (right).

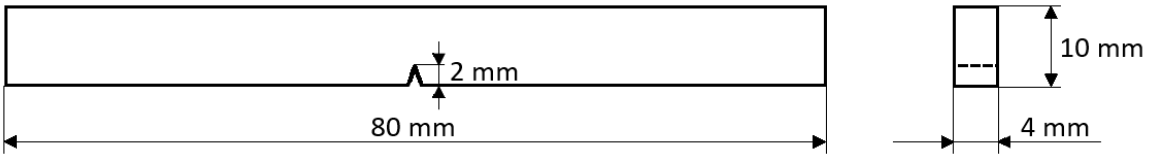


**Fig. 3.4:** Charpy test specimen dimensions according to DIN EN ISO 179-1.

The raw data obtained was evaluated using Python (Python Software Foundation, US) (Python evaluation file can be found in the appendix) (Messiha unpublished). For this purpose, the areas ($A_{tot}$, $A_{max}$, $A_{prop}$) under the recorded load-displacement curves were determined (see Fig. 3.5), which were divided by $A_n$ of the specimen afterwards. The obtained specific energy components $U_{tot}$ (=$A_{tot}/A_n$), $U_{max}$ (=$A_{max}/A_n$), $U_{prop}$ (=$A_{prop}/A_n$) as well as the energetic ratios $U_{max}/U_{tot}$, $U_{prop}/U_{tot}$ are set against the temperature. The energy $U_{tot}$ corresponds to the total energy absorbed during the test and consists of an energetic fraction used for crack initiation $U_{max}$ as well as for crack propagation $U_{prop}$ (Grellmann and

Altstädt 2011; Martinez et al. 2009). The energetic ratios should provide information about the amount of energy required to initiate ($U_{max}/U_{tot}$) or propagate ($U_{prop}/U_{tot}$) a crack in relation to the total energy.

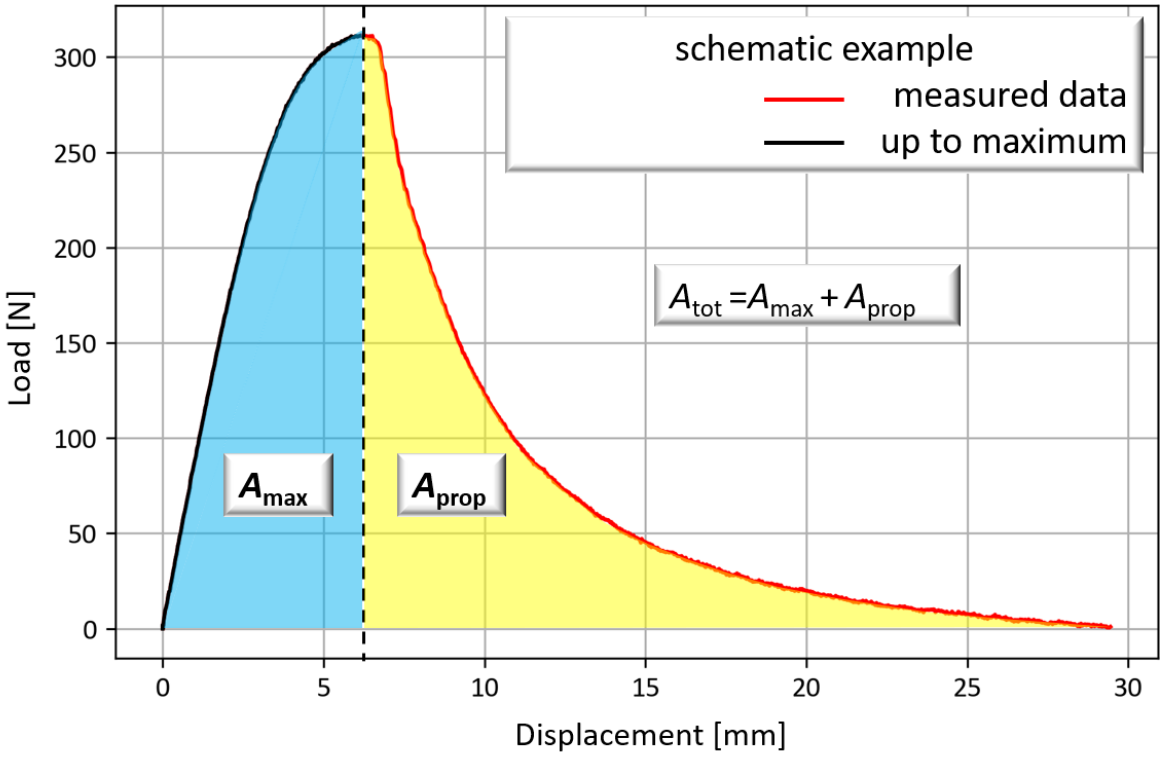


**Fig. 3.5:** Typical load-displacement curve of a modified Charpy test; $A_{tot}$ is the total energy, $A_{max}$ is initiation energy and $A_{prop}$ is the crack propagation energy.

### 3.2.2 Notched Hoop-stressed Impact (NHI) Test

In order to characterise the resistance to RCP, two methods established in practice (FS test and S4 test) have already been explained in the background. With the NHI test, a low-cost, quick RCP ranking tool is now being evaluated. A pipe (Fig. 3.6) of length *L,* external diameter $D_{out}$ and thickness *t* under internal pressure $p_{int}$ can be characterized by three acting main stresses: a tangential- or hoop-stress $\sigma_{hoop}$ (red), an axial-stress $\sigma_{ax}$ (blue) and a radial-stress $\sigma_r$ (green). These stresses can be determined using Barlow´s equations (Eq. 3.1-3.2) which can be applied when dealing with rotationally symmetrical and thin-walled geometries (e.g. pipes under internal pressure, gas containers) (Läpple 2016):

$$\sigma_{hoop} = p_{int} \cdot \frac{D_{out} - t}{2t} \tag{3.1}$$

$$\sigma_{ax} = p_{int} \cdot \frac{D_{out} - t}{4t} \tag{3.2}$$

As the radial-stress is $\sigma_r = -p_{int}$ at the inner wall of the pipe as well as $\sigma_r \approx 0$ (unloaded surface) at the outer wall, $\sigma_r$ becomes negligible compared to $\sigma_{ax}$ which itself equals 0,5 $\sigma_{hoop}$.

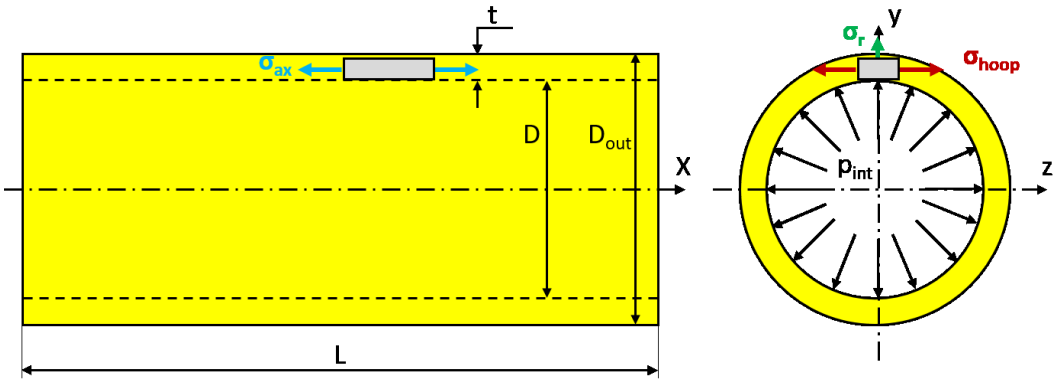


**Fig. 3.6:** Stress conditions of a pipe under internal pressure with the length *L*, internal diameter *D*, external diameter $D_{out}$, pipe wall thickness *t* and the stresses occurring in the pipe wall: $\sigma_{hoop}$ (hoop-stress), $\sigma_{ax}$ (axial-stress) and $\sigma_r$ (radial-stress) (Messiha unpublished).

When a striker hits a pressurized pipe during S4 testing, the crack opens up perpendicular to the pipe axis. Hence, the basic intention of the NHI test is to imitate this highest acting crack driving force $\sigma_{hoop}$ as it exists in the S4 test. Instead of using complete pipe sections, simple or modified specimen geometries of e.g. Charpy or Single-Edge-Notched Bend (SENB) specimens were used. This basic concept is illustrated in Fig. 3.7. In the S4 test, it is generally possible to vary the stresses (variable via $p_{int}$), the temperature *T* and also the loading speed *v* and thereby the crack propagation speed. Exactly the same parameters can be varied as desired in the NHI test by means of a special setup, whereby the highest stresses can be realised by a tensile stress perpendicular to the notch. Thus, it is possible to simulate different stress states and to influence the fracture behavior, from brittle to ductile.

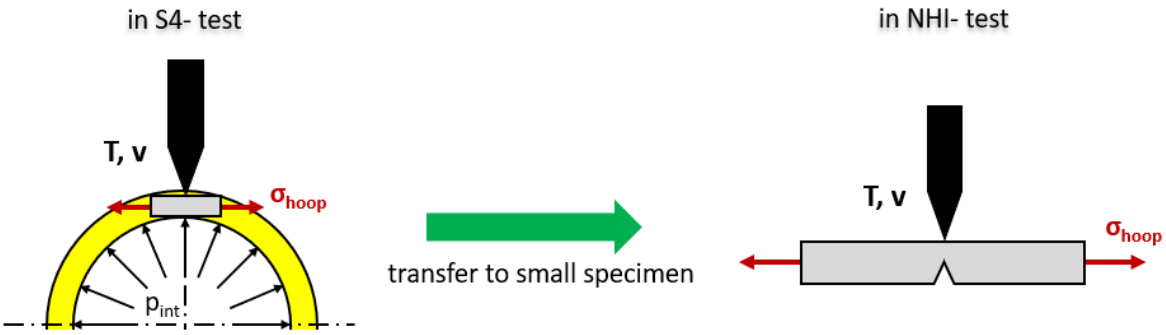


**Fig. 3.7:** Basic idea behind the NHI test; stress conditions in the pipe are transferred to a small test specimen (Messiha unpublished).

It can be expected that due to the similarities in the local loading conditions during the impact of the specimen, a correlation of the material response in the NHI test with the reference data of the S4 Test is possible. To achieve the aforementioned test conditions, the so-called "Hoop-Stress Device", which was recently developed in an on-going project (see Fig. 3.8, Messiha (unpublished)), was installed in a drop tower CEAST 9350 from INSTRON, Darmstadt (GER). The fin of the drop tower was equipped with a load cell of 45 kN. In addition, the Hoop-Stress Device as well as the specimens can be cooled (lower limit: -70 °C) or heated (upper limit: 150 °C) via an integrated temperature chamber. The Hoop-Stress Device itself works as follows: A specimen (1) is supported at both ends via a fixture (2), where it is free to move up and down (vertical). The fixtures are inserts which can be exchanged at any time to accommodate variable test specimen thicknesses. They are hinged (3) to the clamping jaws (4) of the construction so that the specimen can freely rotate and bend during testing without additional constraints compared to a standard three-point-bending setup. The fixtures are further connected to elastic bands (5) on the upper movable carriage (6), so that broken specimen halves can be pulled back easily. The carriage is able to move along a linear guide (7). The supports (8) used for NHI testing can be fixed at different location with the aid of slotted grooves (9) allowing for a certain range of distance between both supports, which are also adjustable for height variations. This is important in some applications, as for example SENB and Charpy test specimens do not have the same height. Via a thread and a nut (10), an open-end spanner can be used to apply a desired axial force to the test specimen, which is detected via a load cell (11). The load cell of 1 kN is manufactured by Lorenz Messtechnik GmbH, Alfdorf (GER). On the other

side of the Hoop-Stress Device, the carriage is fixed via nuts (12) to ensure the application of a chosen pre-stress on the selected specimen.

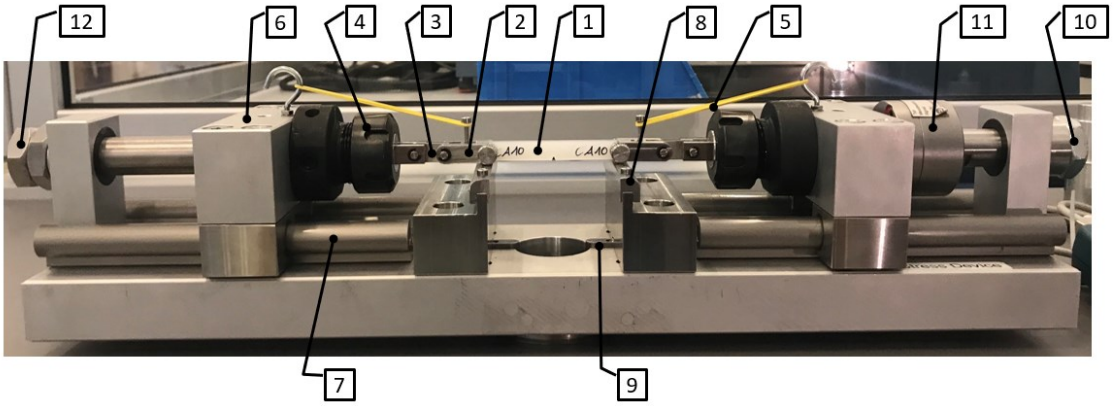


**Fig. 3.8:** Hoop-Stress Device (specimen [1], clamping [2], hinge [3], fixture for clamping [4], elastic bands [5], moveable blocks [6], linear guidance [7], supports [8], parallel key [9], force application [10], load cell [11], axial fixing [12]).

In order to prove the feasibility of testing different PA12 grades with regard to their RCP resistance, two main approaches (A1 & A2) were applied in this study, which differ essentially from each other in the defined failure criterion, specimen production, preparation as well as in the evaluation.

### 3.2.2.1 Approach 1 (A1)

The failure criterion in A1 is termed Break Through (BT) and is basically applicable for simpler testing machines without specialized sensors for instrumentation. The principle behind this failure criterion is to vary the stress in the cross-section of the specimen via the Hoop-Stress Device at different temperatures until the specimen breaks through (Fig. 3.9). However, the kind of fracture is not considered further – it does not matter if it is a brittle or ductile failure. Reason therefore is given from a practical observation generally made during S4 tests of different polymers, particularly PE-HD, where the crack path shows different regions of highly brittle, as well as highly ductile areas (Argyrakis 2010). With the measured stress in the cross-section, the equivalent internal pipe pressure $p_{eq}$ can be calculated with the aid of Barlow´s equations. By varying the applied pressure and temperature conditions, a failure curve $p_{eq}(T)$ similar to that observed by an S4 test can be drawn. Finally, the NHI results can be compared to the reference S4 test data in order to

determine a possible correlation, probably allowing for a reliable prediction of critical pressure and temperature values.

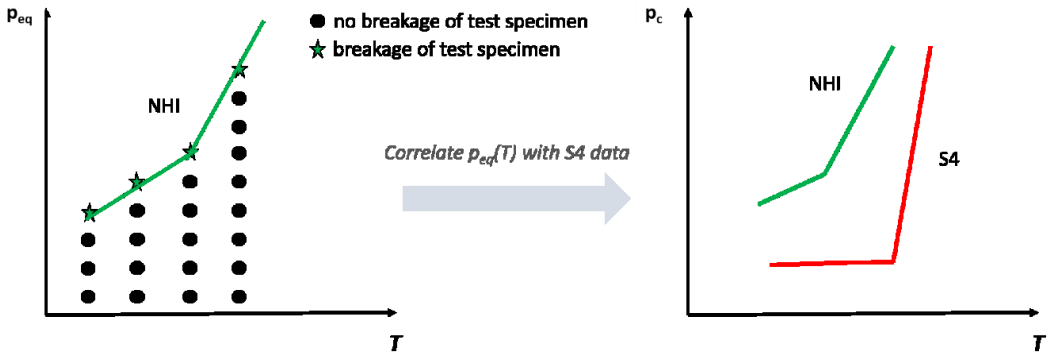


**Fig. 3.9:** Principle of the break-through criterion.

For the implementation of A1, standard Charpy specimens with "V" notch according to DIN EN ISO 179 were used which were milled out of an extruded pipe. The specimens, which were provided by Evonik Operations GmbH, were drilled at both ends (drill hole diameter of 4 mm) for an appropriate mounting within the Hoop-Stress Device. A schematic representation of the test specimens is given in Fig. 3.10. A loading speed of 1 m/s was selected, which corresponds to an energy input of 2,93 J. At higher rates, strong dynamic effects occur that make evaluation highly inaccurate. Different temperatures and tensile loads $F_{hoop}$ (via the Hoop-Stress Device) were applied for individual pipe grades, depending on the material and whether a specimen breaks or or not. Temperatures ranged from 23 °C to 50 °C and $F_{hoop}$ from 0 N to a maximum of 500 N. Three specimens were used per $F_{hoop}$ and temperature level. All selected materials were tested by using this approach (see Table 3.1).

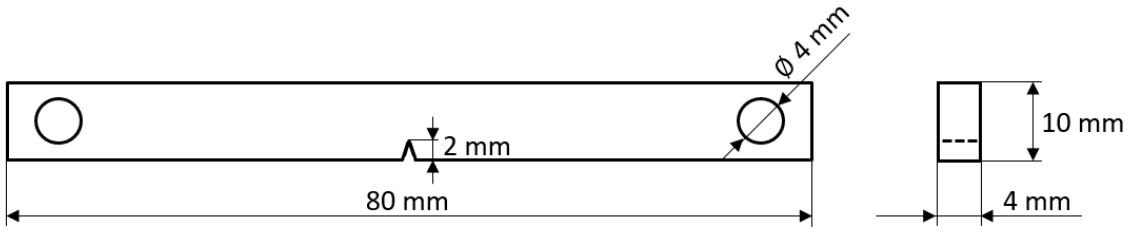


**Fig. 3.10:** Charpy test specimen dimensions with additional drill holes for mounting in Hoop-Stress Device.

Evaluation of A1 was done by using the applied $F_{hoop}$ and the measured $A_n$. The stress in the critical cross-section can be calculated in this way by Eq. 3.3 (Böge and Böge 2019):

$$\sigma_{hoop} = \frac{F_{hoop}}{A_n}. \tag{3.3}$$

A transformation to an equivalent internal pipe pressure $p_{eq}$ is given by Eq. 3.4:

$$p_{eq} = \frac{\sigma_{hoop} \cdot 2t}{(D_{out} - t)} \tag{3.4}$$

To evaluate the internal pressure, a wall thickness of 10 mm and an external diameter of 110 mm were used. This corresponds to the pipe dimensions on which S4 testing has been carried out. By varying $F_{hoop}$ or the equivalent $p_{eq}$ and temperature conditions, a failure curve $p_{eq}(T)$ similar to that observed by an S4 test were determined.

### 3.2.2.2 Approach 2 (A2)

The failure criterion in A2 involved the determination of the Brittle-Tough Transition (BTT) and is applicable for testing machines with specialized sensors for instrumentation. Polymers often exhibit a sharp and abrupt transition from brittle to ductile failure behavior. This behavior can be strongly influenced by the temperature, the loading speed, the specimen geometry as well as by the presence of hydrostatic pressure. (Argyrakis 2010; Özbek 2008). Analogous to the BT criterion of approach A1, a failure curve $p_{eq}(T)$ is to be determined by varying acting equivalent pressures and temperatures (see Fig. 3.11). In contrast to BT, the BTT criterion considers the nature of different failure behaviors. By a precise evaluation of measured load-displacement curves as well as the fracture surface of each specimen, a clear distinction between brittle and non-brittle (i.e. ductile, semi-ductile, semi-brittle, etc.) fractures is possible. Again, NHI results will be used for comparison to RCP resistances determined by S4 testing.

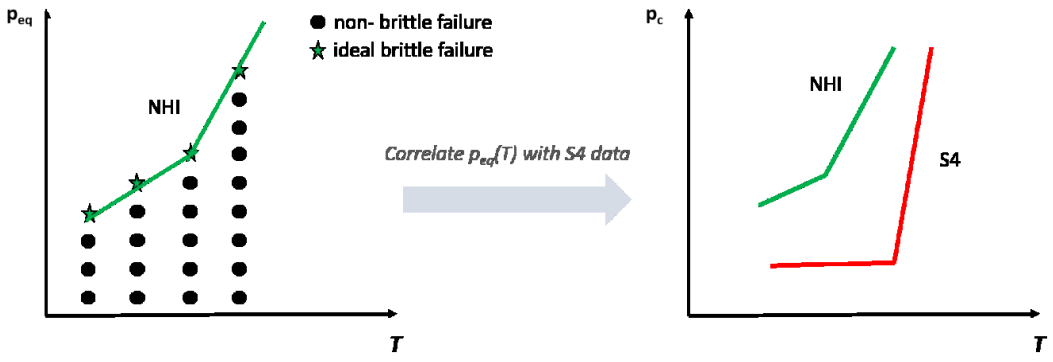


**Fig. 3.11:** Principle of the brittle-tough transition criterion.

For the implementation of A2, standard Charpy specimens with "V" notch according to DIN EN ISO 179 were used which were taken from an injection-molded multi-purpose specimen. These specimens also had to be drilled at both ends, as in A1. In addition, side groove of 0,5 mm depth as well as an additional razor blade notch of 0,2 mm was introduced to provoke brittle fractures. The side grooves were machined with a saw DIADISC 5200 from Mutronic GmbH & Co KG, Rieden bei Füssen (GER), razor blade notches were introduced via a microtome RM 2255 from Leica, Nussloch (GER). A schematic representation of the test specimens is given in Fig. 3.12. Due to dynamic effects, a loading speed of 1 m/s was chosen, like in A1. Tensile load $F_{hoop}$ was chosen to be 0 N, 350 N and 700 N. The specimens were tested at temperatures of 23/ 0/ -20/ -40/ -70 °C. All selected materials were tested by using this approach (see Table 3.1).

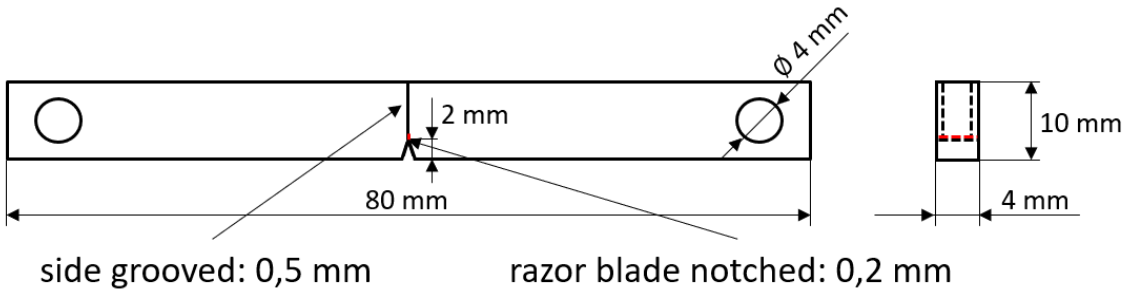


**Fig. 3.12:** Charpy test specimen dimensions with additional drill holes for mounting in Hoop-Stress Device, side grooves and razor blade notch.

For better understanding of the evaluation according to A2, the individual steps are schematically shown for three different Materials (A, B & C) in Fig. 3.13. The raw data obtained is evaluated using Python (Python Software Foundation, US; evaluation file can be found in the appendix (Messiha unpublished)). For this purpose, the areas ($A_{tot}$, $A_{max}$, $A_{prop}$) under the recorded load-displacement curves were determined, which were divided by $A_n$ afterwards to obtain the specific energy components $U_{tot}$, $U_{max}$ and $U_{prop}$ (Step 1). Applied $F_{hoop}$ and the measured $A_n$, were used to calculated the stress in the critical cross-section. The resulting $\sigma_{hoop}$ is then substituted into the transformed Barlow´s equation to obtain an equivalent internal pipe pressure $p_{eq}$ (Step 2). After determining $U_{prop}$ and $p_{eq}$ for all pipe grades, they are plotted together in a $U_{prop}(p_{eq})$ diagram (note that the graph is shown for one temperature). The data points are extrapolated afterwards, if necessary, to determine the pressure at which a theoretical “ideal” brittle failure occurs

(marked with a star) (Step 3). The pressures obtained are plotted over several temperatures, which should result in a ranking of the materials that correlates with the ranking from S4 Test (Step 4).

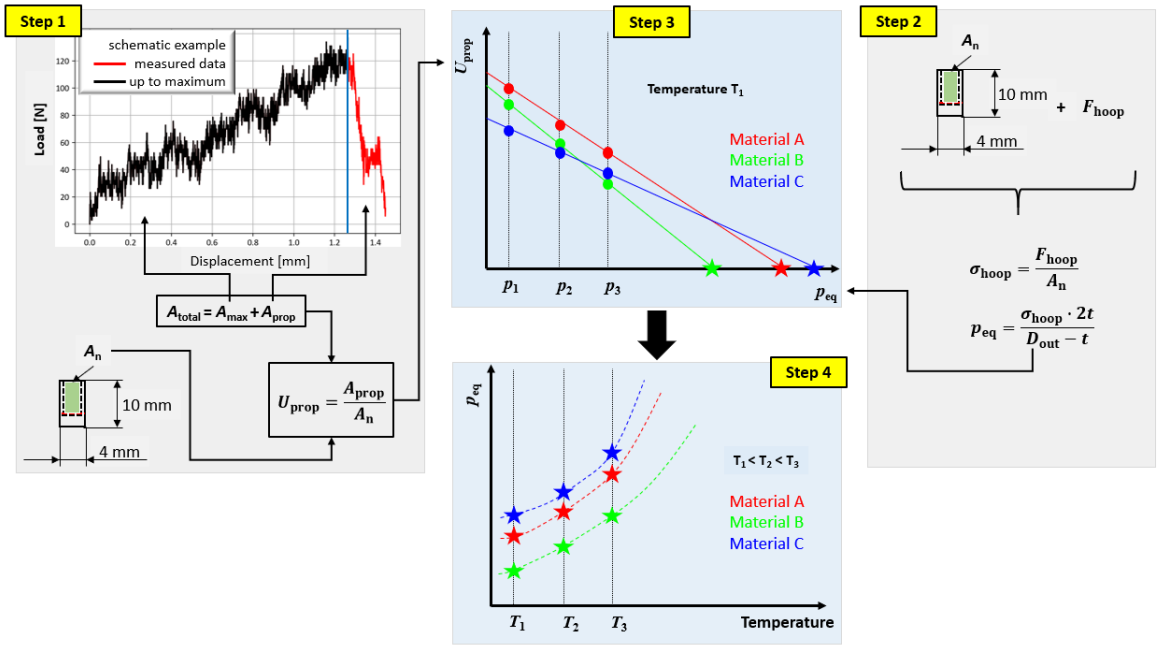


**Fig. 3.13:** Individual steps for the data evaluation according to A2.

### 3.2.3 Quasi- Dynamic $K_{ID,eq}$

Polymers exhibit strong time and temperature dependence in their behavior, which is due to pronounced molecular movement and rearrangement processes. These processes run faster at elevated temperatures, which leads to a shift of the relaxation and retardation spectra to shorter times (Pilz 2014; Retting 1969, 1973). However, it must be noted that only the speed of rearrangements (and not the number and type of rearrangements) is allowed to change with increasing temperature, so that the shape of these spectra and thus the shape of a polymer's viscoelastic characteristic remains unchanged. This behavior is well-known as time-temperature equivalence (see Fig. 3.14) (Grellmann and Altstädt 2011). If the characteristics of a viscoelastic parameter (e.g. E(t)) is known at different temperatures ($T_0$, $T_1$, $T_2$, $T_3$) within a certain time interval (measurement range), the individual curves can be brought into coincidence by a horizontal shift, known as master curve. Thereby, log($a_T$) describes the temperature dependent shift function. In many cases this can be described in the form of an Arrhenius approach, or in the region of $T_g$ with the

aid of the Williams-Landel-Ferry (WLF) equation (Grellmann and Altstädt 2011; Pilz 2001, 2014).

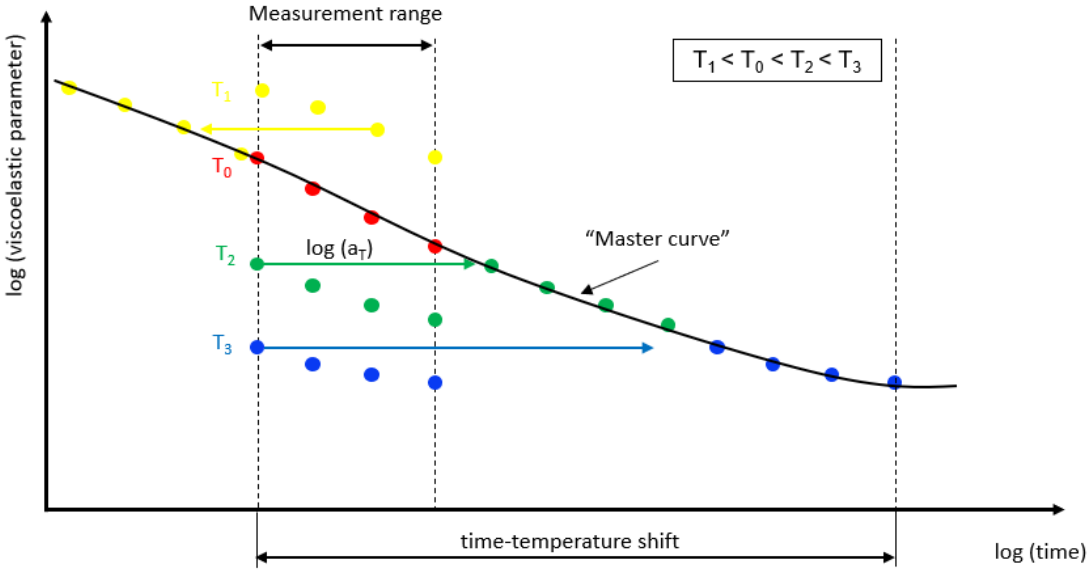


**Fig. 3.14:** Schematic master curve construction by using the time-temperature shift principle (according to Pilz (2001) and Grellmann and Altstädt (2011)).

However, this principle can only be applied if the measurements were carried out in the linear viscoelastic range of a material, where the characteristic functions only depend on time and temperature but not on the loading level. A good overview of this principle can be found in the work of Moser (2013), Pilz (2001) and Grellmann and Altstädt (2011).

Almost in the same way, a time and temperature shift can be applied in the quasi-dynamic $K_{ID,eq}$ test using the quasi-static $K_{IC}$ value, determined at different temperatures as well as different loading speeds (Fig. 3.15). The fracture toughness parameter depends on the geometry of the component and the crack as well as on the external loading situation. Thus, it is possible to influence the $K_{IC}$ value with temperature and loading speed. With increasing loading speed ($v_1$ to $v_2$) or decreasing temperature ($T_1$ to $T_3$), the $K_{IC}$ value is expected to decrease (Anderson 2005b). However, at extremely low temperatures it should be theoretically possible to reach a state of ideal brittleness (nearly no molecular movement), where increasing loading rates do not affect $K_{IC}$ values significantly (compare slope of $T_1$ to $T_3$). Based on the principle of time-temperature equivalence, measured data points may be horizontally shifted to generate a master curve, where a critical $K_{ID,eq}$ value marks the onset of an ideally brittle plateau. This $K_{ID,eq}$ value is termed quasi-dynamic, as it is only measured

under quasi-static load conditions, yet, under very low temperatures allowing for an extrapolation to theoretically very high loading rates, where dynamic fracture conditions might be equivalently preserved.

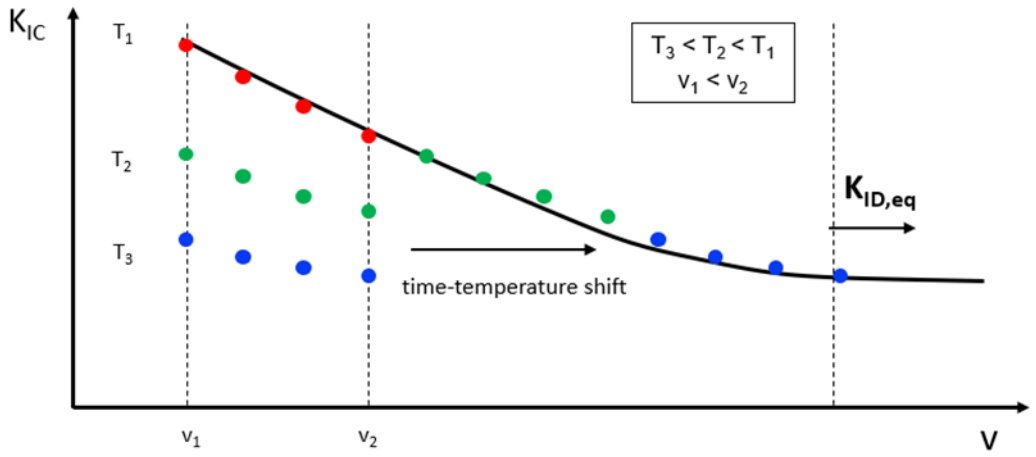


**Fig. 3.15:** Schematic representation of the time-temperature-shift principle used on the $K_{IC}$ to determine the $K_{ID,eq}$ (Messiha unpublished).

For the present thesis, the tests were performed on the same servo-hydraulic testing machine 331.05S from MTS Systems Corporation, Eden Prairie (US), as for the modified Charpy test (Fig. 3.16). To conduct tests at different temperatures, a chamber BT2A1 from BISCUIT, Saugerties (US), was used, whereby the temperature sensor ensures constant conditions in the chamber. To achieve the desired low-temperatures, the chamber was tempered with nitrogen. Test specimens were held at both ends by the clamping devices (screw connection). In addition, a pre-accelerator was used to ensure constant speeds during loading on the specimen. After testing, the fracture surfaces of the specimens were analyzed with a light microscope of the type SZX-ILLB2-200 (Olympus Corporation, Tokyo (J)). Cracked Round Bar (CRB) specimens (Fig. 3.17) were used to verify the test, which were milled out on a CNC machine from solid extruded bars (length: 1000 mm; diameter: 25 mm). The specimens were manufactured to a length of 100 mm and a diameter of 13,8 mm. For fixing the specimens in the servo-hydraulic machine they were provided with a M14 x 1.25 fine thread at both ends. Finally, a razor blade was used to introduce a circumferential notch on a lathe, model K-11A developed by Josef Klippfeld GmbH, Guntramsdorf (A). Notching was carried out at a low rate until the notch depth of 3 mm was reached. Overall, three of the five selected PA 12 grades were tested: C2-im-yw, C3-nc,

C4-im-nc (see also Table 3.1). The tests were carried out at speeds of 10 mm/min, 1000 mm/min and 10 000 mm/min at temperatures of 0/ -30/ -60/ -80/ -100/ -120 °C for the materials C2-im-yw and C4-im-nc. Additionally, C3-nc was measured at the same temperatures, but only at 10 mm/min. For conditioning, the specimens were tempered for about two hours before the test. Three specimens were tested per speed and temperature, for statistical verification.

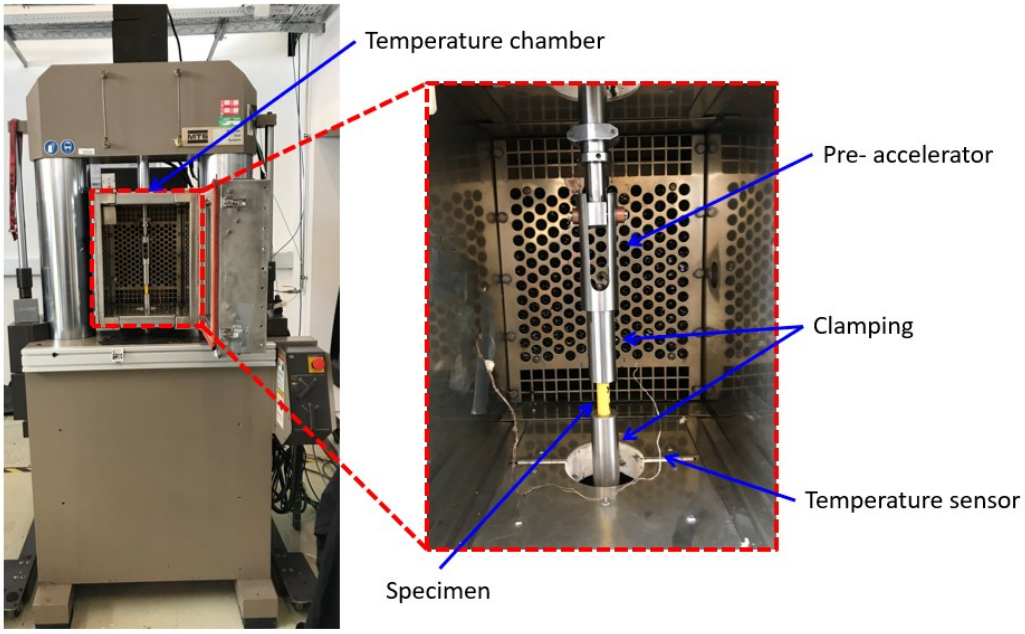


**Fig. 3.16:** left: Machine 331.05S from MTS Systems Corporation with temperature chamber BT2A1 from BISCUIT; right: Test arrangement for quasi dynamic $K_{ID}$ test.

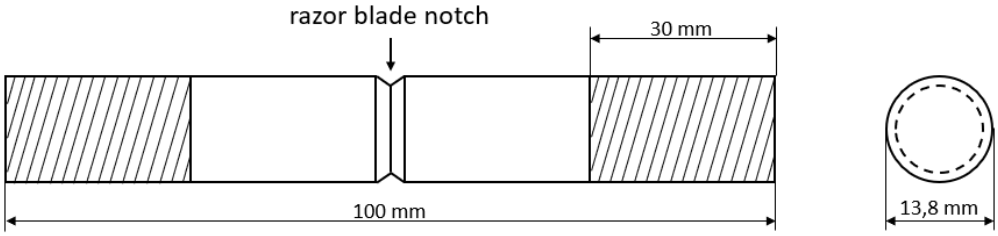


**Fig. 3.17:** Dimensions of the CRB test specimen (schematic representation).

Data evaluation was performed via Python (Python Software Foundation, USA). For this purpose, the formulas of Benthem and Koiter (Eq. 3.5 and Eq. 3.6), which were developed for CRB specimens to determine $K_{IC}$ (Scibetta et al. 2000), were programmed in Python:

$$K_{Ic} = G\left(\frac{b}{R}\right)\frac{P}{\pi b^2}\sqrt{\frac{\pi a b}{R}} \tag{3.5}$$

with:

$$G\left(\frac{b}{R}\right) = \frac{1}{2}\left[1 + \frac{1}{2}\frac{b}{R} + \frac{3}{8}\left(\frac{b}{R}\right)^2 - 0{,}363\left(\frac{b}{R}\right)^3 + 0{,}731\left(\frac{b}{R}\right)^4\right] \quad (3.6)$$

where *b* is the radius of the remaining ligament, *R* the bar radius, *P* the tensile load, *a* the crack length and *G* the gauge length. The following conditions must be fulfilled for a valid evaluation (Eq. 3.7 and Eq. 3.8) (Scibetta et al. 2000):

$$0{,}4 < \frac{a}{R} < 0{,}6 \quad (3.7)$$

and:

$$a, b \geq 0{,}375\left(\frac{K_{Ic}}{\sigma_Y}\right)^2 \quad (3.8)$$

where $\sigma_Y$ is the yield stress of the material.

The energetic counterpart of $K_{IC}$, $G_{IC}$ was also evaluated using Python, which includes the area below the load-displacement curve (= energy) and the fracture area (Anderson 2005b; Grellmann and Altstädt 2011; Kolednik 2012). The complete Python file (Messiha unpublished) can be found in the appendix. In addition to the essential equations, the raw data from the measurements and the dimensions of the real notch depths obtained from the light microscope were fed into the Python file. The results were then processed using Origin (OriginLab Corporation, USA).

# 4 RESULTS AND DISCUSSION

This chapter is divided into four parts. First, the S4 test results of the investigated PA12 pipe grades are presented and discussed. This leads to a ranking of the materials which will be used as reference for the evaluation of the corresponding ranking ability of the new concepts in terms of RCP. Results of the modified Charpy test form the second part of this chapter. Subsequently, results of the NHI test are presented and discussed in detail, which were divided into two approaches A1 and A2 as discussed in section 3.2.2. The final part discusses the outcome of the quasi-dynamic $K_{ID,eq}$ test.

## 4.1 S4 Test Results

The selected PA12 pipe grades were first characterized with regard to their RCP resistance in a S4 Test. These tests were conducted on behalf of Evonik Operations GmbH at SKZ-German Plastics Center, Würzburg (GER), according to ISO 13477. Extruded pipe segments with an outer diameter $D$ of 110 mm, a wall thickness $t$ of 10 mm and a length $L$ of 835 mm were used. Critical pressures were determined on these segments using a pressure range of 1,5 bar to 12 bar and a temperature range of 0 °C and 45 °C with impact speeds of approximately 16 m/s. A valid RCP occurs as soon as the crack moves a distance of at least 4,7$D$. If the crack stops before the minimum length is reached, it is indicated as an arrest. Critical pressure (at 0 °C) and temperature (at 12 bar) results obtained from the S4 test for the individual materials are presented in Fig. 4.1. Obviously, PA12-base and C2-im-yw shows the lowest RCP resistance in the S4 test (Fig. 4.1a). This is evident from the fact that RCP already occurs at relatively low applied pressures at the given temperature. The compound C3-nc, in contrast, shows the highest resistance to RCP in the S4 test, where RCP occurs at very high pressures compared to the remaining pipe grades. Adding an IM to C3-nc systematically results in C4-im-nc. The results demonstrate that in the S4 test an IM leads to lower critical $p_{c\text{-}S4}$ (=4,08 bar) values. By adding a PGM to C4-im-nc, C2-im-yw is obtained and values of $p_{c\text{-}S4}$ (=3,15 bar) decrease again. The last compound C5-im-yw, which equals C2-im-yw with a significantly higher $M_w$, achieves $p_{c\text{-}S4}$ values of 4,41 bar. A further remarkable feature of the values obtained is that the materials can be clustered into different classes. In the first class is the reference of the neat PA12-base and C2-im-yw

materials, with lowest RCP resistances in the S4 test. The second class consists of compounds that contain an IM (C4-im-nc as well as C5-im-yw), which can be further divided in pigmented (C5-im-yw) and not pigmented (C4-im-nc). The third class includes the compounded C3-nc material without further additivation, which shows clear improvements in the RCP resistance in comparison to PA12-base. Based on the critical $T_{c\text{-}S4}$ values (Fig. 4.1b), the resistance of the pipe grades to RCP varies slightly. Obviously, C4-im-nc shows the highest RCP resistance, followed by C5-im-yw, C2-im-yw, C3-nc and PA12-base.

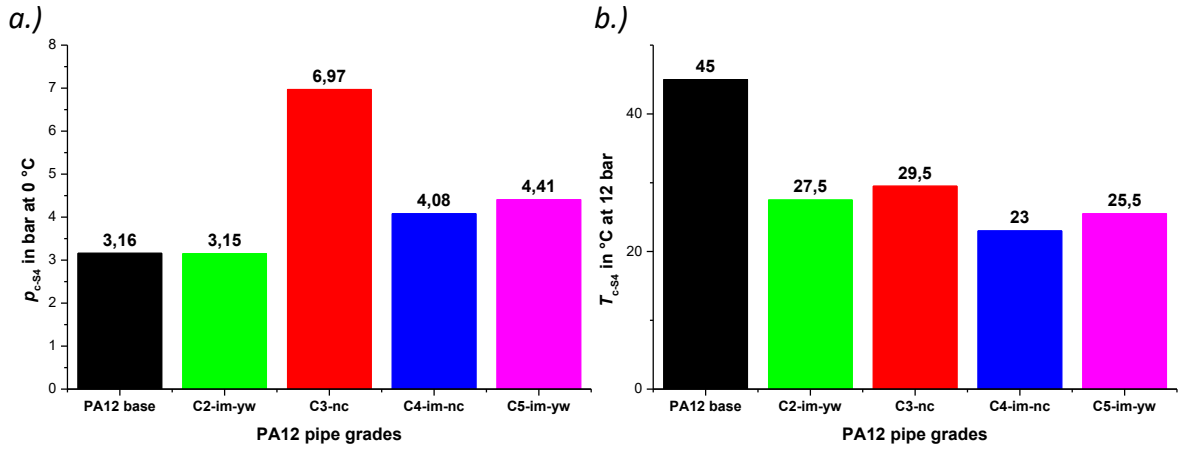


**Fig. 4.1:** Obtained critical pressure values $p_{c\text{-}S4}$ at a temperature of 0 °C (a.) and critical temperature values $T_{c\text{-}S4}$ at a pressure of 12 bar (b.) for the selected PA12 pipe grades.

A possible explanation why compounds containing an IM perform worse (related to $p_{c\text{-}S4}$ in Fig. 4.1a) than those without can be attributed to the strain rate dependence of the IM. It is widely known that polymers behave more brittle with increasing loading rates (Bonten 2016; Grellmann and Altstädt 2011; Pinter 2019). Impact modifiers are also polymers which become increasingly brittle with decreasing temperature and/or increasing loading rates (Perkins 1999; Siviour and Jordan 2016). At low crack propagation speeds, low crack opening strain rates prevail locally at the crack tip, allowing the IM to get easily strained during fracture process and to absorb large amounts of energy (Perkins 1999). In contrast, if the loading rate is high, the local strain rate at the crack tip increases too. Once the strain rate reaches an upper limit (at a given temperature), the IM is unable to follow the applied deformations and becomes ineffective. Similar observations have been published by Perkins (1999) and Leevers (1996) with decreasing temperatures at a given strain rate. As a result, at higher strain rates (as given in the S4 test) a reduction of the RCP resistance can be ascribed to additional negative influence provoked by the implementation of an IM.

Therefore, it is important for new accelerated methods to create similar conditions as in the S4 test (e.g. low temperatures or high loading rates) to account for strain rate effects brought about the IM. Finally, the S4 material ranking of all pipe grades, which is further used as benchmark for the evaluation of the novel concepts, is deduced from the critical $p_{c\text{-}S4}$ levels:

1) PA12-base and C2-im-yw
2) C4-im-nc and C5-im-yw
3) C3-nc

or the critical $T_{c\text{-}S4}$ levels:

1) PA12-base
2) C3-nc and C2-im-yw
3) C5-im-yw and C4-im-nc

The criterion used to rank materials in the industry depends on the polymer. Usually polyolefin grades used in pressurized pipe applications are ranked according to $T_{c\text{-}S4}$. In case of PA12, $p_{c\text{-}S4}$ provides the more favorable ranking, since critical S4 test temperatures are in the region of ambient temperatures.

## 4.2 Modified Charpy

The total absorbed energy $U_{tot}$ and the associated standard deviation of the Charpy specimens is plotted over a wide temperature range from -120 °C to 60 °C in Fig. 4.2. Starting at -120 °C, the total absorbed energy increases with increasing temperature, followed by a decrease at approx. 20 °C to 40 °C for all PA12 pipe grades. The values of $U_{tot}$ are relatively low (10-20 kJ/mm$^2$) at lower temperatures and the fracture is entirely brittle, as can be asserted from load-displacement curves, as well as from fracture surface analysis. In addition, it appears that the grades end in a plateau at around -120 °C, with the exception of C3-nc and C4-im-nc, which show rather unstable values. In contrast, at higher temperatures $U_{tot}$ reaches values ranging from 70-130 kJ/mm$^2$ and the fracture becomes strongly ductile. In this context, the average energy required for ductile failures is about four to five times higher than for brittle fractures. In the range of 20 °C and 60 °C a decrease in $U_{tot}$ for all grades gets evident, which can be explained by the fact that measurements

were taken in the area of $T_g$ (see Fig. 3.1). The sharp transition from brittle to ductile is visible in all investigated materials. The neat PA12-base (black graph) has a BTT which is in the range of -15 °C and 40 °C. The BTT from compound C3-nc (red graph) is between 0 °C and RT. The addition of an IM significantly broadens the BTT starting from -15 °C to RT for C4-im-nc. Similar influences were also observed by Hassan and Haworth (2006), Nijhof et al. (1999), Muratoglu et al. (1995) as well as Deblieck et al. (2017) on different polymers. Pigmentation in C2-im-yw has an opposite effect: the transition range becomes narrower and shifts to higher temperatures which are in the range of 0 °C and RT. In contrast, the research group around Kanu et al. (2001) observed an improvement in impact properties through the addition of a pigment to PP, which results in a shift of the transition to lower temperatures. Increasing the $M_W$ has a positive effect on BTT (C2-im-yw → C5-im-yw), which is shifted to lower temperatures, entering the brittle regime at about -30 °C. This consequence results from improving the impact properties by increasing $M_W$ (Kayanot et al. 1998). Results of the ranking at -120 °C (yellow marking) are compared with the ranking results of the S4 test in Fig. 4.4.

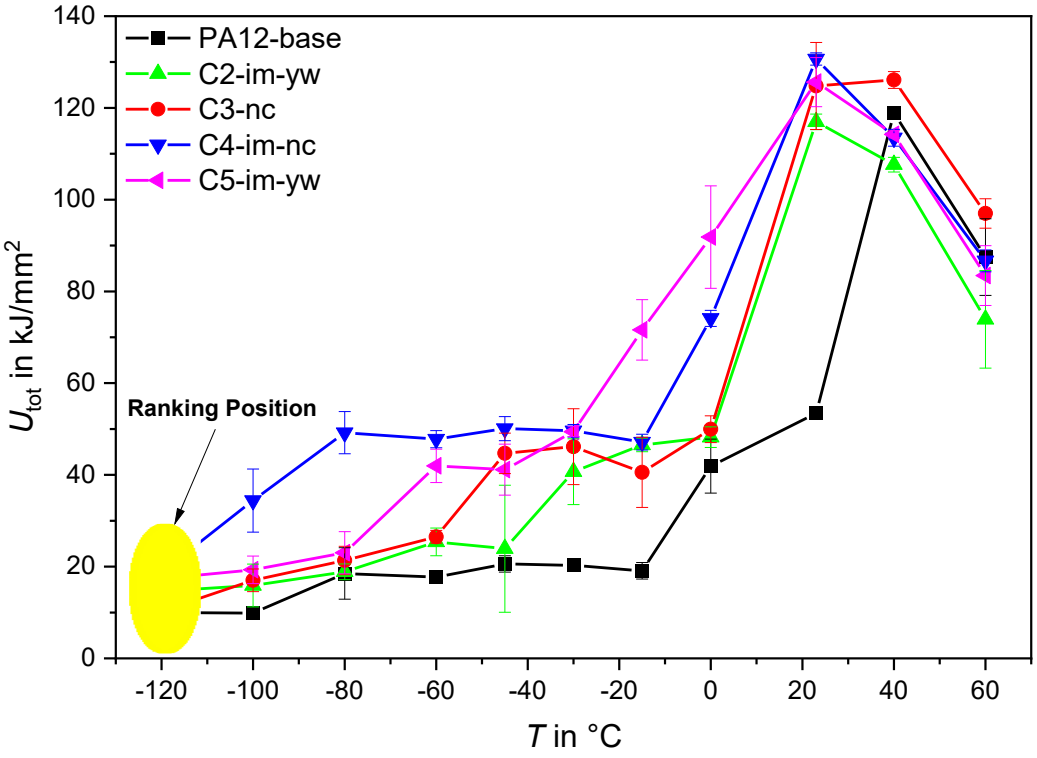


**Fig. 4.2:** Total absorbed energy $U_{tot}$ as a function of temperature ranging from -120 °C to 60 °C at a constant loading rate of 0,1 m/s.

Considering the values obtained from a fracture mechanics point of view, basically a fracture process can be divided into two stages. The first stage is fracture initiation, where significant plastic deformation may occur, followed by crack propagation (Nijhof et al. 1999). The energy required to propagate a crack in relation to the total energy $U_{prop}/U_{tot}$ is shown in Fig. 4.3a as a function of temperature $T$ (from -120 °C to 60 °C). The energies required to drive a crack throughout a material increase strongly with increasing temperature. The research group around Nijhof et al. (1999) reported the same trend in PP-rubber blends. Furthermore, crack initiation behavior was reported to be far less sensitive to temperature increases than crack propagation. Based on data obtained from PE100 pipe grades, this statement can be confirmed by Deblieck et al. (2017). From this work it can also be inferred that at low temperatures the entire fracture process is dominated by crack initiation and at higher temperatures by crack propagation. However, at low temperatures, in the brittle region, the required energies are in a range between approximately 0 % and 20 % of the total energy (Fig. 4.3a), while the remaining energy (80 %-100 %) dissipates to resist crack initiation (Fig. 4.3b). At a certain temperature, the energy content increases and the fracture mode changes from brittle to ductile. In this transition area, the materials behave as described previously, impact modifiers and an increase in $M_W$ lead to a shift of the transition to lower temperatures, that is an increased fracture toughness behavior, whereas pigments counteract this effect. Additionally, $T_{BD}$ transitions illustrated in $U_{prop}/U_{tot}(T)$ and $U_{max}/U_{tot}(T)$ are clearer than observed in $U_{tot}(T)$. At higher temperatures, in the ductile range, it can be seen that the main contribution to the total energy comes from $U_{prop}$. The proportions are roughly between 50 % and 70 %. The energy required for initiation is thus approximately between 30 % and 50 %. Results of the ranking at -120 °C (yellow marking) for Fig. 4.3a are compared with the ranking results of the S4 test in Fig. 4.4.

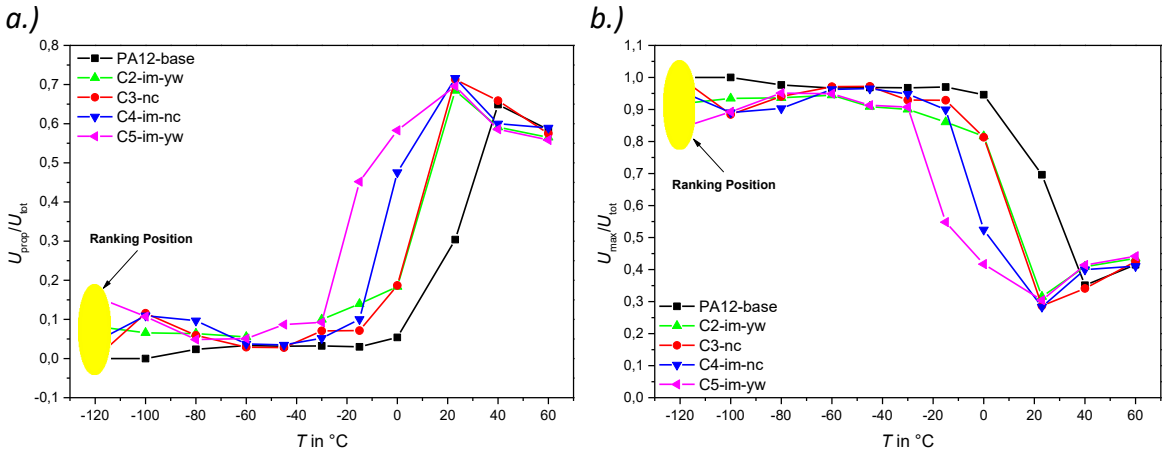


**Fig. 4.3:** a) Proportion of crack propagation energies in relation to the total absorbed energy $U_{prop}/U_{tot}$ as a function of temperature $T$ (a); b) Proportion of crack initiation energies in relation to the total absorbed energy $U_{max}/U_{tot}$ as a function of $T$ in a range from -120 °C to 60 °C with a loading speed of 0,1 m/s.

The modified Charpy test originally aimed for a state of ideal brittleness, that is a clear plateau value at very low temperatures, by which a ranking could have been obtained. Yet, no distinctive plateau was reached for the pipe grades, except for PA12-base. Thus, it becomes apparent that the ranking obtained (see Fig. 4.4) does not match the S4 results in terms of $p_{c\text{-}S4}$, also not if $U_{prop}/U_{tot}$ values are considered. In contrast, regarding the ranking of $T_{c\text{-}S4}$ from the S4 test, it seems that there is an agreement with the values obtained from $U_{tot}$. Agreement of $U_{prop}/U_{tot}$ with the critical temperature values is not obtained.

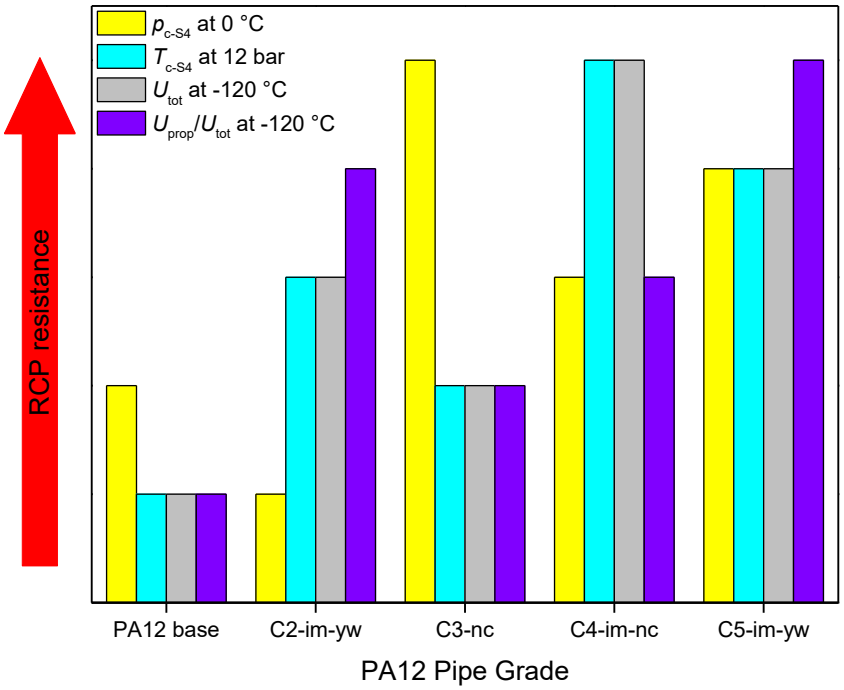


**Fig. 4.4:** Qualitative comparison of ranking results – S4 vs. $U_{tot}(T)$ and $U_{prop}/U_{tot}(T)$ at -120 °C.

Referring to the work of Deblieck et al. (2017), there are further possibilities to rank materials in terms of their RCP resistance, e.g. by using an average initial slope parameter $\phi$. To determine $\phi$, a straight line is drawn through all data points that are in the brittle region (from -120 °C to onset of $T_{BD}$). The greater the slope, the greater the resistance to RCP. The slopes of all materials and whether the ranking corresponds to the S4 test is shown in Table 4.1.

**Table 4.1:** Overview of calculated average initial slopes $\phi$ of the PA12 pipe grades; (✓) indicates a match and (×) indicates no match.

| Material | $\Phi$ ($U_{tot}(T)$) [(kJ/mm²)/°C] | | $\Phi$ ($U_{prop}/U_{tot}(T)$) [1/°C] | | $\Phi$ ($U_{max}/U_{tot}(T)$) [1/°C] | |
|---|---|---|---|---|---|---|
| **PA12-base** | 0,11 | ✓ | 3,9E-4 | × | -3,9E-4 | × |
| **C2-im-yw** | 0,34 | × | 8,1E-4 | × | -8,1E-4 | × |
| **C3-nc** | 0,31 | × | 7,4E-4 | × | -7,4E-4 | × |
| **C4-im-nc** | 0,25 | × | -2,8E-5 | × | 2,8E-5 | × |
| **C5-im-yw** | 0,39 | × | -6,7E-4 | × | 6,7E-4 | × |

Ranking the materials according to their slope in the brittle region also leads to a result that deviates from the S4 test. Discrepancies between the results from the S4 test and the modified Charpy may be due to the different loading speeds. Rapid loading and low temperatures basically lead to RCP (Swallowe 1999). In S4 testing, impact rates of approx. 10-20 m/s are used (Argyrakis 2010). Due to these high rates, the crack initiation is strongly reduced (compare to Fig. 2.5) and the crack propagates at very high speeds. In modified Charpy the specimens were loaded at a speed of 0,1 m/s to avoid dynamic effects. Thus, not only the temperature, even the loading rate as well as the stress state in the specimen have an influence on whether RCP occurs or not (Argyrakis 2010).

## 4.3 Notched Hoop-stressed Impact Test (NHI)

To evaluate the applicability of the NHI test as a substitute for an S4 test, RCP conditions must be warranted in the specimens. In S4 test RCP speeds between 100 and 300 m/s are expected (Ivankovic and Venizelos 1998; Leevers et al. 1991; Ritchie et al. 1998). For this reason, a high-speed camera PHOTRON FASTCAM NOVA S6 from Photron Limited, Tokyo (J), was attached to evaluate the effect of preloading the Charpy specimen through the Hoop-Stress Device. In fact, increased velocities were perceived (see Fig. 4.5 – shown for PA12-base). The unloaded condition ($F_{hoop}$ = 0 N) is shown in Fig. 4.5a, the loaded condition

($F_{hoop}$ = 550 N) in Fig. 4.5b, both measured at RT. In each case, the path of the crack *da* over the time was evaluated. The slope between the single data points provides information about the instantaneous crack propagation speed. For the unloaded case, a maximum crack propagation speed of 90 m/s was determined. The maximum crack propagation speed in the loaded case is approximately 277 m/s. Thus, it can be seen that the application of a pre-stress, induced via the Hoop-Stress Device, leads to an increase in the crack propagation speed, which is about three times higher than in standard impact test.

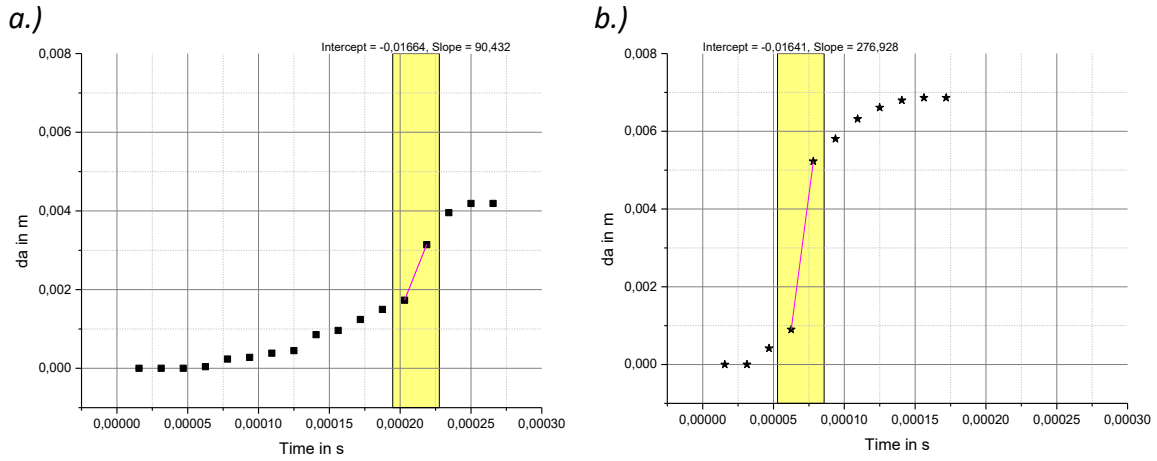


**Fig. 4.5:** Path of the crack *da* as a function of time measured on PA12-base at RT; a.) unloaded ($F_{hoop}$ = 0 N) and b.) loaded with $F_{hoop}$ = 550 N.

With the given certainty that the Hoop-Stress Device creates RCP like crack propagation speeds, the fundamental theory behind the two approaches A1 and A2 according to section 3.2.2.1 and 3.2.2.2, respectively, was tested.

### 4.3.1 Approach 1 (A1)

Results of the A1 are shown in Fig. 4.6. The pressure $p_{eq}$ in bar (from 0 bar to 34 bar) is plotted over a temperature range *T* from RT to 50 °C. Filled symbols are representative for a BT of the specimen, the unfilled symbols for no BT. Dotted lines were fitted approximately between the data points using an exponential fitting function. They are supposed to distinguish the arrest regime from the propagation regime as is often observed in S4 data (compare to Fig. 2.9). The PA12 grade C5-im-yw (magenta dotted line) performs best in this approach. At RT, fracture was detected for the first time at about 2 bar. At temperatures above RT, however, no breakage of the specimen was detected up to a maximum pressure of 34 bar. Compound C4-im-nc (blue dotted line), in contrast, shows no break at RT,

whereas BT of specimen occurs above 9 bar around 27 °C. At temperatures above 27 °C, no breakage was observed up to an equivalent pipe pressure of 34 bar. At 0 °C and temperatures above 27 °C, no breakage was detected up to a pressure of 34 bar for C2-im-yw (green dotted line). A break was determined at 27 °C and approx. 0,5 bar. Pipe grade C3-nc (red dotted line) exhibits BT at approximately 6 bar and a temperature of 35 °C, above which no breakage was achieved up to the maximum applicable pressure level. The neat PA12-base (black dotted line) exhibits BT at around 2 bar and a temperature of 40 °C. At temperatures above, no breakage was detected up to 34 bar. In summary, the results show that, as the temperature increases, generally higher pressures are required to propagate a crack and cause a BT fracture. This can be explained by the increasingly ductile material behavior coupled to rising temperatures (Albiter 2018). Assuming a constant temperature, failure or non-failure of the specimen occurs depending on the level of pressure and on the material structure. In fact, polymers undergo a transition from tough to brittle when exposed to successively increasing pressures (Argyrakis 2010). A summary of the critical pressure and temperature levels with regard to measured S4 data is shown in Table 4.2.

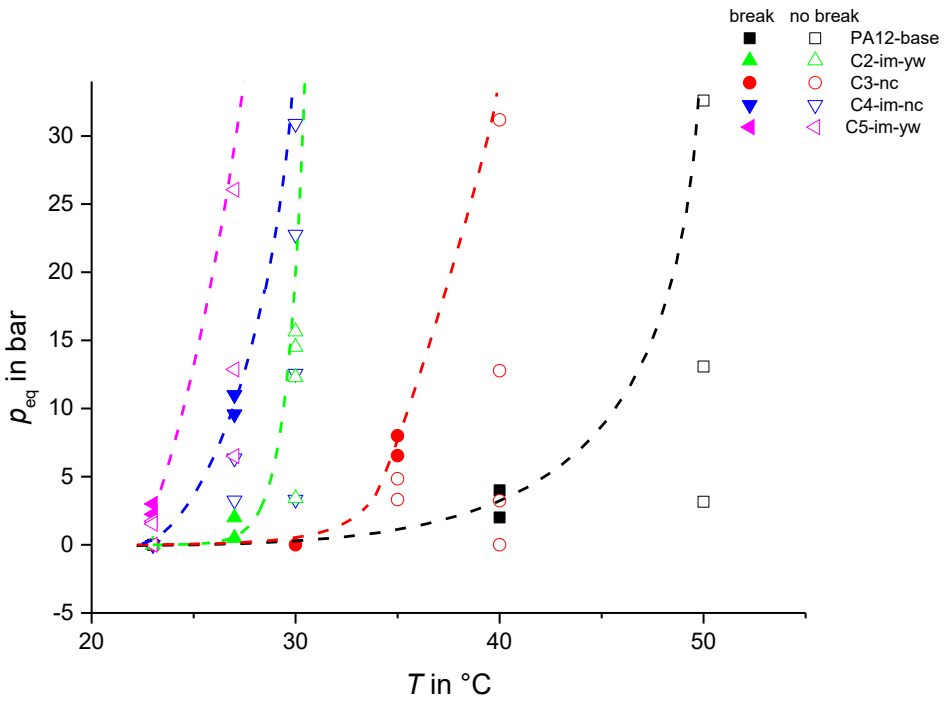


**Fig. 4.6:** Applied equivalent pipe pressure $p_{eq}$ as a function of temperature $T$, recorded at an impact velocity of 1 m/s.

**Table 4.2:** Comparison of the critical pressure ($p_{c\text{-}S4}$, $p_{c\text{-}A1}$) and temperature ($T_{c\text{-}S4}$, $T_{c\text{-}A1}$) values from S4 test and A1.

| Material | S4 | | A1 | |
|---|---|---|---|---|
| | $p_{c\text{-}S4}$ [bar] | $T_{C\text{-}S4}$ [°C] | $p_{c\text{-}A1}$ [bar] | $T_{C\text{-}A1}$ [°C] |
| **PA12-base** | 3,16 | 45,0 | 0,0 | 50 |
| **C2-im-yw** | 3,15 | 27,5 | 0,0 | 30 |
| **C3-nc** | 6,97 | 29,5 | 0,0 | 40 |
| **C4-im-nc** | 4,08 | 23,0 | 0,0 | 29 |
| **C5-im-yw** | 4,41 | 25,5 | * | 27 |

* Exceeds 0 bar at lower temperatures

The results of Fig. 4.6 and Table 4.2 demonstrate that in comparison with the S4 test no correlation in the ranking according to critical $p_{c\text{-}S4}$ occurs at A1. A ranking based on $T_{c\text{-}A1}$ at the highest applied equivalent pressure (34 bar) seems possible and agrees with the ranking of the S4 test (ascending order):

1) PA12-base
2) C3-nc
3) C2-im-yw, C4-im-nc and C5-im-yw.

From the presented data, it can be observed that ranking by critical pressure does not seem to be possible. Deviations from the result of the S4 test might be caused by pronounced shear lips due to dominant plane stress (compare with Fig. 2.4) within the crack plane of the standard Charpy specimens (Fig. 4.7a). Moreover, unwanted deformations around the clamping region of the specimens at high hoop-stress preloads and $T \geq 23$ °C were observed, see Fig. 4.7b.

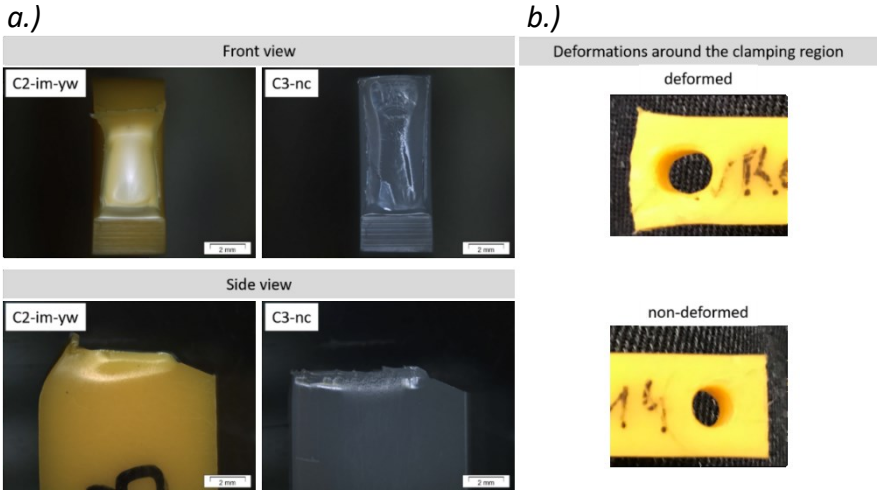


**Fig. 4.7:** Shear lips formation shown for two pipe grades (C2-im-yw & C3-nc) in front and side view (a.); Specimen deformation around the clamping region (b.).

At this point it should also be mentioned that the conditions under which the S4 data are determined may not be sufficiently reached at NHI testing with A1. In contrast to the NHI test, the S4 test uses relatively high impact velocities of 16 m/s, leading to a strong decrease of a rate-sensitive material's (e.g. PA12) crack initiation toughness $G_{Ic}(v)$ (Anderson 2005a; Buchar 1987). The idea leading to A2 is shown schematically in Fig. 4.8, for two materials, material A (black curve) and material B (red curve). Plotted is $G_{Ic}(v)$ as a function of loading rate $v$, for rate sensitive materials with dominating embrittlement (compare with Fig. 2.5). At very low impact velocities (e.g. 1 m/s), the values of $G_{Ic}(v)$ are generally higher compared to higher velocities (e.g. 16 m/s). If materials are ranked at lower loading speeds, it is possible that they will rank differently than at higher loading speeds, where the minimum value of $G_{Ic}(v)$ equals the minimum crack propagation toughness $G_{Id,min}(\dot{a})$. This would result in material A having a higher $G_{Ic}(v)$ than material B in the NHI test, while being more resistant to RCP according to S4 results at higher impact loads, where influences of crack initiation are diminishing.

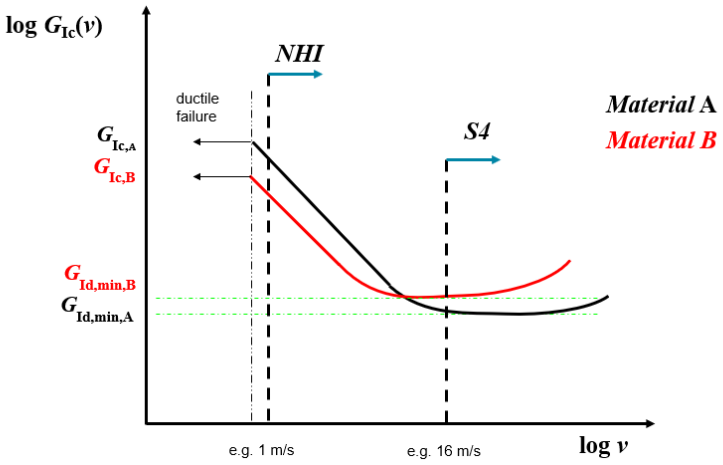


**Fig. 4.8:** Crack initiation toughness $G_{Ic}(v)$ as a function of loading rate $v$, for rate sensitive materials with dominating embrittlement, shown schematically for two materials, A and B (Messiha unpublished).

The underlying idea behind A2 is illustrated in Fig. 4.9. The value of $G_{Ic}(v)$ is not a material constant – it depends on temperature, loading rate and stress state in a structure, thus, on the geometry and shape of the specimen (Bertram 2008). Low temperatures and increasing triaxiality levels at the notch tip (e.g. by introducing a razor blade notch) can lower $G_{Ic}(v)$, which has been confirmed by some researchers in literature (Anderson 2005b; Henry and Luxmoore 1997; Narasimhan and Rosakis 1990; Perkins 1999). Perkins (1999) also mentions

other ways to partially eliminate plasticity effects resisting crack initiation, namely by reducing the molecular mass, the notch radius or by increasing the impact velocity. Therefore, the insertion of a razor blade notch, while simultaneously performing the measurements at low temperatures are intended to create conditions more similar to those in the S4 test, yet, at low impact speeds.

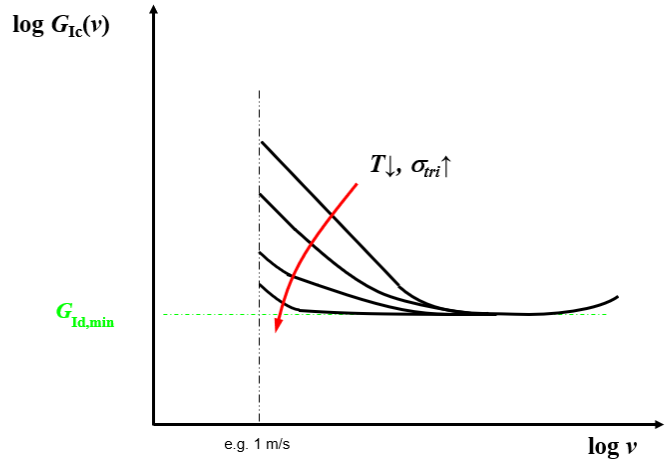


**Fig. 4.9:** Crack initiation toughness $G_{Ic}(v)$ as a function of loading rate $v$, for rate sensitive materials with dominating embrittlement; Influence on the required energy of crack initiation due to decreasing temperature $T$ and increasing triaxiality $\sigma_{tri}$ at the notch tip (Messiha unpublished).

In addition to a razor blade notch and lower temperatures, the specimens in A2 are also notched with side grooves, which are intended to suppress the formation of shear lips when pressure is applied. The effect of side grooves on the embrittlement of materials is widely reported in the literature (Beerbaum 1999; Dabiri et al. 2016; Kadhim et al. 2020; Pinter 2019) as well as the influence of temperature (Beerbaum 1999; Bonten 2016; Grellmann and Altstädt 2011; Pinter 2019). Furthermore, the kind of failure (brittle or tough) is included, which was neglected in A1.

### 4.3.2 Approach 2 (A2)

In the following Fig. 4.10a-b, $U_{tot}(T)$ is plotted as a function of $T$ in a range from -70 °C to -10 °C, once for the unloaded state (Fig. 4.10a) and for a load of $F_{hoop}$= 700 N (Fig. 4.10b) for all PA12 grades. The proportions of energy required for crack propagation relative to the total energy $U_{prop}/U_{tot}$ are plotted in Fig. 4.10c-d as a function of $T$, in a range from -70 °C to -10 °C. Results of the unloaded case can be seen in Fig. 4.10c and those for the loaded case ($F_{hoop}$= 700 N) in Fig. 4.10d. In the unloaded case, the values of $U_{tot}$ are in a

range of approximately 4 J to 12 J. Furthermore, it can be seen from the figure that the values of $U_{tot}$ do not change significantly over the temperature range. The impact modified materials (C2/C5-im-yw & C4-im-nc) tend to be higher than those without (C3-nc and PA12-base). Pigmentation also causes a decrease in the totally absorbed energy (from C4-im-nc to C2/C5-im-yw). Applying a tensile force of approx. $F_{hoop}$= 700 N to the specimen drops $U_{tot}$ to a range of 0,3 J to 6,5 J – less energy (about 50 %) is required to cause the specimen to fracture when hoop-stress is applied. Looking at $U_{tot}$ over $T$, a more pronounced increase with rising temperature is noticeable, particularly for the impact modified grades. Less fracture energy (average 50 %) is needed at low temperatures (-70 °C) than at higher temperatures (-10 °C). In both cases, the proportion of crack propagation energy to the total energy is between 2,5 % and 30 % (Fig. 4.10c-d). The difference to 100 % corresponds to the energy required for crack initiation, in both cases this is approximately between 70 % and 97,5 %, depending on the pipe grade. Comparing the two states to each other, it is noticeable that in the unloaded state, $U_{prop}/U_{tot}$ are almost constant over the entire temperature range, while in the loaded state they tend to fall slightly with decreasing temperature.

In addition to the values obtained from the tests, the fracture surfaces were observed. This supports the understanding where all of the introduced energy is absorbed. The fracture surfaces were examined with a light microscope using 10x magnification (Fig. 4.11). A fracture surface in the unloaded and loaded state at different temperatures (from -10 °C to -70 °C) is shown for all PA12 grades. In the unloaded state, PA12-base shows a very smooth surface, plastic deformations and an influence of the temperature are not visible. In contrast, loading results in a comminuted fracture surface appearance. Plastic deformations on the fracture surface are recognisable at C2/C5-im-yw and C4-im-nc at the initiation area (lower area) and at the crack propagation zone (upper area). As the temperature decreases, deformations reduce at the initiation zone and remain almost unchanged at the crack propagation zone. By loading the specimens, the plastic deformations at the crack propagation zone disappear, but those at the initiation area remain and become smaller with decreasing temperature. At -70 °C, only slight plastic deformations are visible and the fracture surface seems smoother. An increase of plasticity effects with increasing equivalent pipe pressure is probably attributed to applied

prestresses before the impact load occurs. Thus, materials might be already pre-damaged. However, fracture surfaces of C3-nc seem rather smooth in both cases.

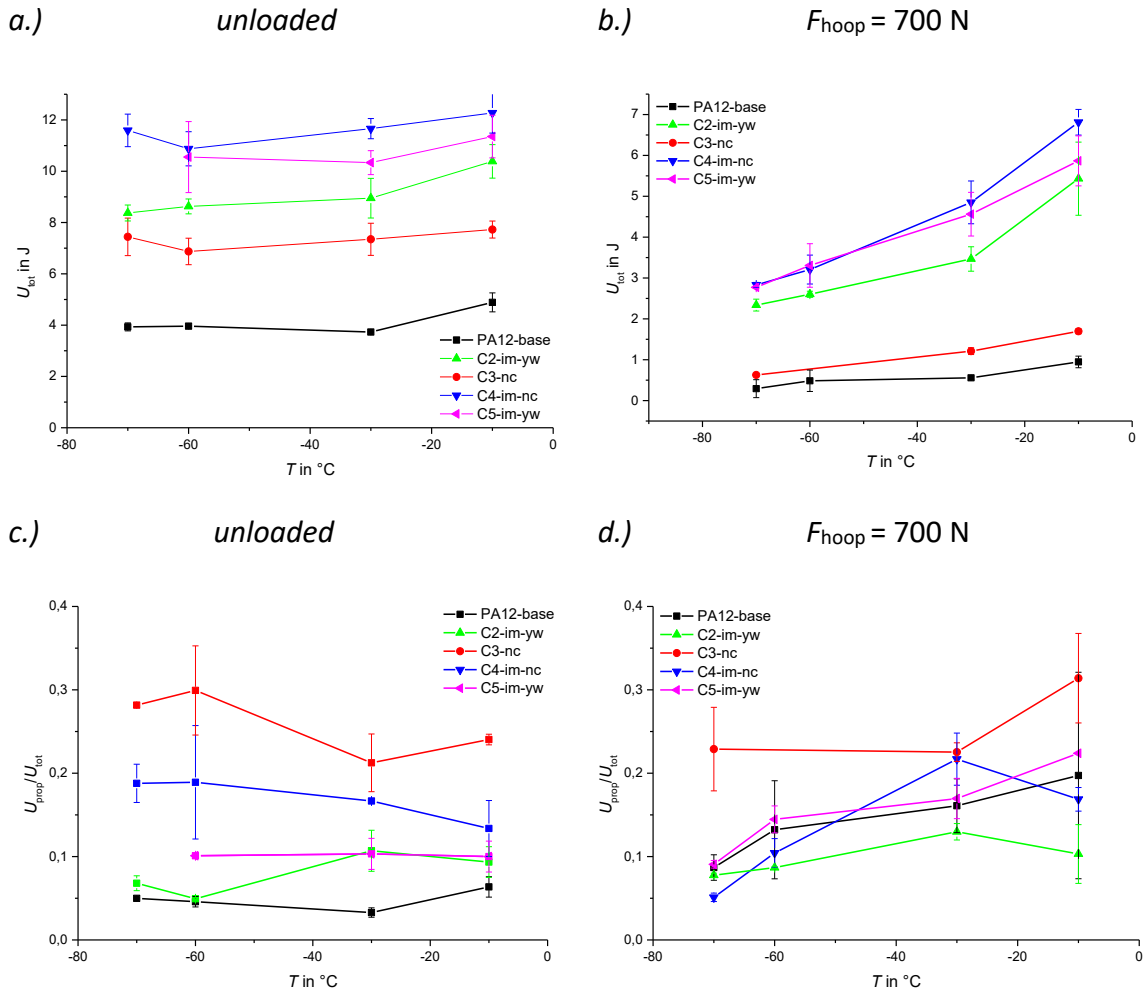


**Fig. 4.10:** Total absorbed energy $U_{tot}$ as a function of temperature $T$ (unloaded condition (a.) and (b.) with a tensile force of $F_{hoop}$ = 700 N (b.)) and proportion of crack propagation energies in relation to the total absorbed energy $U_{prop}/U_{tot}$ as a function of temperature $T$ in a range from -70 °C to -10 °C (unloaded condition (c.) and (d.) with a tensile force of $F_{hoop}$ = 700 N (b.))

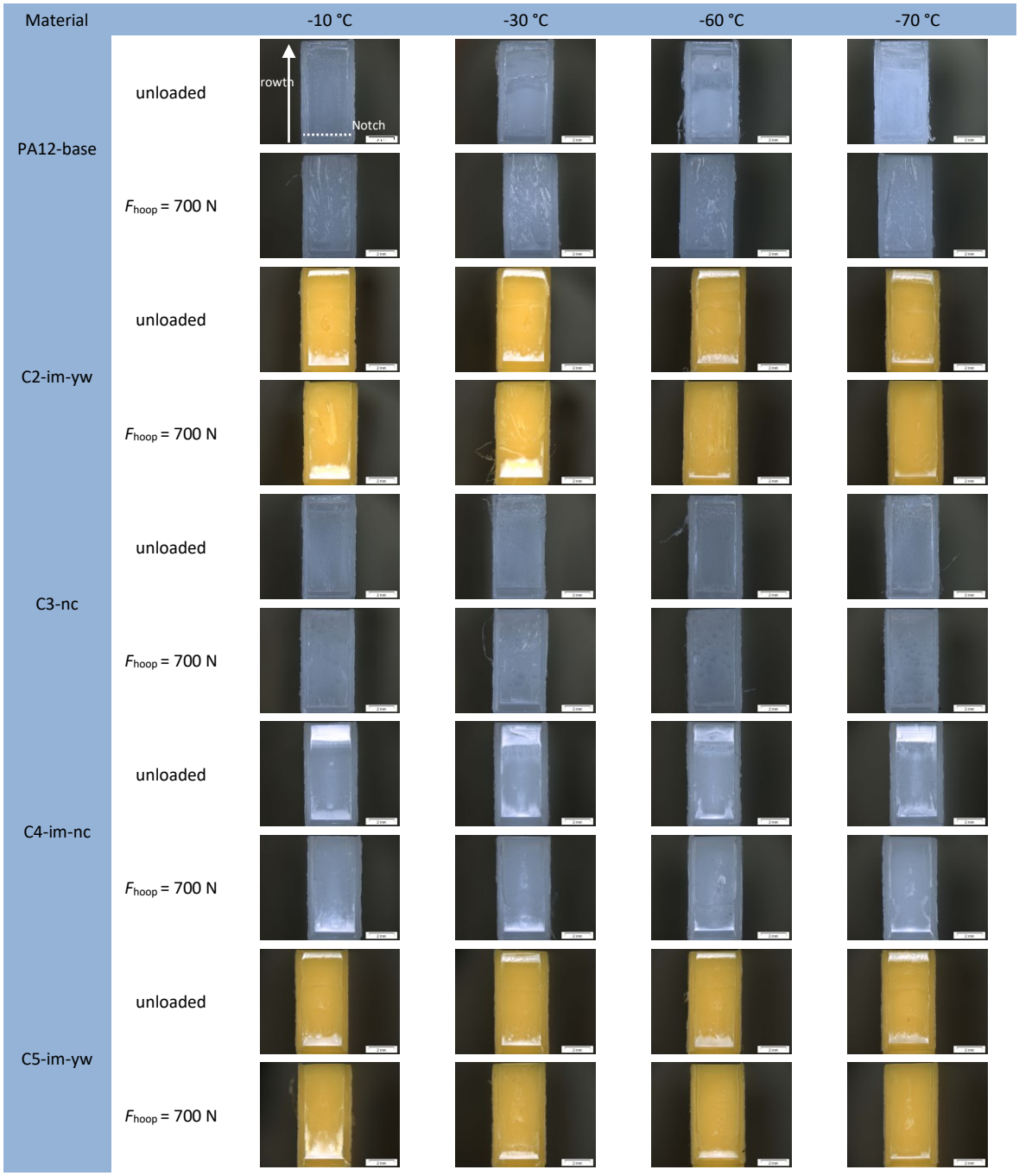


**Fig. 4.11:** Representation of the fracture surfaces in a loaded and an unloaded state of all selected PA12 grades at different temperatures.

Results of A2 are shown in Fig. 4.12. The pressure $p_{eq}$ in bar is plotted over a temperature range $T$ from -70 °C to -10 °C. It can be inferred that at lower temperatures, generally less pressure is required to obtain brittle failure than at higher temperatures. While C2/C5-im-yw and C4-im-nc grades exhibit an almost exponential decrease in pressure with decreasing temperature, neat PA12-base shows an approximately linear decrease in the measured range. Compound C3-nc exhibits an increase in the pressure required to achieve

"ideal" brittle failure between -10 °C and -30 °C. From -60 °C, the values seem to end in a plateau (except C2-im-yw). A summary of the critical pressure levels with regard to measured S4 data is presented in Table 4.3.

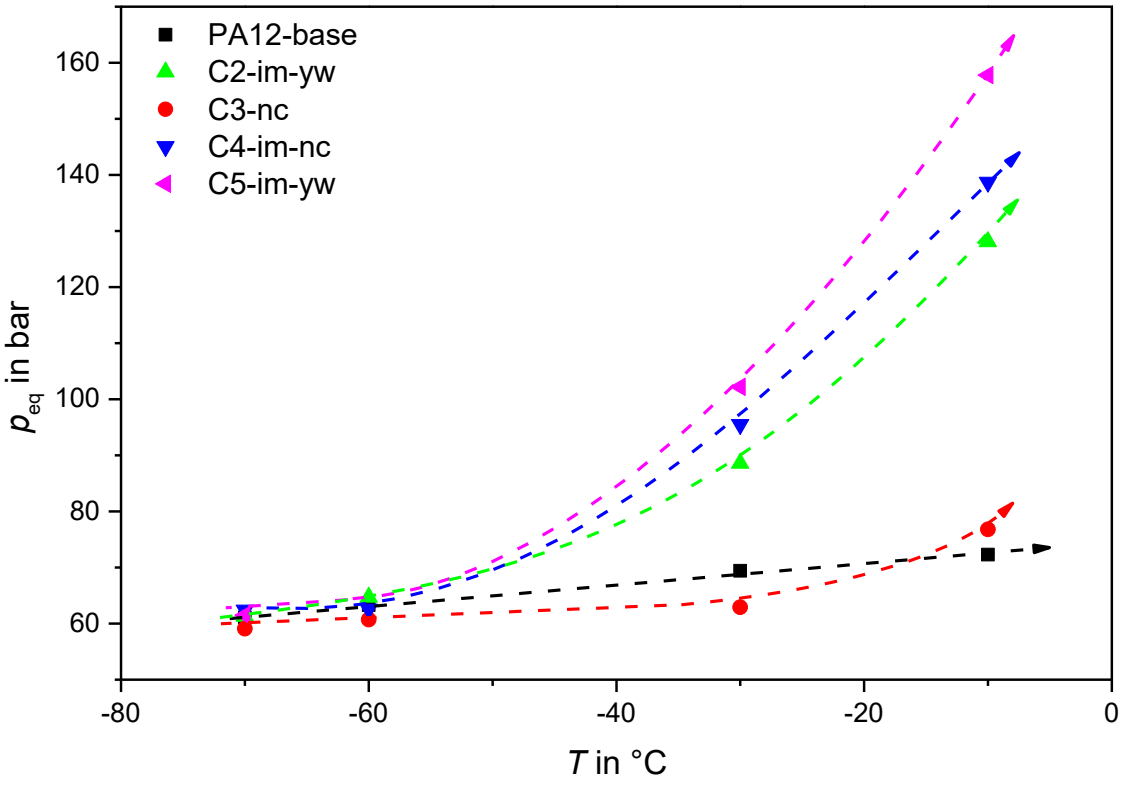


**Fig. 4.12:** Applied equivalent pipe pressure $p_{eq}$ as a function of temperature $T$, recorded at an impact velocity of 1 m/s.

**Table 4.3:** Comparison of the critical pressure ($p_{c\text{-}S4}$, $p_{c\text{-}A2}$) values from S4 test and A2.

| Material | S4 | A2 |
|---|---|---|
| | $p_{c\text{-}S4}$ [bar] | $p_{c\text{-}A2}$ [bar] |
| **PA12-base** | 3,16 | 61,0 |
| **C2-im-yw** | 3,15 | 61,3 |
| **C3-nc** | 6,87 | 59,0 |
| **C4-im-nc** | 4,08 | 62,0 |
| **C5-im-yw** | 4,41 | 61,5 |

From Fig. 4.12 and Table 4.3 it can be seen that no ranking occurs using A2 which is comparable to the ranking in the S4 test. The pipe grades which are impact modified rank significantly better in A1 than those without impact modifier. A ranking based on $p_{c\text{-}A1}$ at a temperature of -70 °C would result in the following (descending order):

1) C4-im-nc, C5-im-nc and C2-im-yw
2) PA12-base

3) C3-nc.

Deviations from the A2 could be due to the fact that the selected conditions are not close enough to those prevailing in the S4 test. The presence of the IM must be considered. According to Perkins (1999) and Leevers (1996), a critical temperature exists at which the IM loses effectiveness. The used IM in the PA12 grades has a $T_g$ of approx. -58 °C. Therefore, the temperatures of -70 °C were possibly not set low enough to eliminate its effect. At this point, it should also be mentioned that a technological limit of the used drop tower is reached at -70 °C. Furthermore, the selected impact velocity of 1 m/s is probably far below the velocity required to exclude strain rate dependence of the IM. Other measurement uncertainties result from the used striker, which is equipped with a load cell of 45 kN. Recorded forces, however, were in a range between 50 N and a maximum of 700 N. Measurements were taken at the lowest limit of the striker, which can lead to deviations. Also, the hoop-stress device cannot reproduce residual stresses as they occur in extruded pipes (more information can be found, e.g., at: Pilz (2001), Hutař et al. (2013), Poduška et al. (2016)), which can lead to additional deviations.

## 4.4 Quasi-Dynamic $K_{ID,eq}$

The following Fig. 4.13 shows the determined $K_{IC}$ values at different temperatures as a function of the loading rate $v$ in a range of 10 mm/min to 10 000 mm/min. Results of C2-im-yw and C4-im-nc are plotted in Fig. 4.13a and Fig. 4.13b, respectively. Both grades were measured at temperatures from -120 °C up to 0 °C. However, the data at -60 °C can be neglected as both materials have secondary relaxation regions around this temperature, that highly alter the results (compare to DMA results, Fig. 3.1). For C2-im-yw as well as for C4-im-nc the $K_{IC}$ values are higher at low temperatures compared to higher temperatures. The received values for low $v$ are in the range of 3,8 $MPam^{1/2}$ to 4,8 $MPam^{1/2}$ for C2-im-yw and in the range of 3,8 $MPam^{1/2}$ to 5,2 $MPam^{1/2}$ for C4-im-nc. With regard to the loading rate, a trend can be observed as well. It is evident for both grades that $K_{IC}$ generally decreases with increasing $v$ at different $T$.

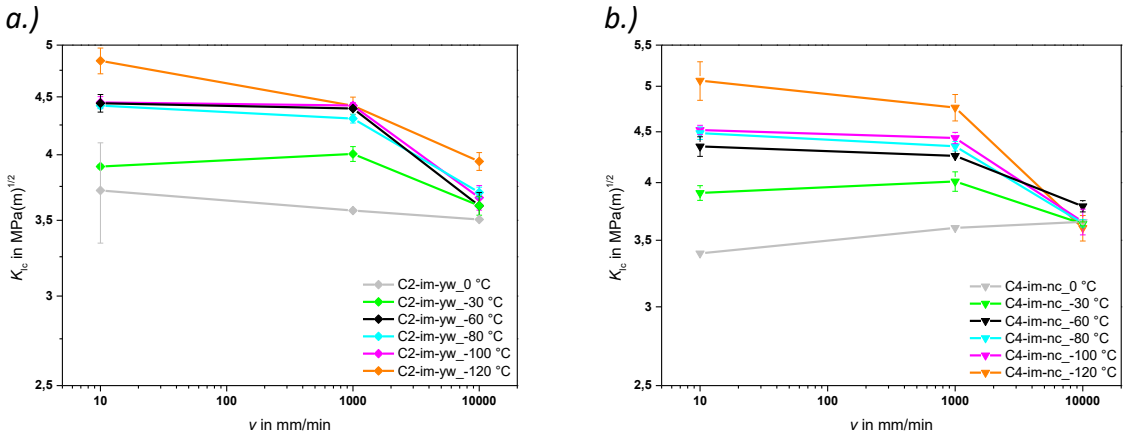


**Fig. 4.13:** $K_{IC}$ as a function of loading rate $v$ at different temperatures for C2-im-yw (a.) and C4-im-nc (b.).

From the obtained data it is evident that the primary intention of the method cannot be carried out. To apply a time-temperature shift on the measured $K_{IC}$ data to obtain an equivalent quasi-dynamic $K_{ID,eq}$, the values would have to decrease with decreasing temperature or increasing loading rate. The latter could be demonstrated, but interestingly $K_{IC}$ decreased with increasing temperature, violating the basic assumptions of the time-temperature equivalence principle. In order to exclude evaluation errors and measurement artefacts, the load-displacement curves and the associated fracture surfaces were examined in more detail. Thus, representative average curves calculated from a number ($n$) of three individually recorded load-displacement curves at each temperature and loading rate are shown in Fig. 4.14a-f (Fig. 4.14a-c the load-displacement curves for C2-im-yw are shown, in Fig. 4.14d-f those of C4-im-nc). Both materials show similar behavior with respect to the temperature influence on the shape of the curves. As the temperature decreases, there is an increase in strength and elongation at break, but the stiffness remains approximately constant. At temperatures around -80 °C, the material behavior changes. The stiffness as well as the strength increases and the elongation at break decreases. Increasing the loading rate essentially reduces the strength and elongation at break of all curves, the shape remains approximately unchanged. However, for many semi-crystalline polymers it is widely known that stiffness and strength increase with increasing loading rate and decreasing temperature. Deformation until fracture, is decreasing (Amjadi and Fatemi 2020). These general observations are basically valid for unnotched specimens. In the case of notched specimens, however, this behavior cannot be always transferred, as different stress states affect the material behavior at the vicinity of

a crack tip. In the present results, the strength increases with decreasing temperature, but the elongation at break hardly decreases and in some cases even increases (Fig. 4.14b,e). As the CRB specimens were taken from extruded solid bars, processing influences may also affect the fracture behavior.

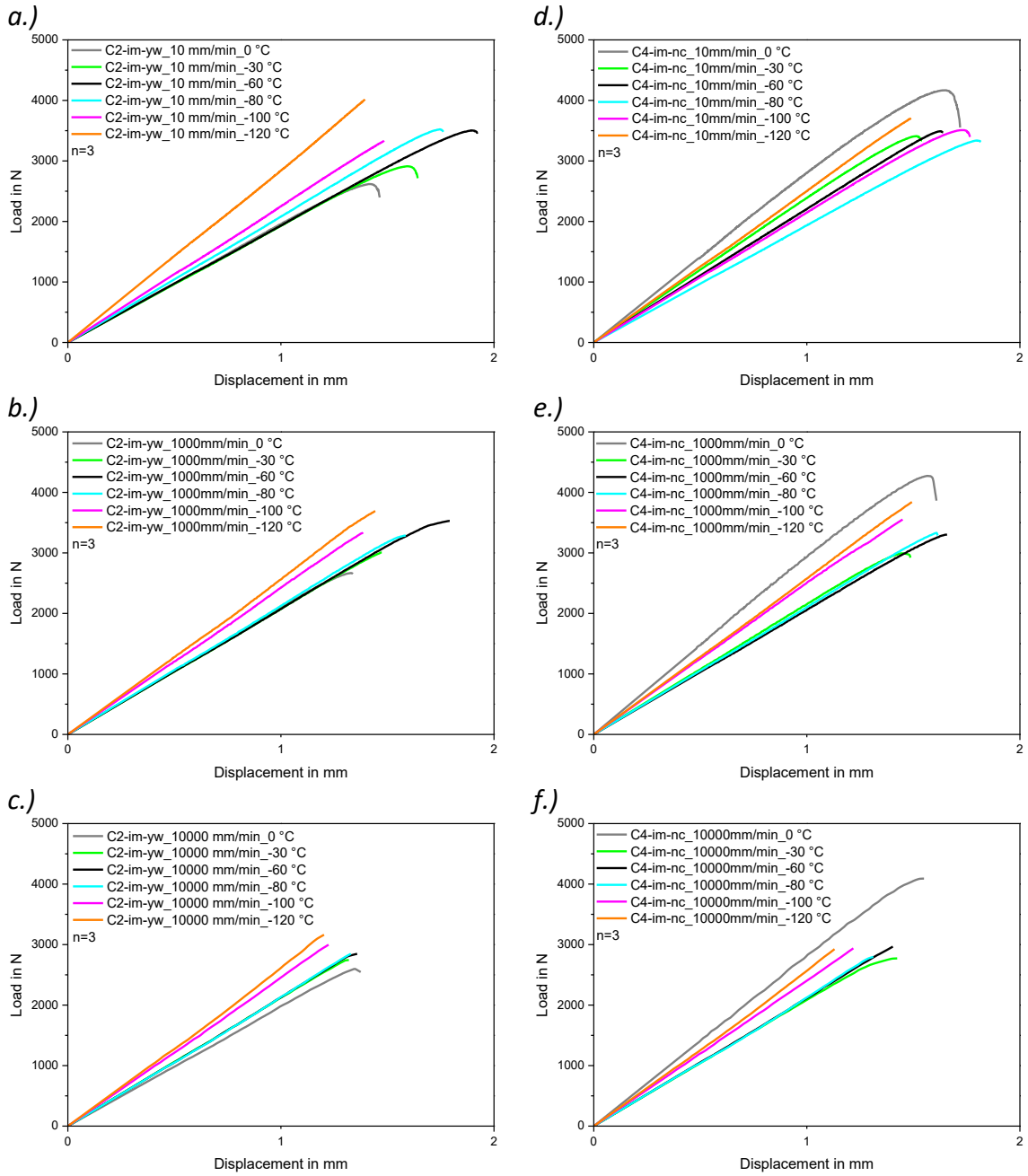


**Fig. 4.14:** Representative load-displacement curves at different temperatures and loading rates (a.-c.) for C2-im-yw and (d.-f.) for C4-im-nc.

The influence of temperature and loading rate can be analysed on the basis of the fracture surfaces (see Fig. 4.15). In both materials, a reduction in plastic deformation can be observed with decreasing temperature and increasing loading rate. This effect on

increasing fracture surface embrittlement is widely known and can be found in many basic literature, e.g. Grellmann and Altstädt (2011) or Bonten (2016). However, at -30 °C and low loading rate (10 mm/min) a high plastic deformation is evident, whereas at -120 °C the fracture surface is highly brittle. Between these two extremes, there are areas that are partly ductile and partly brittle. The last plastic regions, evident by formations of thin white rings surrounding the razor blade notch are visible up to $T$ = -100 °C and $v$ = 1000 mm/min.

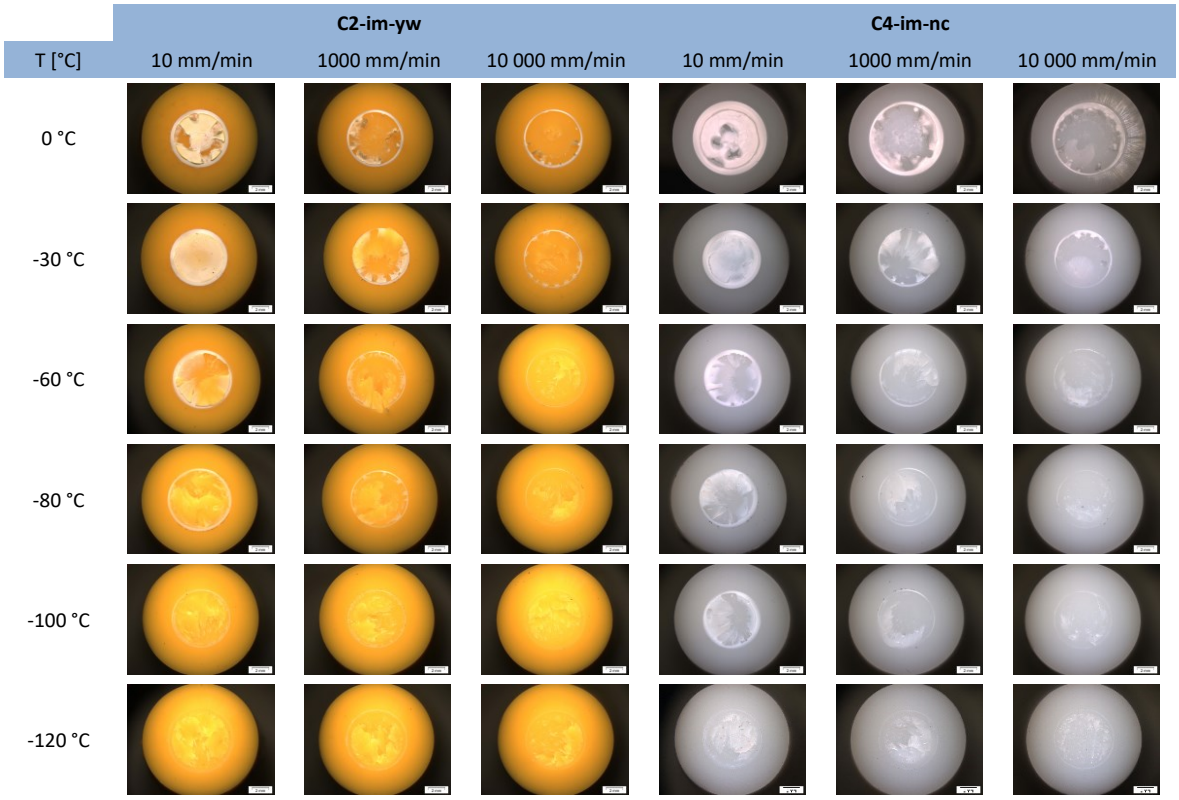


**Fig. 4.15:** Fracture surfaces of the investigated materials C2-im-yw and C4-im-nc at different temperatures (-120 °C to 0 °C) and loading rates (10/1000/10 000 mm/min).

Supplementary to C2-im-yw and C4-im-nc, C3-nc was investigated, but only at a loading rate of 10 mm/min. The reason for choosing C3-nc is due to its high resistance to RCP in the S4 test compared to C2-im-yw and C4-im-nc. Furthermore, this additional measurement makes it possible to investigate the influence of the IM and the addition of PGM on the $K_{IC}$, separately. In the following Fig. 4.16 the load-displacement curves at different temperatures are shown. Over the entire temperature range, a gradually constant stiffness can be seen from the load-displacement curves, while the strength as well as the elongation at break increases. The fracture surfaces of C3-nc are shown in Fig. 4.17, at different temperatures and a loading speed of 10 mm/min. Influence of temperature on

the fracture surfaces is not so clearly visible as it was in case of the impact modified grades, regardless of pigmentation. From -30 °C, surface chipping can be seen, but plastic deformation is not clearly visible, the fracture surfaces seems to be entirely brittle. The remaining question is therefore, where all the energy introduced is consumed, as the fracture surfaces at low temperatures exhibit no plastic deformation areas. In ductile polymers, the main fracture mechanism is either multiple crazing or shear yielding. First involves a high volume of material that can absorb large amounts of energy. The latter creates bands of highly oriented, stretched material (45° to the applied stress) (Beerbaum 1999; Perkins 1999). In reference to Tanrattanakul et al. (1997) who performed tests on notched PolyEthyleneTerephthalate (PET) and blends with Styrene-Butadiene-Styrene (SBS) elastomer specimens, it was found that under all test conditions (temperature and speed) the main mechanism was crazing, which led to brittle fracture. Thus, a possible explanation might be a large-volume damage, which is not directly visible using light microscopic examinations, since the damage is below the fracture surface.

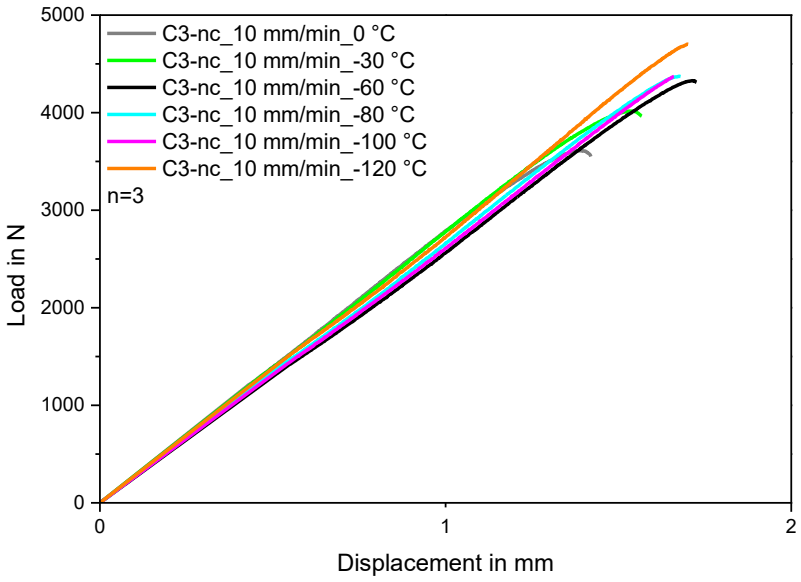


**Fig. 4.16:** Representative load-displacement curves at different temperatures ranging from -120 °C to 0 °C with a loading rate of 10 mm/min for C3-nc.

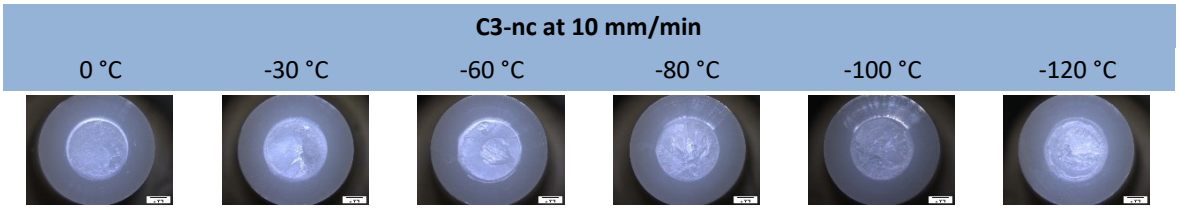


**Fig. 4.17:** Fracture surfaces of C3-nc at different temperatures (-120°C to 0 °C) and a loading rate of 10 mm/min.

For the investigated grades, $K_{IC}$ (Fig. 4.18a) and its energetical counterpart $G_{IC}$ (Fig. 4.18b) are shown as a function of temperature (from -120 °C to 0 °C) at a loading rate of 10 mm/min. With respect to $K_{IC}$, a decrease can be observed over the entire temperature range. The values at low temperatures are in a range between 4,8 $MPam^{1/2}$ and 5,4 $MPam^{1/2}$. At higher temperatures, in contrast, the values are in a range between 3,8 $MPam^{1/2}$ and 4,6 $MPam^{1/2}$. Lach and Grellmann (2008) also observed increased $K_{IC}$ values in impact testing at low temperatures for PP. Moreover, they comment that in semi-crystalline polymers the toughness depends significantly on the mobility of the amorphous domains which keep the crystal lamella together, this is also confirmed by Kausch H.-H. et al. (2005). Marshall et al. (1974) reported an increasing $K_{IC}$ with decreasing temperature in polymethylmethacrylate (PMMA). Mai and William (1977) found that $K_{IC}$ (in plane stress state) increases with decreasing temperature. In contrast, $K_{IC}$ (in plane strain state) is minimal. They performed the measurements on PP and PA6. A cause for the increase of $K_{IC}$ is not given by any of the mentioned researchers. However, values of C3-nc are above those of C2-im-yw and C4-im-nc over the entire temperature range. It can also be observed that C4-im-nc has higher $K_{IC}$ values than C2-im-yw over the entire temperature range, except for the values at -30 °C, where the values seem to coincide. With respect to $G_{IC}$, at low temperatures, the values are in a range of 40 $kJ/mm^2$ and 52 $kJ/mm^2$. It is evident from the graph in Fig. 4.18b that $G_{IC}$ decreases with increasing temperature in case of C3-nc. The impact modified compounds first increase with increasing temperature, reach a maximum and then decrease. In both $K_{IC}(T)$ and $G_{IC}(T)$ it appears that the impact modifier becomes ineffective at temperatures around -80 °C. In $K_{IC}(T)$, this is manifested by the fact that, from this point on, the material differences with respect to RCP are resolved. Differences between C4-im-nc and C2-im-yw become apparent. In $G_{IC}(T)$, this is manifested by the fact that, from this point on, the values of $G_{IC}$ fall with decreasing temperature, since the IM might act as a defect in C2-im-yw and C4-im-nc. In contrast, C3-nc remains unaffected. This observation supports the statement of Leevers (1996) and Perkins (1999) regarding the ineffectiveness of the IM with lower temperatures.

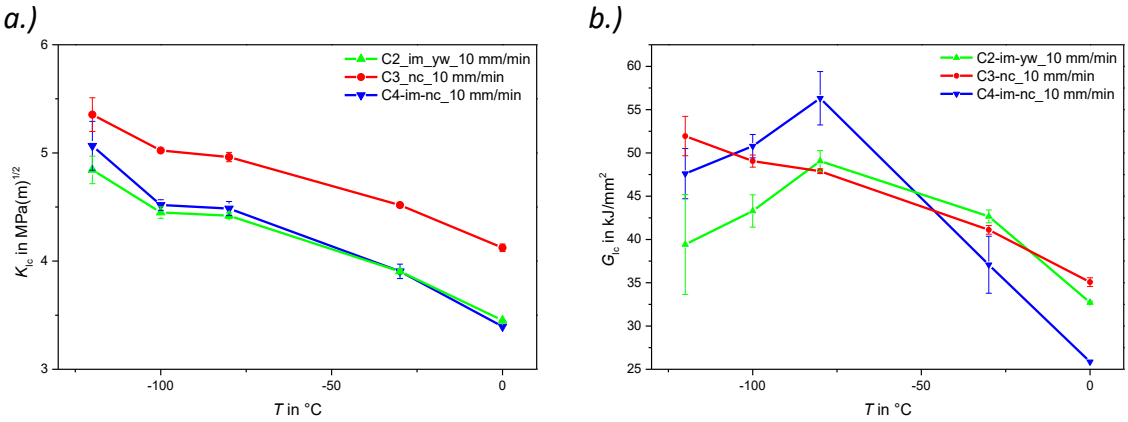


**Fig. 4.18:** $K_{IC}$ (a.) and $G_{IC}$ (b.) as a function of temperatures in a range of -120 °C to 0 °C at a loading speed of 10 mm/min.

However, materials are to be ranked in terms of their RCP resistance. In principle, this seems possible, although the original way of ranking via $K_{ID,eq}$ has been lost. Low temperatures and the advantages of CRB specimens contribute to RCP conditions. The CRB specimens offer several advantages over other commonly used test specimens, e.g. plane strain conditions prevail and the formation of plastic zones is reduced to a minimum (Frank 2010; Lang et al. 2005). Furthermore, high constraints ensure faster crack initiation and subsequent accelerated crack propagation (Frank 2010). All combined, the method seems to provide a good agreement with the ranking (based on $p_{c\text{-}S4}$) from the S4 test. However, at the moment, a more precise statement cannot be made, as the method requires further research.

## 4.5 Comparison of novel concepts

To determine comparable material characteristic parameters to the S4 test, aforementioned concepts were carried out on Charpy (razor blade notched, side grooved, etc.) and CRB specimens. Whereas the S4 test is performed on real pipe structures. In order to be able to transfer characteristic parameters (i.e. $T_{c,A1}$, $T_{c,A2}$ or $K_{Id,eq}$) from miniaturized specimens to components, the so-called "crack tip similitude concept" must be valid (Fig. 4.19). The fracture phenomena that occur at the notch of a specimen must therefore be the same as those that occur at initial defects of a structure (Anderson 2005b). It is therefore important to investigate suitable specimens as well as test conditions under which a specimen reflects same behavior as in a structure under S4 conditions.

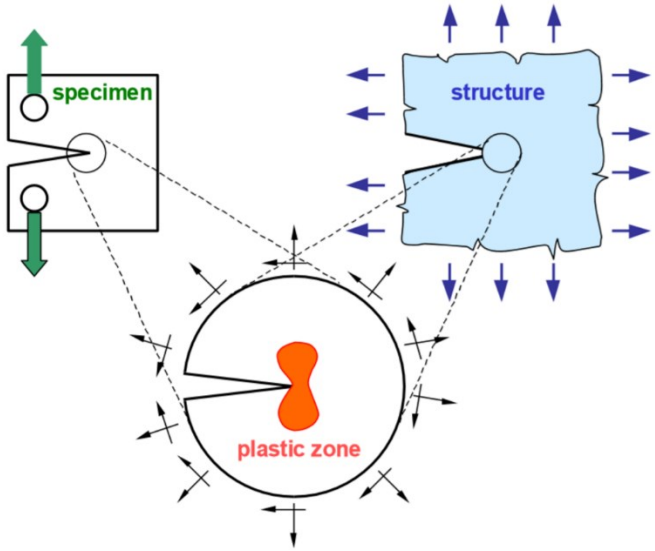


**Fig. 4.19:** Concept of crack tip similitude according to Anderson (2005b) and Pinter (2019).

Comparing the results of the presented concepts to each other, similar rankings are obtained (Fig. 4.20). In both modified Charpy and NHI (A1), the ranking results are identical. Impact modified materials show highest RCP resistance, followed by C3-nc and PA12-base. In contrast, A2 ranking slightly differs from A1 and the modified Charpy. However, a general statement can be made, that impact modified materials show highest fracture toughnesses, while non-toughened grades (PA12-base and C3-nc) maintain lower resistances in the modified Charpy and NHI approach. The quasi-dynamic $K_{ID,eq}$ test, is the only method that portrays higher fracture resistances for non-toughened materials than for impact modified grades.

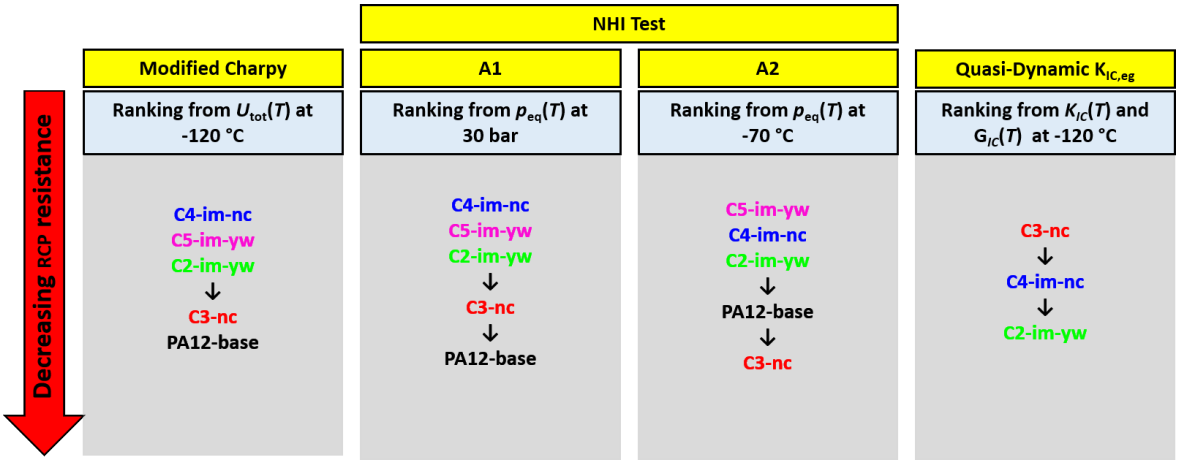


**Fig. 4.20:** Comparison of ranking results from the investigated novel concepts.

# 5 SUMMARY AND CONCLUSION

To characterize the resistance against Rapid Crack Propagation (RCP) in pipes, two established methods are available nowadays, the Full Scale (FS) and the Small-Scale Steady-State (S4) test. Both test methods are very cost and time consuming, which makes the development of accelerated methods very interesting for material producers. In this thesis, three new accelerated, specimen based, test concepts were investigated for their suitability to characterize materials in terms of RCP resistance. These novel concepts include a modified form of a Charpy impact test, called "Modified Charpy", a novel test apparatus designed to imitate stress conditions in a pipe under internal pressure, called the "Notched Hoop-stressed Impact (NHI)" test and finally the presentation of a fracture mechanics test method, termed "Quasi-Dynamic $K_{ID,eq}$". In order to quantify a reliable material ranking with regard to RCP resistances, five different PA12 pipe grades, which differ in their molecular structure and use of additives, were tested via S4 test according ISO 13477. Results of the newly developed approaches were then compared to S4 results in order to check for their reliability in terms of proper material ranking.

Ranking results obtained from the different methods examined are shown in Fig. 5.1, in comparison with the results achieved from S4 testing. In S4, based on the critical pressure $p_{c\text{-}S4}$, C3-nc shows the best resistance to RCP, followed by the impact modified materials C5-im-yw and C4-im-nc and the neat PA12-base and C2-im-yw grade. Based on the critical temperature $T_{c\text{-}S4}$ the following ranking is obtained: highest resistance to RCP is exhibited by C4-im-nc and C5-im-yw, followed by C2-im-yw and the C3-nc. Neat PA12-base shows the worst resistance. With aid of the modified Charpy, the influence of the additives on the material behavior was characterized over a wide temperature range from -120 °C to 60 °C. Unfortunately, with this simple method it was not possible to classify the materials according to $p_{c\text{-}S4}$ ranking of the S4 test. Nevertheless, a ranking regarding to $T_{c\text{-}S4}$ values seems to be possible. Impact modified materials show highest RCP resistance, followed by C3-nc and PA12-base. Limitations of applicable loading rates and a different stress state within the test specimen, compared to pipes during S4 testing, are possible reasons for observed deviations. The underlying idea of reaching a plateau of unchanging ideal brittleness was also not achieved due to experimental restrictions. With the NHI test it was

possible to induce a similar stress state in the specimen as it occurs in a pipe under internal pressure. Likewise, crack speeds similar to RCP were determined. However, a ranking of the materials in terms of their RCP resistance does not result in a correlation to the S4 results, when considering $p_{c\text{-}S4}$ for both approaches A1 and A2. Nevertheless, this method is able able to rank the RCP resistance of the investigated PA12 types as long as the classification remains within a certain material class. In this way, impact modified and non-impact modified, or neat PA12 grades and compounds, can be distinguished from each other and thus also ranked correctly as far as a ranking after the critical temperature is concerned. In contrast, the quasi-dynamic $K_{ID,eq}$ shows high potential for ranking the materials with regard to their RCP resistance similar to $p_{c\text{-}S4}$ from the S4 test. Even if the initial intention of a time-temperature shift was not valid after reviewing the obtained data. It seems, that $K_{ID,eq}$ tests at low temperatures, appropriate loading rates (from 10 mm/min up to 10 000 mm/min or even higher) and the extraordinary plane strain conditions of CRB test specimens create results which are in good agreement with ranking of S4 test results. For the time being, a more precise statement cannot be made, as the method requires further research.

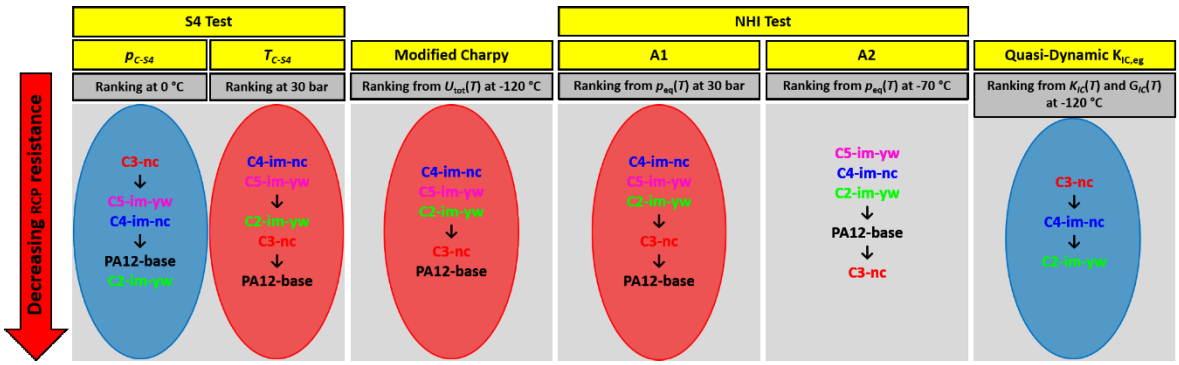


**Fig. 5.1:** Comparison of ranking results from the investigated methods.

# 6 OUTLOOK

This chapter is intended to give a brief overview of possible improvements regarding the investigated methods. In case of the modified Charpy, a brittle plateau could be achieved by testing at even lower temperatures or by modifying the specimens, e.g. by notching. For the $K_{ID,eq}$, further work will be dedicated to test the two remaining PA12 pipe grades. Secondly, the underlying failure mechanism should be investigated in more detail. The fracture surfaces of the test specimens are to be compared with those from the S4 test using Scanning Electron Microscopy (SEM). An investigation using Micro Computer Tomography (µCT) could also provide further information about underlying failure mechanism. A characterization using these methods could at least show if the failure mechanism as given in the S4 test is the same or similar to that observed with this method. To obtain an improved ranking using the NHI test, a striker with reasonable measuring range might be of advantage. More attention should be given to the specimens (thickness, preparation, etc.) and the deformation at the fixing locations. Furthermore, considerations should also be given to determine residual stresses that prevail in extruded pipes due to different cooling conditions, and whether these could additionally be simulated via the hoop-stress device.

# 7 REFERENCES

Albiter, N. L. 2018. *On the fracture behavior of ductile polymer films: Notch quality, essential work of fracture, J-integral, and crack tip opening displacement,* PhD Thesis, Universitat Politècnica de Catalunya-BarcelonaTech.

Alewelt, W., L. Bottenbruch, and G. W. Becker. 1998. *Polyamide*, München: Hanser.

Amjadi, M., and A. Fatemi. 2020. "Tensile Behavior of High-Density Polyethylene Including the Effects of Processing Technique, Thickness, Temperature, and Strain Rate." *Polymers*, 12(9). https://doi.org/10.3390/polym12091857.

Anderson, T. L. 2005a. *Fracture Mechanics: Fundamentals and Applications: Third Edition,* Chapter 4, Boca Raton: CRC Press.

Anderson, T. L. 2005b. *Fracture Mechanics: Fundamentals and Applications: Third Edition,* Chapter 2, Boca Raton: CRC Press.

Argyrakis, C. 2010. *Models for designing pipe-grade polyethylenes to resist rapid crack propagation,* Dissertation, Imperial College London.

Baron, C., Baumann, H. Daebel, J. Mügge, and U. Rhode Liebenau. 1998. "Polyamide: Polyamid 11 und 12.".

Beerbaum, H. 1999. *Ermittlung strukturbezogener bruchmechanischer Werkstoffkenngrößen an Polyethylen-Werkstoffen,* Dissertation, Martin-Luther-Universität Halle-Wittenberg.

Bertram, A. 2008. "Bruchenergie laufender Risse in Gestein.", 2008.

Böge, A., and W. Böge. 2019. *Technische Mechanik: Statik- Reibung- Dynamik- Festigkeitslehre- Fluidmechanik*: Springer Verlag.

Bonten, C. 2016. *Kunststofftechnik: Einführung und Grundlagen*, München: Hanser.

Broek, D., ed. 1982. *Elementary engineering fracture mechanics*, Dordrecht: Springer Netherlands.

Brömstrup, H. 2012. *PE 100 Pipe Systems*, Essen: Oldenbourg Industrieverlag.

Buchar, J., ed. 1987. *The effect of strain rate sensitivity on crack initiation under dynamic loading: Macro-and micro-mechanics of high velocity deformation and fracture*, Berlin, Heidelberg: Springer, Berlin, Heidelberg.

Dabiri, M., T. Skriko, M. Amraei, and T. Björk. 2016. "Effect of Side Grooves on Plane Stress Fracture Behavior of Compact Tension Specimens Made of Ultra-High Strength Steel." *Key Engineering Materials, 713, 159–162.*

Deblieck, R. A.C., D.J.M. L. van Beek, M. McCarthy, P. Mindermann, K. Remerie, B. Langer, R. Lach, and W. Grellmann. 2017. "A simple intrinsic measure for rapid crack propagation in bimodal polyethylene pipe grades validated by elastic-plastic fracture mechanics analysis of data from instrumented Charpy impact test." *Polym Eng Sci*, 57(1): 13–21. https://doi.org/10.1002/pen.24380.

Domininghaus, H., P. Elsner, P. Eyerer, and T. Hirth. 2012. *Kunststoffe*, Berlin, Heidelberg: Springer Berlin Heidelberg.

Flüeler, P., and M. Farshad. 1995. "Arrest of rapid crack propagation in polymer pipes." *Materials and Structures*, 28(2): 108–110. https://doi.org/10.1007/BF02473181.

Frank, A. 2010. *Fracture Mechanics Based Lifetime Assessment and Long-term Failure Behavior of Polyethylene Pressure Pipes,* Dissertation, Montanuniversität.

Frank, A., F. Arbeiter, I. Berger, P. Hutař, L. Náhlík, and G. Pinter. 2019. "Fracture Mechanics Lifetime Prediction of Polyethylene Pipes." *In J. Pipeline Syst. Eng. Pract. 10 (1), p. 4018030.*, (DOI: 10.1061/(ASCE)PS.1949-1204.0000356.).

Gensler, R., C.J.G. Plummer, C. Grein, and Kausch H.-H. 2000. "Influence of the loading rate on the fracture resistance of isotactic polypropylene and impact modified isotactic polypropylene." *Polymer 41 (2000) 3809–3819*.

Grellmann, W., and V. Altstädt. 2011. *Kunststoffprüfung*, München: Hanser.

Griffith, A. A. 1921. "The Phenomena of Rupture and Flow in Solids." *In Philos T Roy Soc A 221 (582-593), pp. 163–198.*, (DOI: 10.1098/rsta.1921.0006.).

Gross, D., and T. Seelig. 2016. *Bruchmechanik: Mit einer Einführung in die Mikromechanik*, Berlin, Heidelberg: Springer Vieweg.

Hahn, G. T., R. G. Hoagland, and M. F. Kanninen. 1973. "A preliminary study of fast fracture and arrest in the DCB test specimen." *Proceedings of an international conference on Dynamic Crack Propagation, G. C. Sih, Ed., pp. 649–662*.

Hartmann, M. 2014. "Polyamid 12-Rohre im Gas-Hochdruckbereich." *KRV Nachrichten, 15-.*

Hassan, A., and B. Haworth. 2006. "Impact properties of acrylate rubber-modified PVC: Influence of temperature." *Journal of Materials Processing Technology*, 172(3): 341–345. https://doi.org/10.1016/j.jmatprotec.2005.07.015.

Henry, B. S., and A. R. Luxmoore. 1997. "THE STRESS TRIAXIALITY CONSTRAINT AND THE Q- VALUE AS A DUCTILE FRACTURE PARAMETER." *Engineering Fracture Mechanics Vol. 57, No. 4, pp. 375-390, 1997*.

Hertlin, J. 1999. "Ausbreitungsgeschwindigkeit von instabilen Rissen in Polymeren bei tiefen Temperaturen.".

Hitesh, P. 2006. "Evaluation of Polyamide 12 (PA12) for high pressure gas distribution applications." *Edited by Gas Technology Institute. Gas Technology Institute.*

Höffin, F. 1995. *Bruchmechanische Untersuchungen zur Wirkungsweise von Oligo- und Polyetherestern mit Poly(oxytetramethylen)-Segmenten als Zähmodifikatoren von anhydridgehärteten Epoxidharzen,* Dissertation, Universität Freiburg, Deutschland.

Hutař, P., M. Ševčík, A. Frank, L. Náhlík, J. Kučera, and G. Pinter. 2013. "The effect of residual stress on polymer pipe lifetime." *Engineering Fracture Mechanics*, 108: 98–108. https://doi.org/10.1016/j.engfracmech.2013.04.014.

Irwin, G. R. 1957. "Analysis of Stresses and Strains Near the End of a Crack Traversing a Plate." *Journal of Applied Mechanics, vol. 24, pp. 361-362*.

Ivankovic, A., and G. P. Venizelos. 1998. "RAPID CRACK PROPAGATION IN PLASTIC PIPE: PREDICTING FULL-SCALE CRITICAL PRESSURE FROM S4 TEST RESULTS." *Engineering Fracture Mechanics Vol. 59, No. 5, pp. 607±622, 1998*.

Jandke Joachim, and Reinicker Roger A., eds. 2016. *Handbuch Kunststoffadditive: Farbmittel*: Carl Hanser Verlag München.

Janostik, V., and V. Senkerik. 2017. "Effect of Pigment Concentration on Mechanical Properties of Polycarbonate." *MATEC Web Conf.*, 125: 2052. https://doi.org/10.1051/matecconf/201712502052.

Jareneck, D., and P. Armstrong. 2010. "Advancing the Adoption of PA12 for High-Pressure Applications.".

Kadhim, M. H., N. A. Latif, M. A. Harimon, A. A. Shamran, and D. R. Abbas. 2020. "Effects of side-groove and loading rate on the fracture properties of aluminium alloy AL-6061." *Materialwiss. Werkstofftech.*, 51(6): 758–765. https://doi.org/10.1002/mawe.201900262.

Kalthoff, J. F., ed. 1990. *Crack Dynamics in Metallic Materials: Experimental Fracture Dynamics*.

Kanninen, M. F. 1983. *Dynamic Fracture Mechanics and its Applications to Material Behavior under High Stress and Loading Rates,* in Material Behavior under High Stress and Ultrahigh Loading Rates, Boston, MA: Springer.

Kanu, R. C., T. H. Spotts, and M. Checebrough. 2001. "The Effects of Some Organic and Inorganic Pigments on the Tensile and Impact Properties of Injection-molded Polypropylene." <https://www.ijme.us/issues/fall2001/articles/polypropylene.htm>.

Kausch H.-H., C. Grein, P. Bequelin, and R. Gensler. 2005. "FRACTURE MECHANICAL CHARACTERIZATION OF SEMICRYSTALLINE THERMOPLASTICS." *ICF 1001-007 OR*.

Kayanot, Y., Keskkula H., and D. R. Paul. 1998. "Fracture behaviour of polycarbonate blends with a core-shell impact modifier." *Polymer Vol. 39 No. 4, pp. 821-834, 1998*.

Kolednik, O. 2012. "FRACTURE MECHANICS." *A221, p.163*.

Kopp, J.-B., C. Fond, and G. Hochstetter. 2018. "Rapid crack propagation in PA11: An application to pipe structure." *Engineering Fracture Mechanics*, 202: 445–457. https://doi.org/10.1016/j.engfracmech.2018.08.025.

Kurzböck, M., G. M. Wallner, and R. W. Lang. 2012. "Black pigmented polypropylene materials for solar absorbers." *Energy Procedia*, 30: 438–445. https://doi.org/10.1016/j.egypro.2012.11.052.

Lach, R., and W. Grellmann. 2008. "Time- and Temperature-Dependent Fracture Mechanics of Polymers: General Aspects at Monotonic Quasi-Static and Impact Loading Conditions." *Macromol. Mater. Eng.*, 293(7): 555–567. https://doi.org/10.1002/mame.200700417.

Lang, R. W., G. Pinter, and W. Balika. 2005. "Ein neues Konzept zur Nachweisführung für Nutzungsdauer und Sicherheit von PE-Druckrohren bei beliebiger Einbausituation." *3R international, 44(1-2), 33-41*.

Läpple, V. 2016. *Einführung in die Festigkeitslehre: Behälter unter Innen- und Außendruck*: Springer Vieweg, Wiesbaden.

Leevers, P. 1995. "Impact and dynamic fracture of tough polymers by thermal decohesion in a Dugdale zone." *International Journal of Fracture 73: 109-127*.

Leevers, P. 1996 *Polym. Eng. Sci. (Polymer Engineering & Science) 36*, 1996.

Leevers, P. 2004. "MODELLING IMPACT FRACTURE and RCP RESISTANCE of THERMOPLASTICS from COHESIVE PROPERTIES." *Society of Plastics Engineers*.

Leevers, P., and R. Morgan. 1995. "IMPACT FRACTURE OF POLYETHYLENE: A NON-LINEAR-ELASTIC THERMAL DECOHESION MODEL." *Engineering Fracture Mechanics Vol. 52, No. 6, pp. 999-1014*.

Leevers, P. S., S. Hazra, and S. Hillmansen. 2000. "Impact resistance of thermoplastics Prediction from bulk properties." *Plastics, Rubber and Composites*, 29(9): 460–467. https://doi.org/10.1179/146580100101541300.

Leevers, P. S., P. Yayla, and M. A. Wheel. 1991. "Charpy and dynamic fracture testing for rapid crack propagation in polyethylene pipe." *Plasries, Rubber and Composires Processing and Applications 17 (1992) 247- 253*.

Lodeiro, M. J., P. E. Tomlins, and A. Pearce. 2000. "THE INFLUENCE OF PIGMENTS ON THE MECHANICAL PROPERTIES OF HIGH DENSITY POLYETHYLENE (HDPE)." *NPL Report CMMT(A) 258*, 2000.

Lohmar, J. 2006. "Polyamide 12 for high pressure gas installations." *In : 23rd Worlg Gas Conference. Amsterdam.*, 2006.

Mai, Y. W., and J. G. William. 1977. "The effect of temperature on the fracture of two partially crystalline polymers: polypropylene and nylon." *Journal of Materials Science, 12(7):1376-82*.

Maiti, S. K. 2015. *Fracture Mechanics: Fundamentals and Applications*: Cambridge Universit Press.

Marshall, G. P., L. H. Coutts, and J. G. Williams. 1974. "Temperature effects in the fracture of PMMA." *JOURNAL OF MATERIALS SCIENCE 9 (1974) 9 1409-1419*.

Martinez, A. B., J. Gamez-Perez, M. Sanchez-Soto, J. I. Velasco, O. O. Santana, and M. Ll Maspoch. 2009. "The Essential Work of Fracture (EWF) method – Analyzing the Post-Yielding Fracture Mechanics of polymers." *Engineering Failure Analysis*, 16(8): 2604–2617. https://doi.org/10.1016/j.engfailanal.2009.04.027.

Messiha, M. unpublished. *A systematic investigation of relevant structure-property-relationsships affecting the general crack growth behavior of unplasticized polamide 12,* unpublished PhD Thesis, Montanuniversität.

Messiha, M., B. Gerets, J. Heimink, A. Frank, F. Arbeiter, and K. Engelsing. 2020. "Slow crack growth resistance of modern PA-U12 grades measured by cyclic cracked round bar tests and strain hardening tests." *Polymer Testing*, 86(38): 106468. https://doi.org/10.1016/j.polymertesting.2020.106468.

Moser, A. 2013. *Zeit- Temperatur- Verschiebung von thermoplastischen polymeren Werkstoffen,* Master Thesis, Montanuniversität.

Muratoglu, O. K., A. S. Argon, R. E. Cohen, and M. Weinberg. 1995. "Microstructural processes of fracture of rubber- modified polyamides." *Poiymer Vol. 36 No. 25, pp. 4171-4186, 1995*.

Narasimhan, R., and A. J. Rosakis. 1990. "Three-Dimensional Effects Near a Crack Tip in a Ductile Three-Point Bend Specimen: Part I—A Numerical Investigation." *Journal of Applied Mechanics SEPTEMBER 1990, Vol. 57 / 607*.

Nijhof, R., A. van der Wal, and R. J. Gaymans. 1999. "Polypropylene–rubber blends: 2. The effect of the rubber content on the deformation and impact behaviour.", 1999.

Özbek, P. 2008. *Rapid Fracture Resistance of Polyethylene: Dependence on Polymer Structure,* Dissertation, Imperial College.

Partridge, I. K. 1992. "Rubber Toughened Polymers in Multicomponent Polymer Systems." *Longman Scientific & Technical Ltd.*, 1992.

Perkins, W. G. 1999. "Polymer toughness and impact resistance." *POLYMER ENGINEERING AND SCIENCE*.

Pilz, G. 2001. *Viskoelastische Eigenschaften polymerer Werkstoffe für Rohranwendungen,* Dissertation, Montanuniversität.

Pilz, G. 2014. *Physik und Werkstoffkunde der Kunststoffe II,* Vorlesungsunterlagen, Montanuniversität.

Pinter, G. 1999. *Rißwachstumsverhalten von PE-HD unter statischer Belastung,* Dissertation, Montanuniversität.

Pinter, G. 2019. *Vorlesungsunterlagen zu Bruchmechanik der Kunst- und Verbundwerkstoffe,* Vorlesungsunterlagen, Montanuniversität.

Poduška, J., P. Hutař, J. Kučera, A. Frank, J. Sadílek, G. Pinter, and L. Náhlík. 2016. "Residual stress in polyethylene pipes." *Polymer Testing*, 54: 288–295. https://doi.org/10.1016/j.polymertesting.2016.07.017.

Pritchard, G., ed. 1998. *Plastics Additives: Impact modifiers: (1) mechanisms and applications in thermoplastics*, Dordrecht: Springer Science+Business Media.

Ravi-Chandar, K., and W. G. Knauss. 1984. "An experimental investigation into dynamic fracture: I. Crack initiation and arrest." *International Journal of Fracture*, 25(4): 247–262. https://doi.org/10.1007/BF00963460.

Retting, W., ed. 1969. *Die Angewandte Makromolekulare Chemie: Applied Macromolecular Chemistry and Physics: Zur abhängigkeit der mechanischen eigenschaften von thermoplasten von ihrer thermischen vorgeschichte.*

Retting, W. 1973. "Influence of orientation on the relaxation and ultimate properties of polypropylene." *In Journal of Polymer Science: Polymer Symposia (Vol. 42, No. 2, pp. 605-615). New York: Wiley Subscription Services, Inc., A Wiley Company.*

Ritchie, S., P. S. Leevers, and P. Davis. 1998. "Brittle–tough transition of rapid crack propagation in polyethylene." *Polymer Vol. 39 No. 25, pp. 6657–6663, 1998*, 1998.

Schöngrundner, R. 2010. *Numerische Studien zur Ermittlung der risstreibenden Kraft in elastisch-plastischen Materialien bei unterschiedlichen Belastungsbedingungen,* Dissertation, Montanuniversität.

Scibetta, M., R. Chaouadi, and E. van Walle. 2000. "Fracture toughness analysis of circumferentially-cracked round bars." *International Journal of Fracture 104: 145–168, 2000.*

Shnean, Z.Y. 2012. "MECHANICAL AND PHYSICAL PROPERTIES OF HIGH DENSITY POLYETHYLENE FILLED WITH CARBON BLACK AND TITANIUM DIOXIDE." *Diyala Journal of Engineering Sciences; Vol. 05, No. 01, pp.147-159, June 2012*, 2012.

Siviour, C. R., and J. L. Jordan. 2016. "High Strain Rate Mechanics of Polymers: A Review." *J. dynamic behavior mater.*, 2(1): 15–32. https://doi.org/10.1007/s40870-016-0052-8.

Swallowe, G. M., ed. 1999. *Mechanical Properties and Testing of Polymers: An A-Z Reference*: Springer Netherlands.

Taib, R. M., Z. A. Ghaleb, and Z. A. Mohd Ishak. 2012. "Thermal, mechanical, and morphological properties of polylactic acid toughened with an impact modifier." *J. Appl. Polym. Sci.*, 123(5): 2715–2725. https://doi.org/10.1002/app.34884.

Tanrattanakul, V., W. G. Perkins, F. L. Massey, A. Moet, A. Hiltner, and E. Baer. 1997. "Fracture mechanisms of poly(ethylene terephthalate) and blends with styrene-butadiene-styrene elastomers." *JOURNAL OF MATERIALS SCIENCE 32 (1997) 4749–4758*.

Wagner, B. 2009. *Bruchmechanische Charakterisierung austenitischer Edelstähle bei chloridinduzierter Spannungsrisskorrosion,* Dissertation, Montanuniversität.

Wang, J., X. Zhang, L. Jiang, and J. Qiao. 2019. "Advances in toughened polymer materials by structured rubber particles." *Progress in Polymer Science*, 98: 101160. https://doi.org/10.1016/j.progpolymsci.2019.101160.

Weichert, R., and K. Schönert. 1974. "On the temperature rise at the tip of a fast running crack." *Journal of the Mechanics and Physics of Solids*.

Weßing, W., J. Lohmar, C. Baron, and A. Dowe. 2007. "Polyamid- Rohre vor dem praktischen Einsatz im Gas- Hochdruckbereich." *3R international (2007)*.

Yayla, P. 1991. *Rapid Crack Propagation in Polyethylene Gas Pipes,* PhD Thesis, Imperial College.

Yilmaz, S., O. Gul, and T. Yilmaz. 2015. "Effect of chain extender and terpolymers on tensile and fracture properties of polyamide 6." *Polymer*, 65: 63–71. https://doi.org/10.1016/j.polymer.2015.03.057.

Zhuang, Z., Z. Liu, B. Cheng, and J. Liao. 2014. *Extended Finite Element Method: Dynamic Crack Propagation*: Academic Press.

# APPENDIX

**Python evaluation file for “modified Charpy”**

```
import numpy as np # work with matrices
import matplotlib.pyplot as plt
import sys
import kkv_plt_37
from scipy.interpolate import interp1d
import os
from numpy import trapz
import datetime
files = os.listdir('Messdaten')
for i in files:
   test= open('Messdaten/'+str(i),"r")
   data = test.read()
   data = data.replace(",", ".")
   file = open('Messdaten_korrigiert/'+str(i),"w")
   file.write(data)
   file.close()
day = datetime.datetime.now()
filename = 'Ergebnisse/{}-{}-{}-results.txt'.format(day.year, day.month, day.day)
with open(filename, 'w') as f:
   f.write('Name\tArea tot\tArea max\tArea prop\n')
for i in files:
   data = np.genfromtxt('Messdaten_korrigiert/'+ str(i), delimiter='\t', skip_header=5)
   zeit = data[:,0]
   axialweg = data[:,2]*(-1) - data[0,2]*(-1)
   kraft = data[:,1]*(-1) - data[0,1]*(-1)
   axialweg_list=[]
   axialweg_maxlist=[]
   kraft_maxlist=[]
   kraft_list=[]
   zeit_list=[]
   axialweg_max=axialweg[0]
   for j in range(0,len(axialweg)):
      if j <= np.argmax(axialweg):
         if axialweg[j] < axialweg_max -0.1:
            break
         if kraft[j] < 0 and j >= np.argmax(kraft):
            break
         kraft_list.append(kraft[j])
         axialweg_list.append(axialweg[j])
         zeit_list.append(zeit[j])
         axialweg_max=axialweg[j]
         if j <= np.argmax(kraft):
```

```
            kraft_maxlist.append(kraft[j])
            axialweg_maxlist.append(axialweg[j])
    print(kraft_list, axialweg_list)
    area_max = trapz(kraft_maxlist, axialweg_maxlist)
    area_tot = trapz(kraft_list, axialweg_list)
    area_prop = area_tot - area_max
    print(str(i),"area_max =",'\t', "area_tot =",'\t' ,"area_prop =",'\n', area_max,
'\t',area_tot,'\t',area_prop)
    with open(filename, 'a') as f:
      f.write('{}\t{}\t{}\t{}\n'.format(i, area_tot, area_max, area_prop))
    #Plot Einstellung:
    titlesize = 15
    labelsize = 12
    legendsize = 11
    plt.rcParams = kkv_plt_37.rcParams(titlesize, labelsize, legendsize, font='calibri')
    Groesse_cm = np.array([15.5,10]) # Groesse in cm
    fig, ax = plt.subplots(ncols=1, nrows=1,figsize=Groesse_cm/2.54, dpi = 150)
    ax.plot(axialweg_list, kraft_list, 'r', label='Messdaten')
    ax.plot(axialweg_maxlist, kraft_maxlist, 'k', label='bis Maximum')
    ax.set_xlabel(r'Axialer Weg [mm]')
    ax.set_ylabel(r'Kraft [N]')
    leg = ax.legend(ncol=1)
    leg.set_title(str(i), prop={'size':labelsize})
    ax.grid()
    fig.tight_layout(pad=0.1)
fig.savefig('Plots/'+str(i.replace('dat','png')),dpi=300)
    array1 = np.array(zeit_list)
    array2 = np.array(axialweg_list)
    array3 = np.array(kraft_list)
    array_list = [array1, array2, array3]
    array2d = np.array(array_list)
    final_array = np.transpose(array2d)
    np.savetxt('Ergebnisse/'+str(i), final_array, delimiter='\t')
```

**Python evaluation file for "quasi-dynamic $K_{ID,eq}$"**

```
import numpy as np # work with matrices
import matplotlib.pyplot as plt
import kkv_plt_37
import os
from numpy import trapz
import datetime
from scipy.interpolate import interp1d
from scipy.optimize import bisect
from scipy import optimize as opt
```

```
files = os.listdir('Messdaten')
day = datetime.datetime.now()
filename = 'Ergebnisse/{}-{}-{}-K1c_dyn.txt'.format(day.year, day.month, day.day)
with open(filename, 'w') as f:
   f.write('Name\tvelocity in mm/min\ttemperature in °C\t${F_{max}}/{F_{Q}}$\tK1c in MPam^(-1/2)\tG1c in kJ/m² (aus A_max)\tArea_tot in J\tArea_max in J\tArea_prop in J\n')
for i in range(len(files)):
   if str(files[i])=='desktop.ini':
      continue
   else:
      test= open('Messdaten/'+str(files[i]),"r")
      data = test.read()
      data = data.replace(",", ".")
      file = open('Messdaten_korrigiert/'+str(files[i]),"w")
      file.write(data)
      file.close()
      data = np.genfromtxt('Messdaten_korrigiert/'+str(files[i]), delimiter='\t', skip_header=5)
      zeit = data[:,0]
      axialweg = data[:,2]
      kraft = data[:,1]
      axialweg_list=[]
      axialweg_maxlist=[]
      kraft_maxlist=[]
      kraft_list=[]
      zeit_list=[]
      axialweg_max=axialweg[0]
      for j in range(len(axialweg)):
         if j <= np.argmax(axialweg):
            if axialweg[j] < axialweg_max -0.05:
               break
            if kraft[j] < 0 and j >= np.argmax(kraft):
               break
            kraft_list.append(kraft[j])
            axialweg_list.append(axialweg[j])
            zeit_list.append(zeit[j])
            axialweg_max=axialweg[j]
            if j <= np.argmax(kraft):
               kraft_maxlist.append(kraft[j])
               axialweg_maxlist.append(axialweg[j])
      area_max = trapz(kraft_maxlist, axialweg_maxlist)*10**(-3)
      area_tot = trapz(kraft_list, axialweg_list)*10**(-3)
      area_prop = area_tot - area_max
      #print(str(i),"area_max =",'\t', "area_tot =",'\t' ,"area_prop =",'\n', area_max, '\t',area_tot,'\t',area_prop)
      array1 = np.array(zeit_list)
```

```
    array2 = np.array(axialweg_list)
    array3 = np.array(kraft_list)
    array_list = [array1, array2, array3]
    final_array=np.transpose(array_list)
    np.savetxt('Ergebnisse/'+str(files[i]), final_array, delimiter='\t')
    K1c_array=[]
    v_array=[]
    T_array=[]
    specimens=[]
    print(str(files[i]))
    user_input=input('make calculation: y; skip this specimen: s; one specimen back: b; abort calulation: a; your answer: ')
    if user_input =='s':
      continue
    if user_input == 'a':
      break
    if user_input == 'y':
      i=i
      print(str(files[i]))
      area_CRB = float(input('tell me the whole microscopically measured CRB area for that specimen in mm²: '))*10**(-6)
      lig_area_CRB = float(input('tell me the microscopically measured ligament area for that specimen in mm²: '))*10**(-6)
      velocity = float(input('tell me the test speed for that specimen in mm/min: '))
      temperature = float(input('tell me the test temperature for that specimen in °C: '))
      Fmax=max(kraft_maxlist)
      print(Fmax)
      b=np.sqrt(lig_area_CRB/np.pi) # Ligamentradius
      R=np.sqrt(area_CRB/np.pi) # Radius
      a=R-b #Kerbtiefe
      geom_corr=0.5*(1+0.5*b/R+3/8*(b/R)**2-0.363*(b/R)**3+0.731*(b/R)**4) #Geometriekorrekturfaktor für CRB nach Benthem & Koiter
#Berechnung von Steigungsgerade durch Fmax/3 bzw. 2Fmax/3 und Ermittlung der 5% verschobenen Gerade allerdings problem mit Intersection zwischen Gerade und random dataset
      index_Fmax3=0
      for g in range(len(kraft_maxlist)):
        if kraft_maxlist[g] <= Fmax/3:
          index_Fmax3=g
          g=g+1
      x1=axialweg_maxlist[index_Fmax3]
      y1=kraft_maxlist[index_Fmax3]
      index_2Fmax3=0
      for g in range(len(kraft_maxlist)):
        if kraft_maxlist[g]  <= 2*Fmax/3:
          index_2Fmax3=g
```

```
        g=g+1
x2=axialweg_maxlist[index_2Fmax3]
y2=kraft_maxlist[index_2Fmax3]
d=(x2*y1-x1*y2)/(x2-x1)
k=(y1-d)/x1
x0=-d/k
#print(k,d,y1,y2,x1,x2,x0)
index_x0=0
for g in range(len(axialweg_maxlist)):
    if axialweg_maxlist[g] <= x0:
        index_x0=g
        g=g+1
f=[]
weg_f=[]
for g in range(index_x0, np.argmax(axialweg_maxlist)):
    f.append(k*axialweg_maxlist[g]+d)
    weg_f.append(axialweg_maxlist[g])
    g=g+1
#zweite Gerade mit 5% Steigung versetzt, die aber auch durch x0 geht:
k_5=0.95*k
d_5=-k_5*x0
f_5=[]
weg_f_5=[]
for g in range(index_x0, np.argmax(axialweg_maxlist)):
    f_5.append(k_5*axialweg_maxlist[g]+d_5)
    weg_f_5.append(axialweg_maxlist[g])
    g=g+1
f_arr=np.array(f)
weg_f_arr=np.array(weg_f)
f_5_arr=np.array(f_5)
weg_f_5_arr=np.array(weg_f_5)
f5 = interp1d(weg_f_5_arr, f_5_arr, fill_value="extrapolate")
kraft_func = interp1d(axialweg_maxlist, kraft_maxlist, fill_value="extrapolate")
x_start = x0
x_stop = max(axialweg_maxlist)
#create function
h = lambda x : kraft_func(x) - f5(x)
if np.sign(h(x_start)) == np.sign(h(x_stop)):
    F_q=Fmax
    x_intersect=max(axialweg_maxlist)
else:
    x_intersect = bisect(h, x_start, x_stop, xtol = .001)
    #x_intersect = opt.brentq(h, x_start, x_stop, xtol = .001)
    F_q = kraft_func(x_intersect)
#K1c berechnen
K1c= F_q/(np.pi*b**2)*np.sqrt(np.pi*a*b/R)*geom_corr*10**(-6)
```

```
        #G1c aus K1c
        #G1c aus Fläche: (Formeln nach Scibetta et al_Fracture toughness analysis of circumferentially-cracked round bars S.152 nach Lei & Neale)
        if a/R > 0.65:
           eta=1
        else:
           eta=b/(2*R)*(0.00771+3.05739*(a/R))/(1-0.00771*(a/R)-1.52869*(a/R)**2)
        G1c=eta*area_max/lig_area_CRB*10**(-3) #in kJ/m²
        print(str('K1c='),K1c,str('G1c='),G1c)
           f.write('{}\t{}\t{}\t{}\t{}\t{}\t{}\t{}\n'.format(str(files[i]), velocity, temperature, round(Fmax/F_q,3), K1c, G1c, area_tot, area_max, area_prop)
     if user_input == 'b':
        i=i-1
        print(str(files[i]))
        area_CRB = float(input('tell me the whole microscopically measured CRB area for that specimen in mm²: '))*10**(-6)
        lig_area_CRB = float(input('tell me the microscopically measured ligament area for that specimen in mm²: '))*10**(-6)
        velocity = float(input('tell me the test speed for that specimen in mm/min: '))
        temperature = float(input('tell me the test temperature for that specimen in °C: '))
        Fmax=max(kraft_maxlist)
        print(Fmax)
        b=np.sqrt(lig_area_CRB/np.pi) # Ligamentradius
        R=np.sqrt(area_CRB/np.pi) # Radius
        a=R-b #Kerbtiefe
        geom_corr=0.5*(1+0.5*b/R+3/8*(b/R)**2-0.363*(b/R)**3+0.731*(b/R)**4) #Geometriekorrekturfaktor für CRB nach Benthem & Koiter
        index_Fmax3=0
        for g in range(len(kraft_maxlist)):
           if kraft_maxlist[g] <= Fmax/3:
              index_Fmax3=g
              g=g+1
        x1=axialweg_maxlist[index_Fmax3]
        y1=kraft_maxlist[index_Fmax3]

        index_2Fmax3=0
        for g in range(len(kraft_maxlist)):
           if kraft_maxlist[g]  <= 2*Fmax/3:
              index_2Fmax3=g
              g=g+1
        x2=axialweg_maxlist[index_2Fmax3]
        y2=kraft_maxlist[index_2Fmax3]
        d=(x2*y1-x1*y2)/(x2-x1)
        k=(y1-d)/x1
        x0=-d/k
        #print(k,d,y1,y2,x1,x2,x0)
```

```
index_x0=0
for g in range(len(axialweg_maxlist)):
   if axialweg_maxlist[g] <= x0:
      index_x0=g
      g=g+1
f=[]
weg_f=[]
for g in range(index_x0, np.argmax(axialweg_maxlist)):
   f.append(k*axialweg_maxlist[g]+d)
   weg_f.append(axialweg_maxlist[g])
   g=g+1
k_5=0.95*k
d_5=-k_5*x0
f_5=[]
weg_f_5=[]
for g in range(index_x0, np.argmax(axialweg_maxlist)):
   f_5.append(k_5*axialweg_maxlist[g]+d_5)
   weg_f_5.append(axialweg_maxlist[g])
   g=g+1
f_arr=np.array(f)
weg_f_arr=np.array(weg_f)
f_5_arr=np.array(f_5)
weg_f_5_arr=np.array(weg_f_5)
f5 = interp1d(weg_f_5_arr, f_5_arr, fill_value="extrapolate")
kraft_func = interp1d(axialweg_maxlist, kraft_maxlist, fill_value="extrapolate")
x_start = x0
x_stop = max(axialweg_maxlist)
#create function
h = lambda x : kraft_func(x) - f5(x)
if np.sign(h(x_start)) == np.sign(h(x_stop)):
   F_q=Fmax
   x_intersect=max(axialweg_maxlist)
else:
   x_intersect = bisect(h, x_start, x_stop, xtol = .001)
   #x_intersect = opt.brentq(h, x_start, x_stop, xtol = .001)
   F_q = kraft_func(x_intersect)
#K1c berechnen
K1c= F_q/(np.pi*b**2)*np.sqrt(np.pi*a*b/R)*geom_corr*10**(-6)
#G1c aus K1c:
#G1c aus Fläche: (Formeln nach Scibetta et al_Fracture toughness analysis of
circumferentially-cracked round bars S.152 nach Lei & Neale)
if a/R > 0.65:
   eta=1
else:
   eta=b/(2*R)*(0.00771+3.05739*(a/R))/(1-0.00771*(a/R)-1.52869*(a/R)**2)
#Speichern in filename2:
```

```
        with open(filename, 'a') as f: #öffne das zweite File und appende
          f.write('{}\t{}\t{}\t{}\t{}\t{}\t{}\t{}\t{}\n'.format(str(files[i]), velocity, temperature,
round(Fmax/F_q,3), K1c, G1c, area_tot, area_max, area_prop))
    #Plot einstellung:
    print
    titlesize = 15
    labelsize = 12
    legendsize = 11
    plt.rcParams = kkv_plt_37.rcParams(titlesize, labelsize, legendsize, font='calibri')
    Groesse_cm = np.array([15.5,10]) # Groesse in cm
    fig, ax = plt.subplots(ncols=1, nrows=1,figsize=Groesse_cm/2.54, dpi = 150)
    ax.plot(axialweg_list, kraft_list, 'r', label='Messdaten')
    #ax.plot(axialweg[:idx1], kraft[:idx1], 'g', label='Gesamtkurve')
    ax.plot(axialweg_maxlist, kraft_maxlist, 'k', label='bis Maximum')
    ax.plot(weg_f_arr, f_arr, 'g-.', label='linear elastic line', linewidth=1)
    ax.plot(weg_f_5_arr, f_5_arr, '-.',color='orange', label='$F_{Q}$ correction
line',linewidth=1)
    ax.scatter(x_intersect, F_q, color='grey',edgecolor='k', marker='X', zorder=5)
    ax.annotate('$F_{Q}$',(x_intersect-0.3, F_q))
    ax.scatter(max(axialweg_maxlist), Fmax, color='red',edgecolor='k', marker='X',
zorder=6)
    ax.annotate('$F_{max}$',(max(axialweg_maxlist)+0.1, Fmax))
    ax.annotate('${F_{max}}/{F_{Q}}=$'+str(round(Fmax/F_q,3)),(x_intersect-1.5, F_q))
    ax.set_xlabel(r'Axialer Weg [mm]')
    ax.set_ylabel(r'Kraft [N]')
    leg = ax.legend(ncol=1)
    leg.set_title(str(files[i]), prop={'size':labelsize})
    ax.grid()
    fig.tight_layout(pad=0.1)
    #fig.show()
    fig.savefig('Plots/'+str(files[i].replace('dat','png')),dpi=300)
```

**Python evaluation file for NHI – Approach 2 (A2)**

```
import numpy as np # work with matrices
import matplotlib.pyplot as plt
import sys
import kkv_plt_37
from scipy.interpolate import interp1d
import os
from numpy import trapz
import datetime
files = os.listdir('Messdaten')
# Komma durch Punkte ersetzen
for i in files:
  test= open('Messdaten/'+str(i),"r")
```

```
    data = test.read()
    data = data.replace(",", ".")
    file = open('Messdaten_korrigiert/'+str(i),"w")
    file.write(data)
    file.close()
day = datetime.datetime.now()
filename = 'Ergebnisse/{}-{}-{}-results.txt'.format(day.year, day.month, day.day)
with open(filename, 'w') as f:
f.write('Name\tArea_max\tArea_tot\tArea_prop\tArea_max/Area_tot\tArea_prop/Area_
tot\tArea_prop/Area_max\n')
for i in files:
    print(str(i))
    if str(i)=="desktop.ini":
        continue
    data = np.genfromtxt('Messdaten_korrigiert/'+ str(i), delimiter='\t', skip_header=7,
usecols=np.arange(0,5))
    zeit = data[:,1]
    axialweg = data[:,4]
    kraft = data[:,2]
    #print(zeit, axialweg, kraft)
    axialweg_list=[]
    axialweg_maxlist=[]
    kraft_maxlist=[]
    kraft_list=[]
    zeit_list=[]
    axialweg_max=axialweg[0]
    for j in range(0,len(axialweg)):
        if j <= np.argmax(axialweg):
            if axialweg[j] < axialweg_max -0.1:
                break
            if kraft[j] < 0 and j >= np.argmax(kraft):
                break
            kraft_list.append(kraft[j])
            axialweg_list.append(axialweg[j])
            zeit_list.append(zeit[j])
            axialweg_max=axialweg[j]
            if j <= np.argmax(kraft):
                kraft_maxlist.append(kraft[j])
                axialweg_maxlist.append(axialweg[j])
    area_max = trapz(kraft_maxlist, axialweg_maxlist)
    area_tot = trapz(kraft_list, axialweg_list)
    area_prop = area_tot - area_max
    print(str(i),"area_max =",'\t', "area_tot =",'\t' ,"area_prop =",'\t' ,"area_max/area_tot",
'\t' ,"area_prop/area_tot", '\t', "area_prop/area_max", '\n', area_max,
'\t',area_tot,'\t',area_prop, '\t', area_max/area_tot, '\t', area_prop/area_tot, '\t',
area_prop/area_max)
```

```
    with open(filename, 'a') as f:
        f.write('{}\t{}\t{}\t{}\t{}\t{}\n'.format(i, area_max, area_tot, area_prop, area_max/area_tot, area_prop/area_tot, area_prop/area_max))
    #Plot einstellung:
    titlesize = 15
    labelsize = 12
    legendsize = 11
    plt.rcParams = kkv_plt_37.rcParams(titlesize, labelsize, legendsize, font='calibri')
    Groesse_cm = np.array([15.5,10]) # Groesse in cm
    fig, ax = plt.subplots(ncols=1, nrows=1,figsize=Groesse_cm/2.54, dpi = 150)
    ax.plot(axialweg_list, kraft_list, 'r', label='Messdaten')
    ax.plot(axialweg_maxlist, kraft_maxlist, 'k', label='bis Maximum')
    ax.set_xlabel(r'Axialer Weg [mm]')
    ax.set_ylabel(r'Kraft [N]')
    leg = ax.legend(ncol=1)
    leg.set_title(str(i), prop={'size':labelsize})
    fig.tight_layout(pad=0.1)
    fig.savefig('Plots/'+str(i.replace('txt','png')),dpi=300)
    headers = np.array(['zeit_list [ms]','axialweg_tot [mm]','kraft_tot [N]'])
    headers_max = np.array(['axialweg_max [mm]','kraft_max [N]'])
    array1 = np.array(zeit_list)
    array2 = np.array(axialweg_list)
    array3 = np.array(kraft_list)
    array4 = np.array(axialweg_maxlist)
    array5 = np.array(kraft_maxlist)
    array_list = [array1,array2,array3]
    array_maxlist = [array4,array5]
    #print(array_list)
    array2d = np.array(array_list)
    maxarray2d = np.array(array_maxlist)
    #print(array2d)
    trans_arr = np.transpose(array2d)
    trans_maxarr= np.transpose(maxarray2d)
    np.savetxt('Ergebnisse/A_tot'+str(i), np.vstack((headers,trans_arr)), fmt='%s', delimiter='\t')
    np.savetxt('Ergebnisse/A_max'+str(i), np.vstack((headers_max,trans_maxarr)), fmt='%s', delimiter='\t')
    #np.savetxt('Ergebnisse/'+str(i), array2d, fmt='%s', delimiter='\t', header=headers)
```